TECHNICAL REPORT ARBRL-TR-02367

RECONSTRUCTION OF A BLAST FIELD FROM PRESSURE HISTORY OBSERVATIONS

Aivars Celmiņš

September 1981

US ARMY ARMAMENT RESEARCH AND DEVELOPMENT COMMAND
BALLISTIC RESEARCH LABORATORY
ABERDEEN PROVING GROUND, MARYLAND

Destroy this report when it is no longer needed.
Do not return it to the originator.

Secondary distribution of this report by originating or sponsoring activity is prohibited.

Additional copies of this report may be obtained from the Defense Technical Information Center, Cameron Station, Alexandria, Virginia 22314.

The findings in this report are not to be construed as an official Department of the Army position, unless so designated by other authorized documents.

The use of trade names or manufacturers' names in this report does not constitute indorsement of any commercial product.

UNCLASSIFIED

SECURITY CLASSIFICATION OF THIS PAGE *(When Data Entered)*

REPORT DOCUMENTATION PAGE		READ INSTRUCTIONS BEFORE COMPLETING FORM
1. REPORT NUMBER TECHNICAL REPORT ARBRL-TR-02367	2. GOVT ACCESSION NO.	3. RECIPIENT'S CATALOG NUMBER
4. TITLE *(and Subtitle)* Reconstruction of a Blast Field from Pressure History Observations		5. TYPE OF REPORT & PERIOD COVERED 6. PERFORMING ORG. REPORT NUMBER
7. AUTHOR*(s)* Aivars Celmiņš		8. CONTRACT OR GRANT NUMBER*(s)*
9. PERFORMING ORGANIZATION NAME AND ADDRESS US Army Ballistic Research Laboratory ATTN: DRDAR-BLI Aberdeen Proving Ground, MD 21005		10. PROGRAM ELEMENT, PROJECT, TASK AREA & WORK UNIT NUMBERS 1L161102AH43
11. CONTROLLING OFFICE NAME AND ADDRESS US Army Armament Research & Development Command US Army Ballistic Research Laboratory ATTN: DRDAR-BL Aberdeen Proving Ground, MD 21005		12. REPORT DATE SEPTEMBER 1981 13. NUMBER OF PAGES 89
14. MONITORING AGENCY NAME & ADDRESS*(if different from Controlling Office)*		15. SECURITY CLASS. *(of this report)* UNCLASSIFIED 15e. DECLASSIFICATION/DOWNGRADING SCHEDULE

16. DISTRIBUTION STATEMENT *(of this Report)*

Approved for public release; distribution unlimited

17. DISTRIBUTION STATEMENT *(of the abstract entered in Block 20, if different from Report)*

18. SUPPLEMENTARY NOTES

19. KEY WORDS *(Continue on reverse side if necessary and identify by block number)*

Blast Field	Model Fitting
Overpressure History Data	Numerical Integration
Spherical Blast in Ideal Gas	Variance Estimates

20. ABSTRACT *(Continue on reverse side if necessary and identify by block number)* dll

This report describes a method for the calculation of parts of a spherical blast field from pressure history observations at stations placed at various distances from the blast center. The method consists of a determination of the pressure field by model fitting and of a subsequent numerical integration of the flow governing equations. The results provide a complete flow description (pressure, density, and particle velocity) as well as estimates of the accuracy of the results within the region of observations. A check of some basic

(Continued)

DD FORM 1 JAN 73 1473 EDITION OF 1 NOV 65 IS OBSOLETE

UNCLASSIFIED

SECURITY CLASSIFICATION OF THIS PAGE *(When Data Entered)*

20. Abstract (continued)

assumptions (spherical symmetry and negligible viscosity) is provided by an independent calculation of the particle velocity. Application examples are shown for a theoretically computed strong blast field and for data from a high energy blast experiment.

TABLE OF CONTENTS

LIST OF TABLES

LIST OF FIGURES

LIST OF FIGURES (CONTINUED)

1. INTRODUCTION

For experimental studies of target response to high energy blast, one needs an accurate definition of the blast field which provides the load on the target. The general features of the flow in a blast field can be predicted by solving numerically the governing equations of the flow. However, the accuracy of such calculations is limited because the early stages of an explosion are difficult to model, and the results of the early stage calculations influence subsequent computations for later times. Therefore, direct measurements of the complete flow field would be most desirable; but such measurements are usually restricted, for technical reasons, to pressure history observations, and to shock arrival time and incident shock pressure measurements at various stations. Hence, one has the task to compute other flow variables; e.g., the density and the particle velocity, from the measured pressures.

Directly computable from pressure history observations is the history of the dynamic pressure (internal energy density), if simultaneous measurements of incident and stagnation pressures are available. However, the results are very sensitive to observational inaccuracies. Typically, the relative standard error of the calculated dynamic pressure is ten times as large as the relative standard errors of the pressure observations[1]. Also, the calculations do not provide any other flow variables besides the dynamic pressure.

Generally, one can improve the accuracy of computed results by using additional information. For the present problem, such information is available from two sources: from pressure history observations at stations adjacent to the station of interest and from the governing equations of the flow. Compared to the governing equations of the early stages of the explosion, the governing equations for late stage flow are relatively simple and amenable to numerical solution. Times and distances that are of interest for target response studies typically are within this flow stage. Therefore, one can formulate the problem as a task to solve numerically the governing equations with boundary conditions derived from pressure history and shock observations.

In this formulation, the task is a mathematically ill-posed problem because the boundary conditions overdetermine the solution in some parts of the flow field, and at the same time may not be sufficient to compute the complete flow history for the full duration of a pressure history observation at some other station.

Regularizations of the problem have been achieved by using two opposite approaches. In one approach, one deletes all data that would overdetermine the problem. In the other approach, one uses all pertinent data, but deletes one of the governing equations, using it later for control calculations. The former approach has been used by Gottlieb and Ritzel[2]. The latter approach is described in this report.

---

[1] *George D. Teel, "Free-Field Airblast Definition - Event DICE THROW," Proceedings of the DICE THROW Symposium 21-23 June 1977, Volume I, Defence Nuclear Agency Report DNA 4377P-1, pp. 7-76, July 1977.*

[2] *James J. Gottlieb and David V. Ritzel, "Flow Properties of a Spherical Blast Wave," presentation at the Sixieme Symposium International sur les applications militaires de la simulation de souffle, Cahors, France, 25-27 June 1979.*

An advantage of the approach by Gottlieb and Ritzel is that the problem is immediately reduced to a standard task in numerical mathematics. A disadvantage is that, in a simplistic application of the method, all observational inaccuracies enter directly into the calculations and might be amplified. In order to obtain reasonable results, one has to smooth judiciously the data or to introduce viscosity into the computing scheme. A smoothing of data can be done in different manners so that in effect one may have to manipulate the data in order to obtain reasonable results. The data that are not used for smoothing or as boundary data, could be used for a subsequent check on the calculations, but results of such tests have not been reported in Reference 2.

In our approach, the problem is regularized by discarding one of the governing equations, but using all pressure observations within a region of interest. We assume that the observations suffice to determine a pressure field function $p(r,t)$ within the region. The function is found by a least squares model fitting, which takes the rôle of the data smoothing in the Gottlieb and Ritzel approach. The pressure field function then is substituted into the governing equations which in turn determine the other flow variables. Problems of this type were considered by Makino[3] who observed that one does not need the continuity equation for the flow calculation if $p(r,t)$ is known. We have, in essence, followed Makino's theoretical ideas and established computer programs that compute the flow in the aforementioned manner. The continuity equation is used at the end of the calculations to check the accuracy of the results. We also carried out an analysis of the sensitivity of the results to observational inaccuracies, and included computations of accuracy estimates in the computer programs. In typical examples, the results were found to be quite insensitive to this type of inaccuracy. For example, the relative standard error of the dynamic pressure was found to be of the same order or less than the relative standard error of the overpressure observations.

This report outlines the theory of the flow calculations from pressure measurements (Sections 2 through 6) and demonstrates its application in two examples (Sections 7 and 8). The first example treats a theoretically computed strong blast field. The second example is an application of the technique to real observations.

A description of the use of the computer programs will be published in a forthcoming users' manual.

2. BASIC ASSUMPTIONS AND THEORY

We seek to determine certain parts of the flow field within a blast bubble in air. The area of interest is a relatively narrow strip in the r,t-plane behind the initial shock trajectory at a distance where the shock strength is only moderate. We shall assume that the following conditions are satisfied within the area of interest:

(A) the flowing medium is an ideal gas with zero viscosity and no heat conduction, and

---

[3] *Ray C. Makino, "An Approximation Method in Blast Calculations," BRL Memorandum Report 1034, February 1956.* (AD #114875)

(B) the event is spherically symmetric and the flow has only a radial velocity component u.

The first assumption is satisfied in most applications because typically the maximum overpressure at the target is only of the order of one megapascal. Within this pressure regime, air behaves like an ideal gas. The second condition is nearly satisfied in most experiments, because usually the explosion source and the targets are positioned on the same plane, and the blast bubble is a hemisphere. Deviations from spherical flow symmetry within the bubble may be caused by local surface disturbances, by wind, and by the presence of dust in the flow near the ground surface. The present technique cannot be applied to cases where such disturbances are not negligible.

The governing equations for a flow satisfying the conditions (A) are[4]:

the continuity equation

$$\frac{d\rho}{dt} + \rho \text{ div } u = 0 \ , \tag{2.1}$$

the momentum equation

$$\rho \frac{du}{dt} + \text{grad } p = 0 \ , \tag{2.2}$$

the energy equation

$$\rho \frac{de}{dt} - \frac{p}{\rho} \frac{d\rho}{dt} = 0 \ , \tag{2.3}$$

and the equation of state

$$e = \frac{1}{\gamma - 1} \frac{p}{\rho} \ . \tag{2.4}$$

In Eqs. (2.1) through (2.3) we have used the material derivative symbol

$$\frac{d}{dt} = \frac{\partial}{\partial t} + (u \cdot \text{grad}) \ . \tag{2.5}$$

Because the flow is assumed to be spherically symmetric (condition (B)), we also have the definitions

---

[4] *Richard von Mises, "Mathematical Theory of Compressible Fluid Flow," Academic Press, NY, 1958.*

$$\text{div } u = \frac{1}{r^2} \frac{\partial}{\partial r} (r^2 u) \ , \tag{2.6}$$

and

$$\text{grad } p = \frac{\partial p}{\partial r} \ . \tag{2.7}$$

Eliminating the specific internal energy e between Eqs. (2.3) and (2.4) one obtains

$$\frac{1}{p} \frac{dp}{dt} - \gamma \frac{1}{\rho} \frac{d\rho}{dt} = 0 \ . \tag{2.8}$$

Eq. (2.8) can be integrated along a particle path line. The result is the well known formula for a particle in an adiabatic flow:

$$\frac{\rho}{\rho_A} = \left(\frac{p}{p_A} \right)^{1/\gamma} \ , \tag{2.9}$$

where the subscript A indicates reference values at a point A on the particle path.

The momentum Eq. (2.2) can be reformulated by substituting in it the expression (2.9). The result is

$$\frac{du}{dt} = - \frac{1}{\rho_A} \left(\frac{p_A}{p} \right)^{1/\gamma} \frac{\partial p}{\partial r} \ . \tag{2.10}$$

If the pressure function p(r,t) is given, e.g., by measurements, then the right-hand side of Eq. (2.10) is a known function of r and t. In that case, the equation can be integrated numerically together with the path line equation

$$\frac{dr}{dt} = u \ . \tag{2.11}$$

The integration provides the path line starting at a point A and the particle velocity along it. The density along the same path line is given by Eq. (2.9). All other flow variables, such as, internal energy, dynamic pressure, and sound speed can be computed from p, u, and ρ.

The continuity Eq. (2.1) is not needed for the described calculation of the flow corresponding to an observed pressure field $p(r,t)$. One can use the equation to test the calculated results, as suggested by Makino[3]. In fact, if the pressure $p(r,t)$ is measured precisely then this test provides a check of the validity of the assumptions (A) and (B) about the flow field. In practice, test calculations based on the continuity equation cannot provide exactly the same result as the integration along path lines because the pressure field function $p(r,t)$ contains observational as well as systematic errors. The effects of the former are estimated in our approach using input information about the data accuracy. Systematic errors may manifest themselves by differences between original and control calculations that are larger than predicted by the observational error analysis.

A control calculation based on the continuity equation can be carried out as follows. First, we use Eq. (2.8) and reformulate the continuity Eq. (2.1), obtaining

$$\operatorname{div} u + \frac{1}{\gamma p} \frac{dp}{dt} = 0 \ , \tag{2.12}$$

or

$$\frac{\partial}{\partial r} (r^2 u) + (r^2 u) \frac{1}{\gamma p} \frac{\partial p}{\partial r} + \frac{r^2}{\gamma p} \frac{\partial p}{\partial t} = 0 \ . \tag{2.13}$$

Eq. (2.13) expresses the dependence of the quantity $r^2 u$ on r for $t = \text{const.}$ A formal integration of the equation along a line $t = \text{const.}$ yields

$$r^2 u(r,t) = \left(\frac{p_C}{p(r,t)} \right)^{1/\gamma} \left[r_C^2 u_C + \frac{1}{\gamma} \int_r^{r_C} \xi^2 \left(\frac{p(\xi,t)}{p_C} \right)^{1/\gamma} \frac{1}{p(\xi,t)} \frac{\partial p(\xi,t)}{\partial t} \, d\xi \right] \tag{2.14}$$

or

$$u(r,t) = u_C \left(\frac{r_C}{r} \right)^2 \cdot \left(\frac{p_C}{p(r,t)} \right)^{1/\gamma} + \frac{1}{r^2 \ \gamma \ p(r,t)^{1/\gamma}} \int_r^{r_C} \xi^2 \cdot p(\xi,t)^{(1/\gamma - 1)} \cdot \frac{\partial p(\xi,t)}{\partial t} \, d\xi \tag{2.15}$$

The subscript C in Eqs. (2.14) and (2.15) indicates function values at a point C with the coordinates (r_C,t). Using Eq. (2.15) one can calculate the particle velocity $u(r,t)$ by a numerical quadrature along $t = \text{const.}$, if an initial value $u_C = u(r_C,t)$ and the pressure field function $p(r,t)$ are known.

---

[3] *Ibid.*

In summary, we proceed as follows for the calculation of the flow field. First, we establish a pressure field function $p(r,t)$ by data fitting, whereby all data are used that are located in the vicinity of the point of interest, say B. Next, Eqs. (2.10) and (2.11) are integrated along a particle path AB, as shown in Figure 1. The integration produces the velocity u_B at B. The density ρ_B can be computed using Eq. (2.9), once the path line is established. (The flow variables u_A and ρ_A on the shock are known from the pressure field function and shock relations.) Finally the calculated velocity u_B is compared with another calculation using Eq. (2.15), applied along the line BC. The velocity u_C at the point C is again obtained from shock relations.

3. NUMERICAL INTEGRATION AND ACCURACY ESTIMATES

In most applications, one needs the flow history at some fixed distance, say r_B. We obtain the history, i.e., the values of flow variables at a series of points along the line $r = r_B$, by integrating Eqs. (2.10) and (2.11) along a number of path lines, each starting at a different point of the shock. The test calculation of the velocity is done by integration of Eq. (2.15) along appropriate lines $t = \text{const}$. Figure 2 shows schematically the integration lines and the location of the computed nodes in the r,t-plane. The values of the flow variables at the shock as well as the pressure field function behind the shock that are needed for these integrations, are obtained by model fitting of shock and pressure observations, respectively.

Let the result of the shock model fitting be certain functions of the radial distance r providing shock arrival time t_s, shock overpressure p_s, shock density ρ_s, and particle velocity u_s:

$$
\begin{aligned}
t_s &= t_s(r;\theta) \ , \\
p_s &= p_s(r;\theta) \ , \\
\rho_s &= \rho_s(r;\theta) \ , \\
u_s &= u_s(r;\theta) \ .
\end{aligned}
\tag{3.1}
$$

In these functions, θ is a model parameter vector. We shall give, in Section 4, explicit expressions for the functions t_s through u_s.

The model fitting of the observed pressure histories produces a pressure field function

$$
p = p_f(r,t;\theta) \ , \tag{3.2}
$$

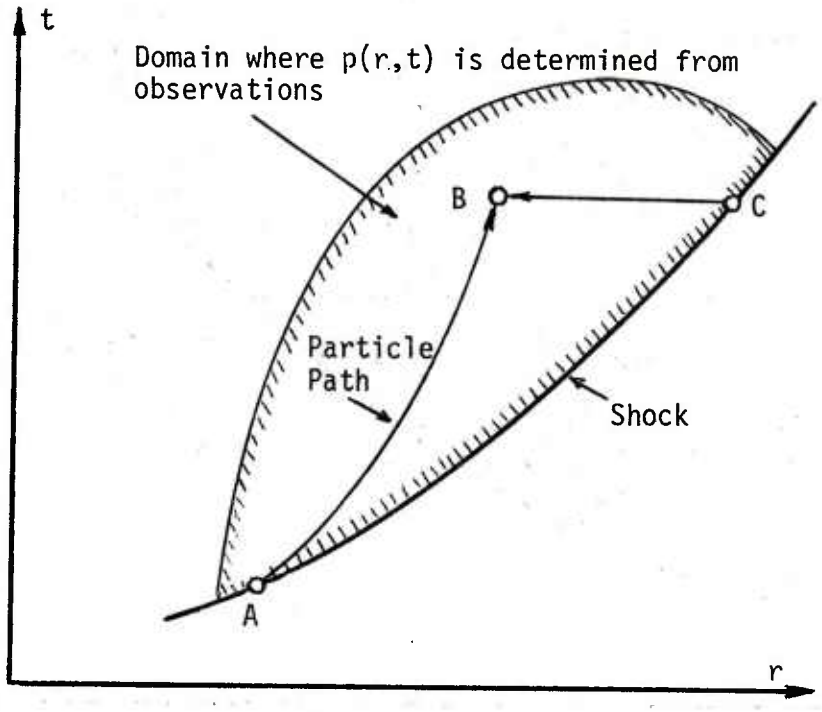

Figure 1. Integration Paths

The flow variables are obtained at the Point B by integration along the path line AB. The computed velocity is checked at B by an integration along the line CB.

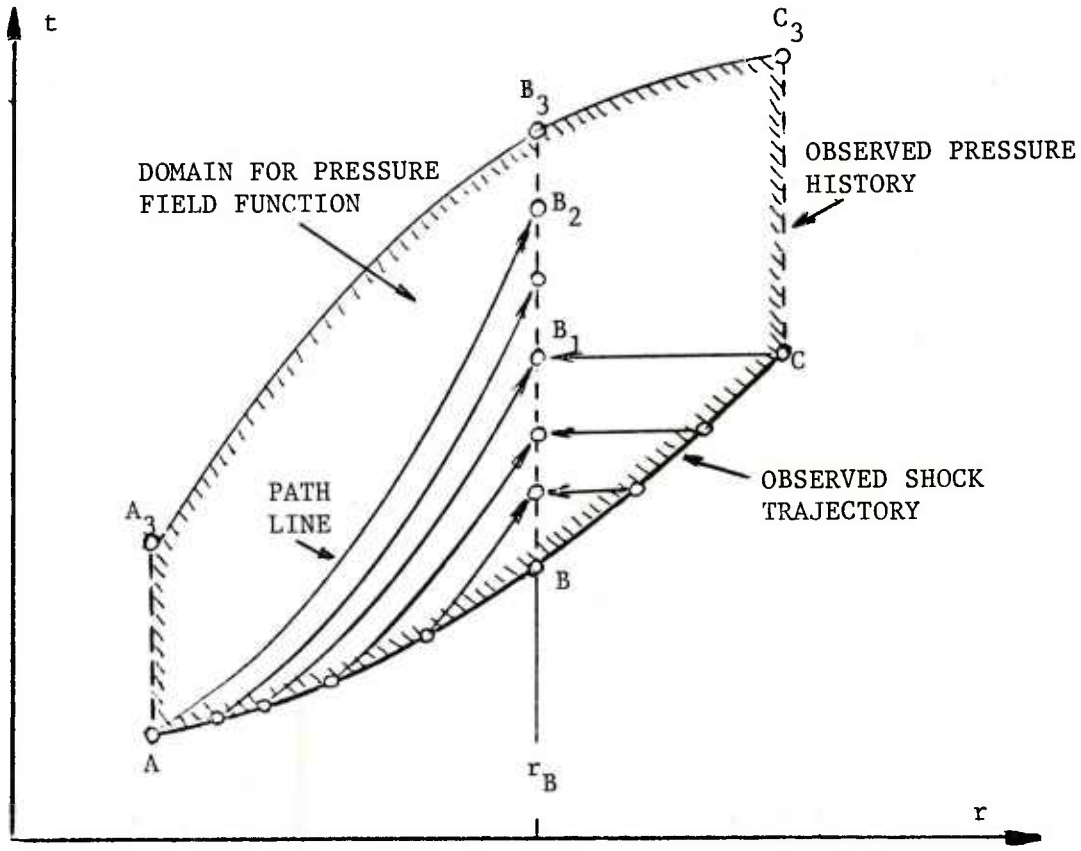

Figure 2. Computation of Flow History at a Given Distance

The pressure field function is determined within the indicated domain from pressure history measurements along the lines AA_3, BB_3, and CC_3, and from shock observations. For $r = r_B$, the flow history can be calculated between B and B_2, and test calculations can be carried out between B and B_1.

that describes the overpressure within a limited region behind the shock. This function will be handled in detail in Section 6. The pressure field function and the shock pressure function are related by

$$p_s(r;\theta) = p_f(r,t_s(r,\theta);\theta) \ . \tag{3.3}$$

The differential equations for the path line, Eqs. (2.10) and (2.11), are in terms of these functions:

$$\left.\begin{aligned} \frac{dr}{dt} &= u \ , \\ \frac{du}{dt} &= F(r,t;\theta) \ , \end{aligned}\right\} \tag{3.4}$$

where

$$\begin{aligned} F(r,t;\theta) &= -\frac{1}{\rho_A}\left(\frac{p_A}{p}\right)^{1/\gamma}\frac{\partial p}{\partial r} = \\ &= -\frac{1}{\rho_s(r_A;\theta)}\left(\frac{p_s(r_A;\theta)+p_o}{p_f(r,t;\theta)+p_o}\right)^{1/\gamma}\frac{\partial p_f(r,t;\theta)}{\partial r} \ , \end{aligned} \tag{3.5}$$

and p_o is the ambient pressure.

The numerical integration of the system (3.4) is done by the following fourth order algorithm:

$$\left.\begin{aligned} t_{k+1} &= t_k + \Delta t \ , \\ r_{k+1} &= r_k + \Delta t \cdot u_k + \Delta t^2\,\dot{u}_k/2 + \Delta t^3\,\ddot{u}_k/6 \ , \\ \hat{u}_{k+1} &= u_k + \Delta t \cdot (\dot{u}_k + \dot{u}_{k+1})/2 \ , \\ \hat{\ddot{u}}_{k+1} &= \frac{\partial}{\partial t}(\dot{u}_{k+1}) + \hat{u}_{k+1}\frac{\partial}{\partial r}(\dot{u}_{k+1}) \ , \\ u_{k+1} &= \hat{u}_{k+1} + \Delta t^2(\ddot{u}_k - \hat{\ddot{u}}_{k+1})/12 \ . \end{aligned}\right\} \tag{3.6}$$

The time derivatives $\dot{u}_k$ and $\ddot{u}_k$ are defined for this algorithm by

$$\left.\begin{aligned} \dot{u}_k &= F(r_k, t_k; \theta) \ , \\ \ddot{u}_k &= \frac{\partial}{\partial t}(\dot{u}_k) + u_k \cdot \frac{\partial}{\partial r}(\dot{u}_k) \ . \end{aligned}\right\} \tag{3.7}$$

The integration errors of the algorithm can be reduced to desired levels by monitoring the time steps Δt. However, the accuracy of the solution is also influenced by the accuracy of the pressure observations which are used to establish the pressure functions $p_f(r,t;\theta)$ and $p_s(r;\theta)$. This sets a limit on the achievable accuracy of any solution of Eq. (3.4).

The basis for the accuracy estimate is an estimate of the variances (or standard errors) of the overpressure observations, which we assume to be obtained by an analysis of the measurement process. The least squares model fitting routines[5] use the data variances to calculate an estimate of the variance-covariance matrix V_θ of the parameter vector θ. Using V_θ, estimates of standard errors of $p_f(r,t;\theta)$ and $p_s(r;\theta)$ can be obtained by applying the linearized law of variance propagation to the formulas for p_f and p_s, respectively. Thus, an estimate of the standard error e_p of p_f is

$$e_p = \left[\frac{\partial p_f}{\partial \theta} V_\theta \left(\frac{\partial p_f}{\partial \theta}\right)^T\right]^{1/2} , \tag{3.8}$$

where $\partial p_f/\partial\theta$ is the Jacobian matrix of the function $p_f(r,t;\theta)$. (The Jacobian matrix is a vector in this case because p_f is a scalar.)

In order to calculate an estimate of the standard error of the velocity u by a corresponding formula one needs to know the derivative vector $\partial u/\partial\theta$. Unlike $\partial p_f/\partial\theta$, that vector cannot be obtained by formal differentiation because u is not given by a formula but obtained by solving numerically the equation system (3.4). Therefore, we differentiate that system producing another system of differential equations where the unknown functions are the derivatives $\partial u/\partial\theta$ and $\partial r/\partial\theta$. The new system is

$$\left.\begin{aligned} \frac{d}{dt}\left(\frac{\partial r}{\partial \theta}\right) &= \frac{\partial u}{\partial \theta} \ , \\ \frac{d}{dt}\left(\frac{\partial u}{\partial \theta}\right) &= \frac{\partial F}{\partial \theta} + \frac{\partial F}{\partial r}\frac{\partial r}{\partial \theta} \ , \end{aligned}\right\} \tag{3.9}$$

where

---

[5] *Aivars Celmiņš, "A Manual for General Least Squares Model Fitting," USA ARRADCOM/Ballistic Research Laboratory Technical Report ARBRL-TR-02167, June 1979.* (AD #B040229L)

$$\frac{\partial F}{\partial \theta} + \frac{\partial F}{\partial r}\frac{\partial r}{\partial \theta} = F \cdot \left\{ - \frac{1}{\rho_A}\frac{\partial \rho_A}{\partial \theta} + \frac{1}{\gamma(p_A+p_o)}\frac{\partial p_A}{\partial \theta} - \frac{1}{\gamma(p_f+p_o)}\left[\frac{\partial p_f}{\partial \theta} + \frac{\partial p_f}{\partial r}\cdot\frac{\partial r}{\partial \theta}\right] + \right.$$

$$\left. + \frac{1}{\partial p_f/\partial r}\left[\frac{\partial^2 p_f}{\partial r \partial \theta} + \frac{\partial^2 p_f}{\partial r^2}\cdot\frac{\partial r}{\partial \theta}\right] \right. . \qquad (3.10)$$

Eqs. (3.9) are integrated numerically concurrently with the path line Eqs. (3.4), and using the same time steps Δt. For simplicity, and because high accuracy is not needed, we use a third-order scheme for the integration of Eqs. (3.9). The third-order scheme is obtained from the algorithm (3.6) by setting $\bar{u}_K$ and $\hat{u}_K$ equal to zero.

The initial values for the integration of Eqs. (3.9) are

$$\left(\frac{\partial r}{\partial \theta}\right)_{r=r_A} = 0 \quad ,$$

and (3.11)

$$\left(\frac{\partial u}{\partial \theta}\right)_{r=r_A} = \frac{\partial}{\partial \theta} u_s(r_A;\theta) \quad .$$

The derivatives $\partial r/\partial \theta$ are zero at the starting point of the path line because $r=r_A$ is a prescribed initial value.

The integration of Eq. (3.10) with the initial conditions (3.11) yields numerical values of the vectors $\partial u/\partial \theta$ and $\partial r/\partial \theta$ at any point along the path line. Of particular interest is the accuracy of the flow at the end point, where the line intersects with $r=r_B$. The end point itself has an uncertainty in the t-direction only that can be estimated by the linearized law of variance propagation, if the derivative $\partial t/\partial \theta$ is known. We obtain a formula for $\partial t/\partial \theta$ at the end point as follows. For a given path line the time value t_B at r_B is a function of the type

$$t_B = t_A + T(r_A, r_B) \quad . \qquad (3.12)$$

Its derivative with respect to θ is

$$\frac{\partial t_B}{\partial \theta} = \frac{\partial t_A}{\partial \theta} + \frac{\partial T}{\partial r_A}\left(\frac{\partial r}{\partial \theta}\right)_{r=r_A} + \frac{\partial T}{\partial r_B}\left(\frac{\partial r}{\partial \theta}\right)_{r=r_B}$$

or, because of Eq. (3.11),

$$\frac{\partial t_B}{\partial \theta} = \frac{\partial}{\partial \theta} t_s(r_A;\theta) + \frac{1}{u_B}\left(\frac{\partial r}{\partial \theta}\right)_{r=r_B} \quad . \qquad (3.13)$$

The derivatives $\partial\rho_B/\partial\theta$, that are needed for the estimation of the accuracy of ρ at the end point, can be calculated by a differentiation of Eq. (2.9):

$$\frac{\partial\rho_B}{\partial\theta} = \rho_B \cdot \left[\frac{1}{\rho_A}\frac{\partial\rho_A}{\partial\theta} - \frac{1}{\gamma(p_A+p_o)}\frac{\partial p_A}{\partial\theta} + \frac{1}{\gamma(p_B+p_o)}\frac{\partial p_B}{\partial\theta}\right] \quad . \tag{3.14}$$

where

$$\frac{\partial\rho_A}{\partial\theta} = \frac{\partial}{\partial\theta}\rho_s(r_A;\theta) \quad , \tag{3.15}$$

$$\frac{\partial p_A}{\partial\theta} = \frac{\partial}{\partial\theta} p_s(r_A;\theta) \tag{3.15}$$

and

$$\frac{\partial p_B}{\partial\theta} = \frac{\partial}{\partial\theta} p_f(r_B,t_B;\theta) + \frac{\partial}{\partial t}\left[p_f(r_B,t_B;\theta)\right]\frac{\partial t_B}{\partial\theta} \quad . \tag{3.16}$$

The flow at the end point of the path line, i.e., at its intersection with the line $r=r_B$ is defined by the four component vector

$$H = (t_B,\ p_B,\ u_B,\ \rho_B)^T. \tag{3.17}$$

The accuracy of the vector can be characterized by a variance-covariance matrix V_H of the components of H, that can be calculated from V_θ by the formula

$$V_H = \frac{\partial H}{\partial\theta} V_\theta \left(\frac{\partial H}{\partial\theta}\right)^T . \tag{3.18}$$

V_H estimates the uncertainties of the flow field that are caused by measurement inaccuracies. The elements of the Jacobian matrix $\partial H/\partial\phi$ in (3.18) are given by the solution of the equation system (3.11) and the formulas (3.13), (3.14), and (3.16), respectively.

4. DETERMINATION OF SHOCK FUNCTIONS BY MODEL FITTING

In order to compute the complete blast field by the method described in previous sections, one needs the pressure field function $p_f(r,t;\theta)$ within the region of interest. We determine that function by a model fitting to pressure

observations, most of which consist of overpressure history recordings at diverse stations. The initial value of most overpressure history recordings is the incident shock overpressure. From the viewpoint of data handling, it is advantageous to use these initial values separately from the rest of pressure data for a determination of the shock functions (3.1). Then one can obtain a shock description that is accurate within a large distance range and use the same shock functions for different field fittings, as will be described in the next sections. Also, in a separate shock fitting one can easily make use of incomplete records from which either the pressure observation or the shock arrival time observation is missing. (Incomplete records do occur occasionally in blast field experiments.) The use of all available data makes the shock functions less sensitive to individual observational inaccuracies. Since the shock functions also can be approximated very accurately by simple expressions, a separate shock fitting is more practical than a concurrent determination of shock and field functions. Details of the shock fitting algorithm will be given in this section. The complementary pressure field fitting will be described in Sections 5 and 6.

The medium into which the shock propagates is assumed to be an ideal gas, characterized by its molar mass M and the ratio γ of its specific heats. We describe the initial state of the gas by its pressure p_o and temperature T_o. The corresponding initial density is

$$\rho_o = \frac{p_o}{T_o} \cdot \frac{M}{R_g} \tag{4.1}$$

where $R_g = 8.31434$ J/(mole·K) is the universal gas constant. The sound speed in the ambient gas is

$$c_o = \sqrt{\gamma p_o/\rho_o} = \sqrt{\gamma T_o R_g/M} \quad . \tag{4.2}$$

Let p_s be the incident shock overpressure. Then the shock velocity, particle velocity and density behind the shock are given in terms of p_s by the following set of formulas[4].

Shock velocity:

$$U = c_o \left(1 + \frac{\gamma+1}{2\gamma} \frac{p_s}{p_o}\right)^{1/2} = \left[\frac{\gamma+1}{2} \frac{p_s}{\rho_o} \left(1 + \frac{2\gamma}{\gamma+1} \frac{p_o}{p_s}\right)\right]^{1/2} . \tag{4.3}$$

Particle velocity behind the stock:

$$u_s = \frac{1}{U} \frac{p_s}{\rho_o} = \frac{c_o^2}{U} \frac{1}{\gamma} \frac{p_s}{p_o} = \frac{2}{\gamma+1} U \left(1 + \frac{2\gamma}{\gamma+1} \frac{p_o}{p_s}\right)^{-1} . \tag{4.4}$$

[4] *Ibid. p. 200 ff.*

Density behind the shock:

$$\rho_s = \rho_o \left(1 + \frac{\gamma+1}{2\gamma} \frac{p_s}{p_o}\right)\left(1 + \frac{\gamma-1}{2\gamma} \frac{p_s}{p_o}\right)^{-1}$$

$$= \rho_o \frac{\gamma+1}{\gamma-1} \left(1 + \frac{2\gamma}{\gamma+1} \frac{p_o}{p_s}\right)\left(1 + \frac{2\gamma}{\gamma-1} \frac{p_o}{p_s}\right)^{-1}. \qquad (4.5)$$

The shock arrival time $t_s(r)$ at a distance r from the center of the explosion and the shock velocity U are related by

$$t_s(r) = t_1 + \int_{r_1}^{r} \frac{dr}{U(r)} \quad . \qquad (4.6)$$

For the numerical treatment of shock data we choose a rational function of r as an approximation of the shock overpressure function $p_s(r)$. The rational function has three parameters and an asymptotic behavior for small and large r as predicted by blast theory. The function is

$$p_s(r;a,b,c) = a/r + b/r^2 + c/r^3 \quad . \qquad (4.7)$$

The corresponding shock arrival time function $t_s(r)$ is obtained by substituting the expression (4.7) into the shock velocity formula (4.3) and the resulting function into the integral (4.6). The final result is

$$t_s(r;a,b,c,d) = d + \int_{r_1}^{r} \frac{dx}{c_o \sqrt{1 + \frac{\gamma+1}{2\gamma p_o}(a/x + b/x^2 + c/x^3)}} \quad . \qquad (4.8)$$

The integral in Eq. (4.8) must be evaluated numerically, and the evaluation provides the shock arrival time t_s at any given distance r. (In the computer programs for shock fitting, the quadrature is done by a Romberg algorithm.) The lower limit r_1 of the integral in Eq. (4.8) can be chosen arbitrarily, e.g., it may be set equal to the smallest observed distance. Once r_1 is fixed, then both model functions, $p_s(r)$ and $t_s(r)$, are completely determined by the four components of the model parameter vector $\theta = (a,b,c,d)^T$.

Appropriate values of the four parameters were found by a least squares data fitting that uses the shock observations as data. Each shock observation

is a three component vector (P_s, T_s, R_s), i.e., the observed shock overpressure, arrival time, and distance. The model constraints for the observations are Eqs. (4.7) and (4.8). They may be formulated as the equation system

$$\left.\begin{aligned} f_1(P_s,T_s,R_s;\theta) &= P_s - p_s(R_s;\theta) = 0 , \\ f_2(P_s,T_s,R_s;\theta) &= T_s - t_s(R_s;\theta) = 0 \end{aligned}\right\} \qquad (4.9)$$

or in some other equivalent form consisting of two simultaneous equations for each three-component vector of observations. Problems of this type can be solved numerically with the aid of the utility program COLSMU[5], that was also used in the present task. The program is sufficiently flexible to accommodate observation sets from which either the pressure or the time observation is missing. (The constraint for such an incomplete set consists of only one of the two equations (4.9).)

The first constraint in Eq. (4.9) was formulated for the model fitting task as follows:

$$f_1(p,t,r;\ a,b,c,d) = r^3p - r^2a - rb - c = 0 . \qquad (4.10)$$

The first order derivatives of f_1 are

$$\partial f_1/\partial(p,t,r) = (r^3,\ 0,\ 3r^2p - 2ar - b) \qquad (4.11)$$

and

$$\partial f_1/\partial(a,b,c,d) = (-r^2,\ -r,\ -1,\ 0) . \qquad (4.12)$$

The non-zero second order derivatives of f_1 are

$$\left.\begin{aligned} \partial^2 f_1/\partial r^2 &= 6rp - 2a , \\ \partial^2 f_1/(\partial r\partial p) &= 3r^2 , \\ \partial^2 f_1/(\partial r\partial a) &= -2r , \\ \partial^2 f_1/(\partial r\partial b) &= -1 . \end{aligned}\right\} \qquad (4.13)$$

[5] *Ibid.*

The second constraint in Eq. (4.9) was used in the model fitting task in the following form

$$f_2(p,t,r;\ a,b,c,d) = \int_{r_1}^{r} \frac{dx}{\sqrt{1 + \Gamma\cdot(a/x+b/x^2+c/x^3)}} + (d-t)c_o = 0 \ , \qquad (4.14)$$

where

$$\Gamma = (\gamma + 1)/(2\gamma p_o) \ . \qquad (4.15)$$

Let

$$Q(x) = \sqrt{1 + \Gamma \cdot(a/x + b/x^2 + c/x^3)} \ . \qquad (4.16)$$

Then the first order derivatives of the model function f_2 are

$$\partial f_2/\partial(p,t,r) = (0,\ -c_o,\ 1/Q(r)) \qquad (4.17)$$

and

$$\frac{\partial f_2}{\partial(a,b,c,d)} = \left(-\frac{\Gamma}{2} \int_{r_1}^{r} \frac{dx}{xQ^3} \ , \ -\frac{\Gamma}{2} \int_{r_1}^{r} \frac{dx}{x^2Q^3} \ , \ -\frac{\Gamma}{2} \int_{r_1}^{r} \frac{dx}{x^3Q^3} \ , \ c_o \right) \qquad (4.18)$$

The non-zero second order derivatives of f_2 are

$$\partial^2 f_2/\partial r^2 = \frac{1}{2}\ \Gamma\cdot(a+2b/r+3c/r^2)/(r^2Q^3(r)) \ , \qquad (4.19)$$

$$\left.\begin{aligned} \partial^2 f_2/(\partial r\partial a) &= -\frac{1}{2}\ \Gamma/(rQ^3(r)) \ , \\ \partial^2 f_2/(\partial r\partial b) &= -\frac{1}{2}\ \Gamma/(r^2Q^3(r)) \ , \\ \partial^2 f_2/(\partial r\partial c) &= -\frac{1}{2}\ \Gamma/(r^3Q^3(r)) \ , \end{aligned}\right\} \qquad (4.20)$$

$$\left.\begin{aligned}
\partial^2 f_2/\partial a^2 &= \tfrac{3}{4}\,\Gamma^2 \int dx/(x^2 Q^5(x)) \ , \\
\partial^2 f_2/(\partial a \partial b) &= \tfrac{3}{4}\,\Gamma^2 \int dx/(x^3 Q^5(x)) \ , \\
\partial^2 f_2/(\partial a \partial c) &= \tfrac{3}{4}\,\Gamma^2 \int dx/(x^4 Q^5(x)) \ , \\
\partial^2 f_2/\partial b^2 &= \partial^2 f_2/(\partial a \partial c) \ , \\
\partial^2 f_2/(\partial b \partial c) &= \tfrac{3}{4}\,\Gamma^2 \int dx/(x^5 Q^5(x)) \ , \\
\partial^2 f_2/\partial c^2 &= \tfrac{3}{4}\,\Gamma^2 \int dx/(x^6 Q^5(x)) \ .
\end{aligned}\right\} \qquad (4.21)$$

The limits of the integrals in Eq. (4.21) are the same as in the constraint Eq. (4.14). All integrals are evaluated numerically by Romberg algorithms.

5. ANALYSIS OF PRESSURE HISTORIES

The data for a determination of the pressure field function consist of a number of pressure histories observed at various locations within an area of interest. Before determining a field function $p_f(r,t)$ that describes the pressure p as a function of r and t within the whole area, we find functions $p_h(t)$ that fit the observed individual pressure histories. The purpose of the fitting of the individual histories is to obtain trends of the histories for increasing distance from the explosion. These trends are needed to construct the pressure field function $p_f(r,t)$, as will be described in the next section.

The model function chosen to fit the individual overpressure histories is

$$p_h(t;\ A,B,C) = (p_s - C)\cdot \exp\left\{A(t-t_s) + B(t-t_s)^2\right\} + C \ , \qquad (5.1)$$

where A, B, and C are model parameters, p_s is the shock overpressure, and t_s is the shock arrival time. The values of p_s and t_s depend on the location of the pressure gage, i.e., on the distance r. They are calculated using the formulas (4.7) and (4.8).

The data consist of two-component vectors (p,t) giving the overpressure p for various time values t. The model fitting problem can be solved numerically by the utility routine COLSAC[5]. The resulting parameters A, B, and C are valid only for the particular history used as input, and they have no general physical significance.

---

[5] *Ibid.*

The constraint function for the model fitting of history data was formulated as follows

$$f(p,t;\ A,B,C) = (P_s - C)\cdot \exp\left(A\cdot(t-t_s) + B\cdot(t-t_s)^2\right) + C - p\ . \tag{5.2}$$

Let

$$E = \exp\left(A\cdot(t-t_s) + B\cdot(t-t_s)^2\right)\ . \tag{5.3}$$

Then the first order derivatives of the constraint function (5.2) are

$$\partial f/\partial(p,t) = \left(-1,\ \left(A + 2B(t_s-t)\right)\cdot(p_s-C)\cdot E\right) \tag{5.4}$$

and

$$\partial f/\partial(A,B,C) = \left((t-t_s)(p_s-C)E,\ (t-t_s)^2(p_s-C)E,\ -E+1\right)\ . \tag{5.5}$$

The non-zero second order derivatives are

$$\left.\begin{aligned}
\partial^2 f/\partial t^2 &= \left[(A + 2B(t-t_s))^2 + 2B\right](p_s-C)E\ , \\
\partial^2 f/\partial A^2 &= (t-t_s)^2(p_s-C)E\ , \\
\partial^2 f/(\partial A\partial B) &= (t-t_s)^3(p_s-C)E\ , \\
\partial^2 f/(\partial A\partial C) &= -(t-t_s)E\ , \\
\partial^2 f/\partial B^2 &= (t-t_s)^4(p_s-C)E\ , \\
\partial^2 f/(\partial B\partial C) &= -(t-t_s)^2E\ ,
\end{aligned}\right\} \tag{5.6, 5.7}$$

$$\left.\begin{aligned} \partial^2 f/(\partial t \partial A) &= \left[1 + \Big(A + 2B(t-t_s)\Big)(t-t_s)\right](p_s - C)E \ , \\ \partial^2 f/(\partial t \partial B) &= \left[2 + \Big(A + 2B(t-t_s)\Big)(t-t_s)\right](t-t_s)(p_s - C)E \ , \\ \partial^2 f/(\partial t \partial C) &= -\Big(A + 2B(t-t_s)\Big)E \ . \end{aligned}\right\} \quad (5.8)$$

After the values of the parameters A, B, and C are obtained for all histories within the area of interest, their trends as functions of the distance r are analyzed. The analysis consists of finding for each parameter a power function of r as an approximation. Let, for example, A_i be the value of the parameter A obtained from a history fitting at the distance r_i. Then one can determine a function $\bar{A}r^{n_A}$ that approximates the data sets $(|A_i|, r_i)$. The function is determined by minimizing an object function W, that is defined as follows

$$W = \sum_i (\ln|A_i| - \ln|\bar{A}| - n_A \ln r_i)^2 A_i^2 \ . \quad (5.9)$$

The solution of the minimization problem is given by the formulas

$$D = \sum_i A_i^2 \sum_i (A_i \ln r_i)^2 - \left[\sum_i A_i^2 \ln r_i\right]^2 \ , \quad (5.10)$$

$$|\bar{A}| = \left[\sum_i (A_i^2 \ln|A_i|) \sum_i (A_i \ln r_i)^2 - \sum_i (A_i^2 \ln|A_i| \ \ln r_i) \sum_i (A_i^2 \ln r_i)\right] \Big/ D \ , \quad (5.11)$$

$$n_A = \left[\sum_i A_i^2 \sum_i (A_i^2 \ln|A_i| \ln r_i) - \sum_i (A_i^2 \ln r_i) \sum_i (A_i^2 \ln|A_i|)\right] \Big/ D \ . \quad (5.12)$$

The sign of $\bar{A}$ is set equal to the sign of that parameter A_i which corresponds to the smallest distance r_i.

Trends of the parameters B and C are calculated by identical formulas that yield the values of $\bar{B}$, n_B, $\bar{C}$, and n_C, respectively. The exponents n_A, n_B, and n_C, are used for the construction of the pressure field function $p_f(r,t)$, as described in the next section. The values of $\bar{A}$, $\bar{B}$, and $\bar{C}$ are used as initial approximations of certain parameters of that function.

Numerical experiments with different data sets have shown that the exponents n_A, n_B, and n_C need not be determined very accurately. Equally good approximations of pressure data can be obtained using field functions with exponents that vary within relatively large ranges. The exponents have no physical significance, because the parameters A_i, B_i, and C_i depend, not only on the distance r_i, but also on various other factors such as the duration of the observed history, its noise level, the number and distribution of the observations, etc.

6. DETERMINATION OF PRESSURE FIELD FUNCTIONS BY MODEL FITTING

A pressure field function describes the overpressure in the blast field as a function of the distance r and the time t. The function is obtained by data fitting of pressure observations and it is, therefore, a valid approximation to the actual pressure field only within the limited region from which the data are selected. In an analysis of a given event, one may use several pressure field functions, each representing the pressure in a different region.

In the present problem, we have used the following five parameter model function as a representation of the overpressure field:

$$p_f(r,t;A_1,A_2,B_1,B_2,C_1) = \left[p_s(r)-C(r;C_1)\right] \exp\left(Q(r,t;A_1,A_2,B_1,B_2)\right)+C(r;C_1) \quad , \tag{6.1}$$

where

$$Q = \left[t-t_s(r)\right](A_1+A_2 r)\cdot r^{n_A}+\left[t-t_s(r)\right]^2(B_1+B_2 r)\cdot r^{n_B} \tag{6.2}$$

and

$$C = C_1 \cdot r^{n_C} \quad . \tag{6.3}$$

The functions $p_s(r)$ and $t_s(r)$ are the shock overpressure and shock arrival time functions, respectively. Both are determined by shock fitting (Section 4). The exponents n_A, n_B, and n_C are assumed to be known from an analysis of the trends of individual history fittings, as described in Section 5. The remaining five parameters, A_1, A_2, B_1, B_2, and C_1 are determined by model fitting to overpressure observations within regions of interest.

The data for the determination of the model parameters are the observed overpressure, time, and distance, i.e., the data are three component vectors (p,t,r). The constraint function is used for the data fitting in the following formulation:

$$f(p,t,r;A_1,A_2,B_1,B_2,C_1) = (p_s-C)e^Q + C-p \quad , \tag{6.4}$$

where Q and C are defined by Eqs. (6.2) and (6.3), respectively. The constraint equations are scalar and, therefore, the model fitting problem can be solved numerically by the utility routine COLSAC[5] for standard least squares problems.

The first and second order derivatives of the constraint function f can be conveniently expressed by the following formalism. Let x and y be any two of the eight arguments of f, and let derivatives with respect to x and y be denoted by corresponding subscripts. Then

$$f_x = e^Q\left[(p_s-C)\ Q_x + (p_s-C)_x\right] - (p-C)_x \quad , \tag{6.5}$$

and

$$f_{xy} = e^Q\left[(p_s-C)(Q_{xy}+Q_xQ_y)+(p_s-C)_xQ_y+(p_s-C)_yQ_x+(p_s-C)_{xy}\right]-(p-C)_{xy} \ . \tag{6.6}$$

The derivatives of Q, $p_s(r)$, p and $C(r;C_1)$ can be easily computed.

The pressure field fitting provides an optimal set of the field parameters A_1, A_2, B_1, B_2, and C_1, and their estimated variances and covariances. The overpressure p_f, computed with the formula (6.1), depends, however, also on the four shock parameters a, b, c, and d through the shock functions $p_s(r)$ and $t_s(r)$. Therefore, when one estimates the accuracy of p_f, one has to take into account the variances and covariances of all nine parameters, namely, the four shock parameters and the five field parameters. Let θ be the vector of all nine parameters and let V_θ be the corresponding variance-covariance matrix of the components of θ. Then an estimate of the variance of p_f is the square of Eq. (3.8), viz.,

$$v_p = \left(\frac{\partial p_f}{\partial \theta}\ V_\theta\ \frac{\partial p_f}{\partial \theta}\right)^T \ . \tag{6.7}$$

The matrix V_θ was composed as follows from the estimated variance-covariance matrix V_{shock} of the shock parameters, and from the corresponding matrix V_{field} of the field parameters:

$$V_\theta = \begin{pmatrix} V_{shock} & 0 \\ 0 & V_{field} \end{pmatrix} \ . \tag{6.8}$$

In the matrix (6.8), correlations between shock parameters and field parameters have been neglected. In reality correlations between both parameter groups

[5] *Ibid.*

exist, because the shock fitting results were used to obtain the field parameters. The neglect of the correlations most likely results in an overestimate of the pressure variance.

The reason for the neglect of the correlations is programming expediency. The correlation could be obtained, e.g., by a joint adjustment of all data (shock data and pressure history data) using the utility program COLSMU[5]. However, this would require an unacceptable investment in programming because of the heterogeneity of the data and constraints. Also, algorithmic difficulties can be expected for this problem, because of the nonlinearities involved, requiring additional effort for their resolution.

7. A THEORETICAL TEST EXAMPLE

The blast field computation method was tested on two examples: on a theoretical strong shock flow field and on real measurements. The former test is described in this section.

The theoretical flow field was obtained by using the computer programs described in Reference 6. The programs are based on self-similar solutions of flow equations[7,8] that approximate the flow of strong blasts. The theory of the approximation is limited to blasts in ideal gas that are generated by point explosions, and for which the ambient pressure is negligible compared to the incident shock pressure. The latter assumption makes the numerical results of the theory ambiguous, because the theoretically computed pressure can be interpreted either as overpressure or as pressure. In our test example, we chose the latter interpretation. Consequently, the overpressure "observations" for the example were obtained by subtracting the ambient pressure from the theoretical pressure values which were supplied by the strong blast computer programs.

The explosion in the test example was assumed to be generated by the release of $209.2 \cdot 10^{12}$ J of energy (equivalent to a 50 kton TNT explosion). Table 1 gives the ambient ideal gas specification and the assumed locations and durations of overpressure observations. The example was chosen such that the strong blast assumption was satisfied reasonably well. (The pressure ratio ranges from 190 at the beginning of the 120 m history reading to 60 at the beginning of the 170 m history.) The locations of the history readings in the r,t-plane are shown in Figure 3 and the assumed data accuracies are listed in Table 2.

---

[5] *Ibid.*

[6] *Aivars Celmiņš, "Strong Blast Wave Computer Programs," USA ARRADCOM/Ballistic Research Laboratory Technical Report ARBRL-TR-02264, September 1980.* (AD #A092346)

[7] *L.I. Sedov, "Similarity and Dimensional Methods in Mechanics," Academic Press, NY, 1959.*

[8] *O. Laporte and T.S. Chang, "Curved Characteristics Behind Strong Blast Waves," Physics of Fluids, 15, pp. 502-504, 1972.*

TABLE 1. PARAMETERS OF THE THEORETICAL TEST EXAMPLE

Explosion

E = 209.2 TJ

Ambient Gas

Molar mass M = 28.96 g/mole

Specific heat ratio γ = 1.40

Temperature T = 293 K

Pressure p_o = 101.325 kPa

Range of Shock Observations

90-170 m

History Observations

Distances	Times
120 m	11.0 - 15.0 ms
130 m	13.4 - 17.9 ms
140 m	16.2 - 21.5 ms
150 m	19.2 - 27.2 ms
160 m	22.6 - 29.6 ms
170 m	26.3 - 32.0 ms

TABLE 2. ASSUMED ACCURACY OF THE THEORETICAL DATA

Time: $\pm$ 0.1 ms

Pressure: $\pm$ 5%

Distance: $\pm$ 0.1 m

Elevation: $\pm$ 0.01 m

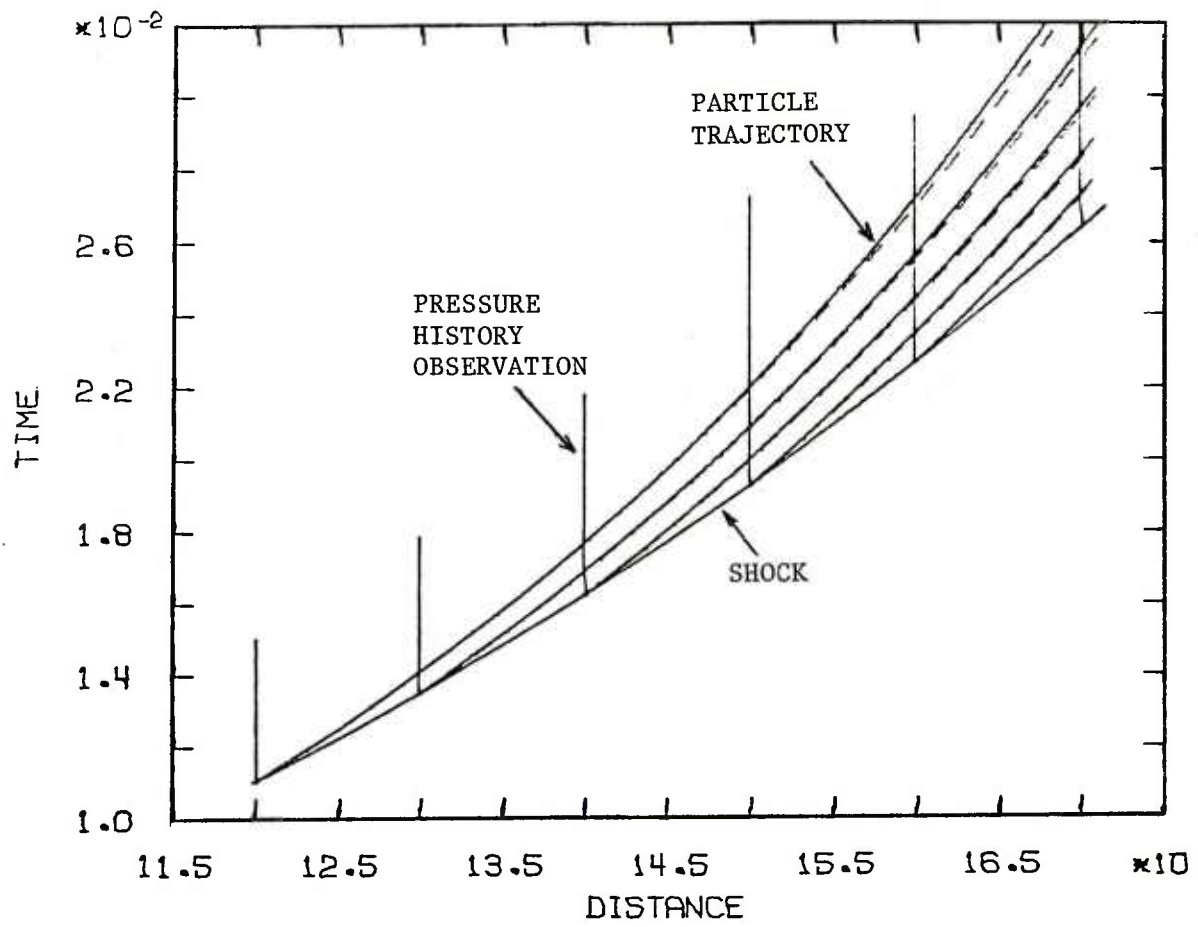

Figure 3. Location of History Observations in Theoretical Test Example

calculated particle trajectories

theoretical particle trajectories

The leftmost particle trajectory limits the region where the complete flow field can be computed.

Distances are expressed in meters and times are expressed in seconds.

Shock arrival times and pressures were assumed to be observed between 90 m and 170 m at 2.67 m intervals. In order to test the program's capability to handle incomplete data sets, it was assumed that from some sets either the pressure or the time observation was missing. Figures 4, 5, and 6 show the shock data and the fitting curves with their three standard error confidence limits. The least squares values of the shock fitting parameters are given in Table 3.

The figures show that the confidence intervals for the fitted curves become very large outside the range of observations. The rapid increase is caused by the redundancy of the parameters a and b, which is manifested also by their large standard errors and the close correlations between the three parameters a, b, and c. (See Table 3.) The reason for the redundancy is the fact that the theoretical shock pressure formula for the strong shock is $p = c/r^3$. One can expect that the increase of the confidence intervals will be less pronounced in cases where the observations are not restricted to either the strong shock regime or to the weak shock regime ($p \approx a/r$).

The next step towards the flow field determination is a fitting of individual pressure histories, as described in Section 5. Figures 7 and 8 show two samples of the results of the fitting.

Each history fitting provides values of three parameters, A, B, and C, which determine the model function (5.1). Figure 9 shows log-log plots of the three parameters versus the distances at which the history recordings were made. The field fitting program calculated trends of the parameters by fitting a power of the distance to the curves shown in Figure 9. The exponents were calculated using Eq. (5.12) and the following results were obtained:

$$n_A = -2.3 ,$$

$$n_B = -4.5 ,$$

$$n_C = -2.9 .$$

The corresponding five parameter overpressure field function is

$$p_f = (p_s(r) - C_1/r^{2.9})\, e^Q + C_1/r^{2.9} \qquad (7.1)$$

with

$$Q = (t-t_s(r))(A_1+A_2 r)/r^{2.3} + (t-t_s(r))^2\,(B_1+B_2 r)/r^{4.5} , \qquad (7.2)$$

where $p_s(r)$ and $t_s(r)$ are the shock overpressure and arrival time, respectively. The numerical results of the pressure field fitting are listed in Table 4. The large parameter error estimates and close correlations between parameters again indicate that probably some of the parameters are redundant for this example.

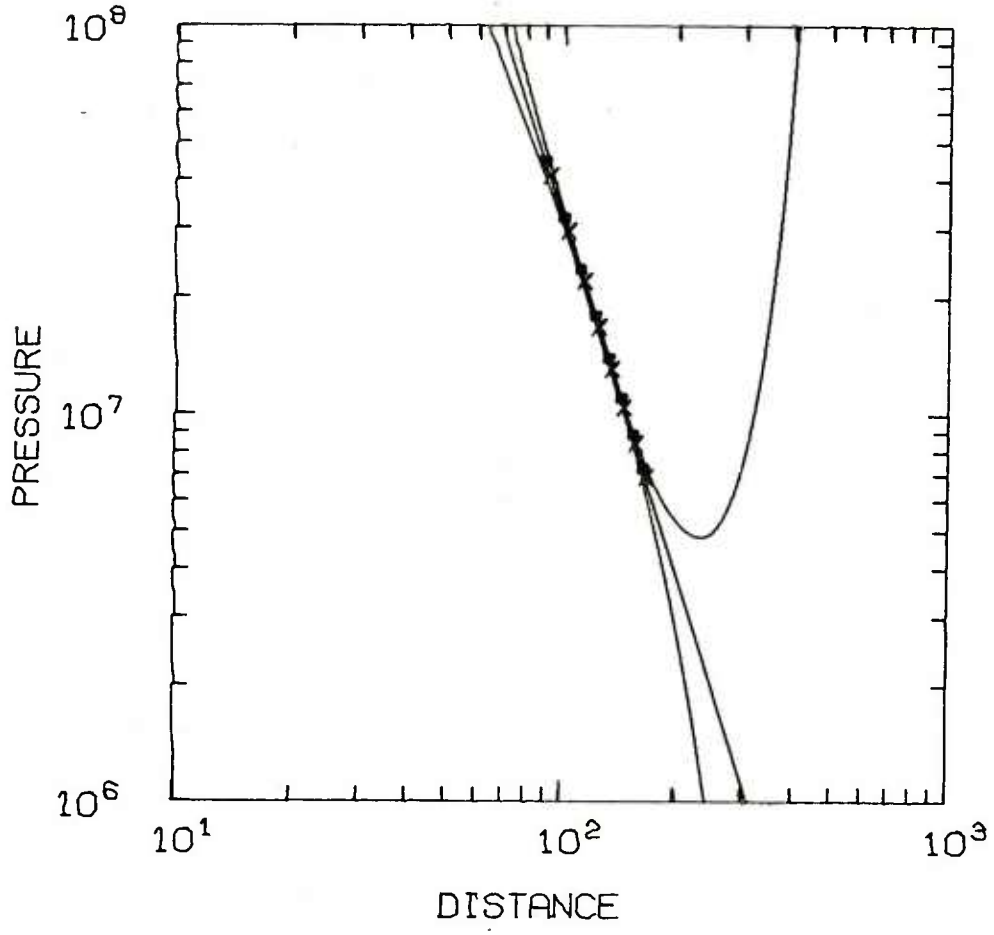

Figure 4. Shock Overpressure vs. Distance in Theoretical Test Example

• Complete observation set
X Set with missing time observation

Distance is expressed in meters and pressure is expressed in pascals.

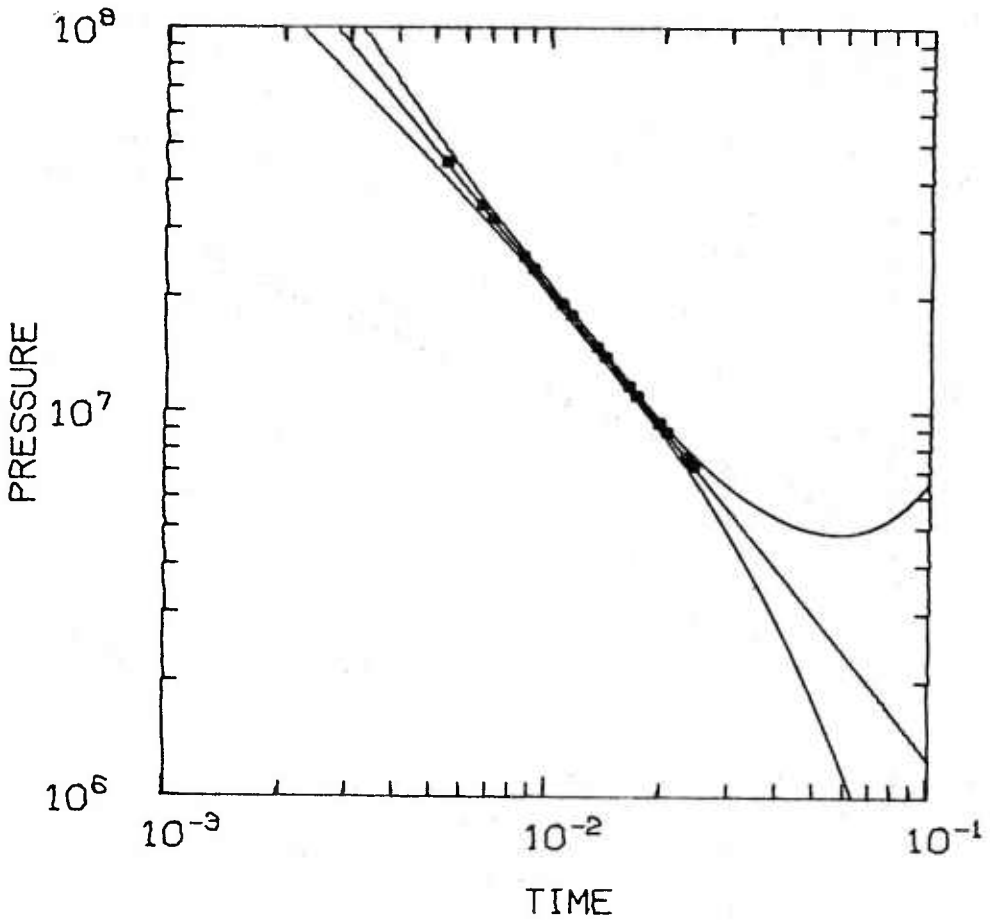

Figure 5. Shock Overpressure vs. Time in Theoretical Test Example

Time is expressed in seconds and pressure is expressed in pascals.

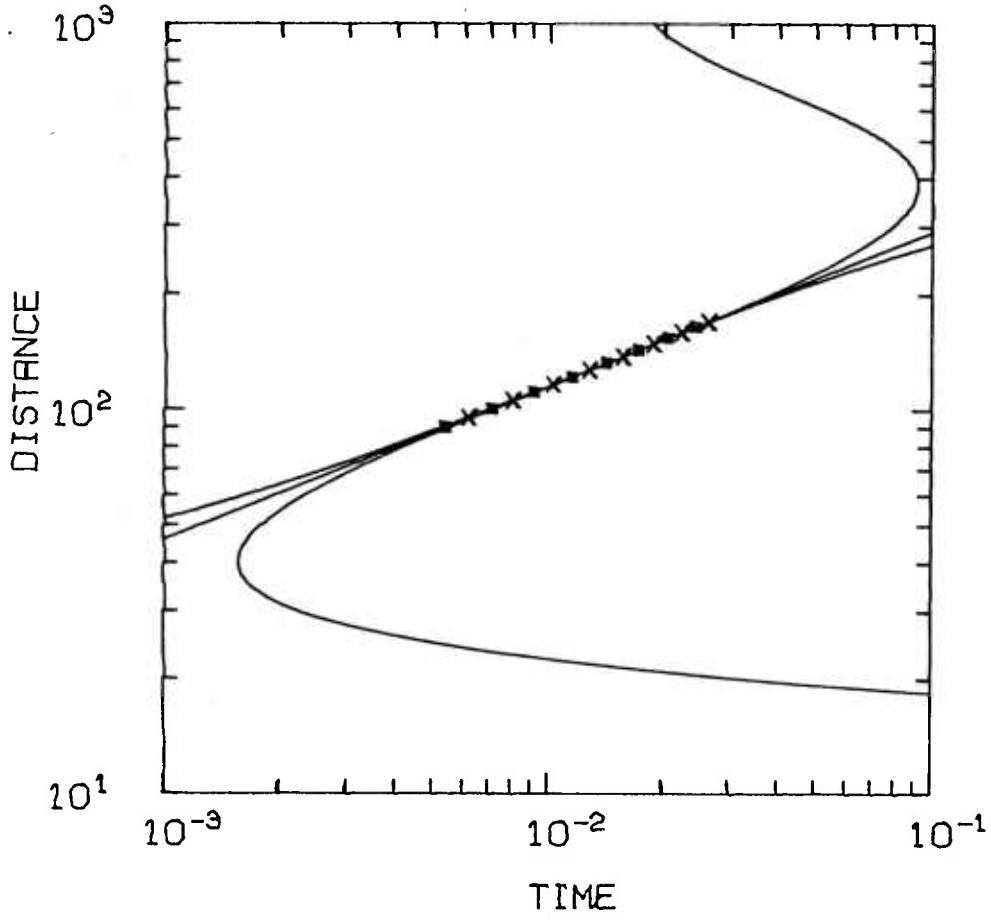

Figure 6. Shock Distance vs. Time in Theoretical Test Example

■ Complete observation set
X Set with missing pressure observation

Time is expressed in seconds and distance is expressed in meters.

TABLE 3. SHOCK PARAMETERS OF THEORETICAL EXAMPLE

The model is given by Eqs. (4.7) and (4.8). The range of fitting is 90 m through 170 m.

Parameters and Standard Errors

$$a = (-26.3 \pm 659.6)\cdot 10^{6} \text{ Pa}\cdot\text{m}$$

$$b = (\ 1.13 \pm 171.5)\cdot 10^{9} \text{ Pa}\cdot\text{m}^2$$

$$c = (32.81 \pm 10.94)\cdot 10^{12} \text{ Pa}\cdot\text{m}^3$$

$$d = (5.380 \pm 0.044) \text{ ms} = \text{arrival at } 90.0 \text{ m}$$

The standard error of weight one, $m_o = 0.01674$, is not included in the standard errors of the parameters.

Correlation Matrix of the Parameters

$$\begin{pmatrix} 1.0 & -0.99682773 & 0.98588603 & 0.04936359 \\ -0.99682773 & 1.0 & -0.99598531 & -0.08560247 \\ 0.98588603 & -0.99598531 & 1.0 & 0.13819642 \\ 0.04936359 & -0.08560247 & 0.13819642 & 1.0 \end{pmatrix}$$

NOTE: The standard error of weight one, m_o, depends on the scatter of data as well as on systematic differences between the model and measurement. For this example the data scatter is zero, because theoretical flow values were used as data. Therefore, the listed m_o characterizes only the systematic difference between the pressure model and the strong blast pressure. Because this difference is small, the value of m_o is also small. The listed standard errors of the parameters are estimates of the parameter inaccuracies that would be caused by data scatter (standard errors) as specified in Table 2.

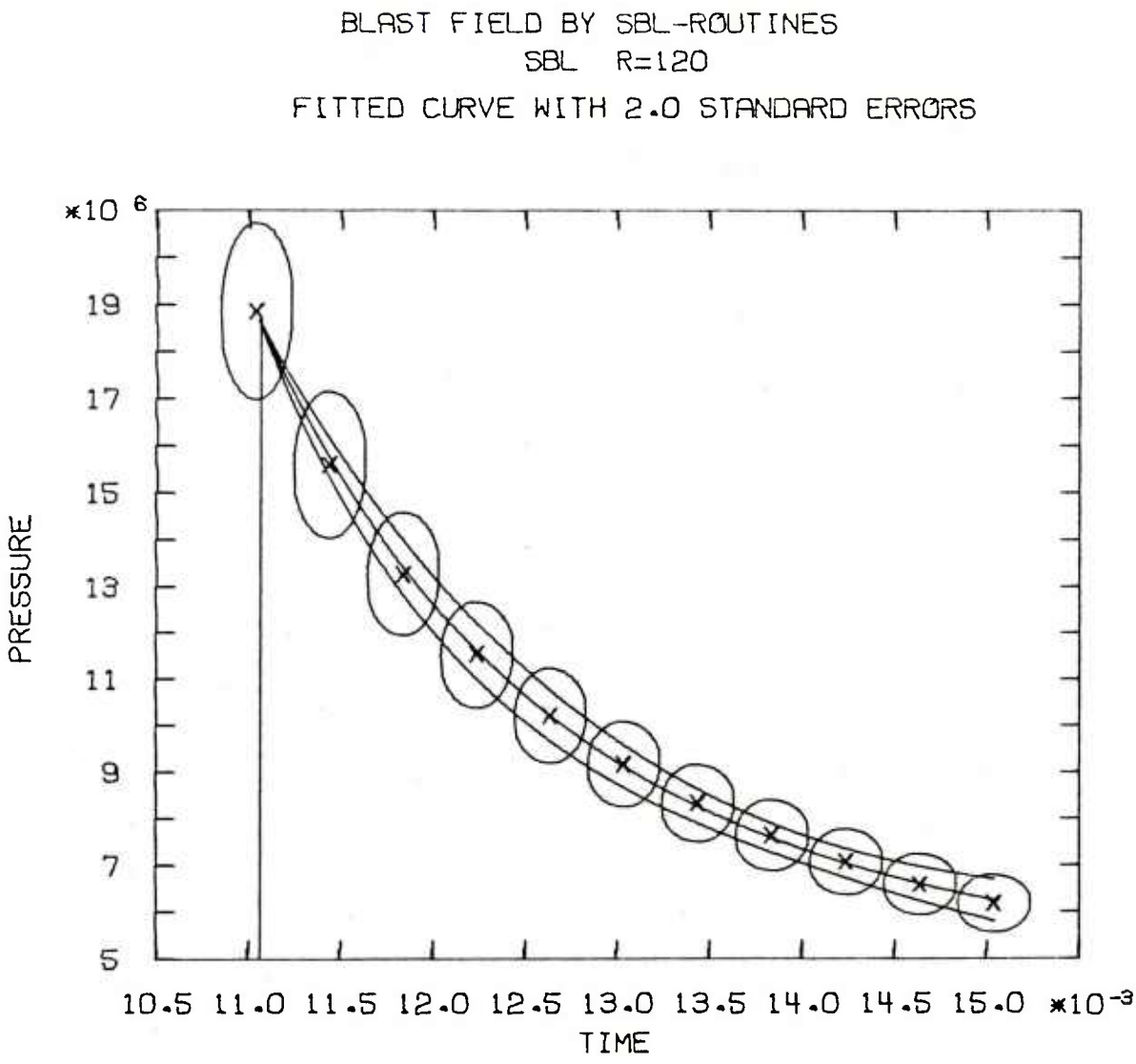

Figure 7. Fitting of Pressure at 120 m in Theoretical Test Example

(The data accuracy is indicated by a two standard error ellipse around each observed point.)

Time is expressed in seconds and pressure is expressed in pascals.

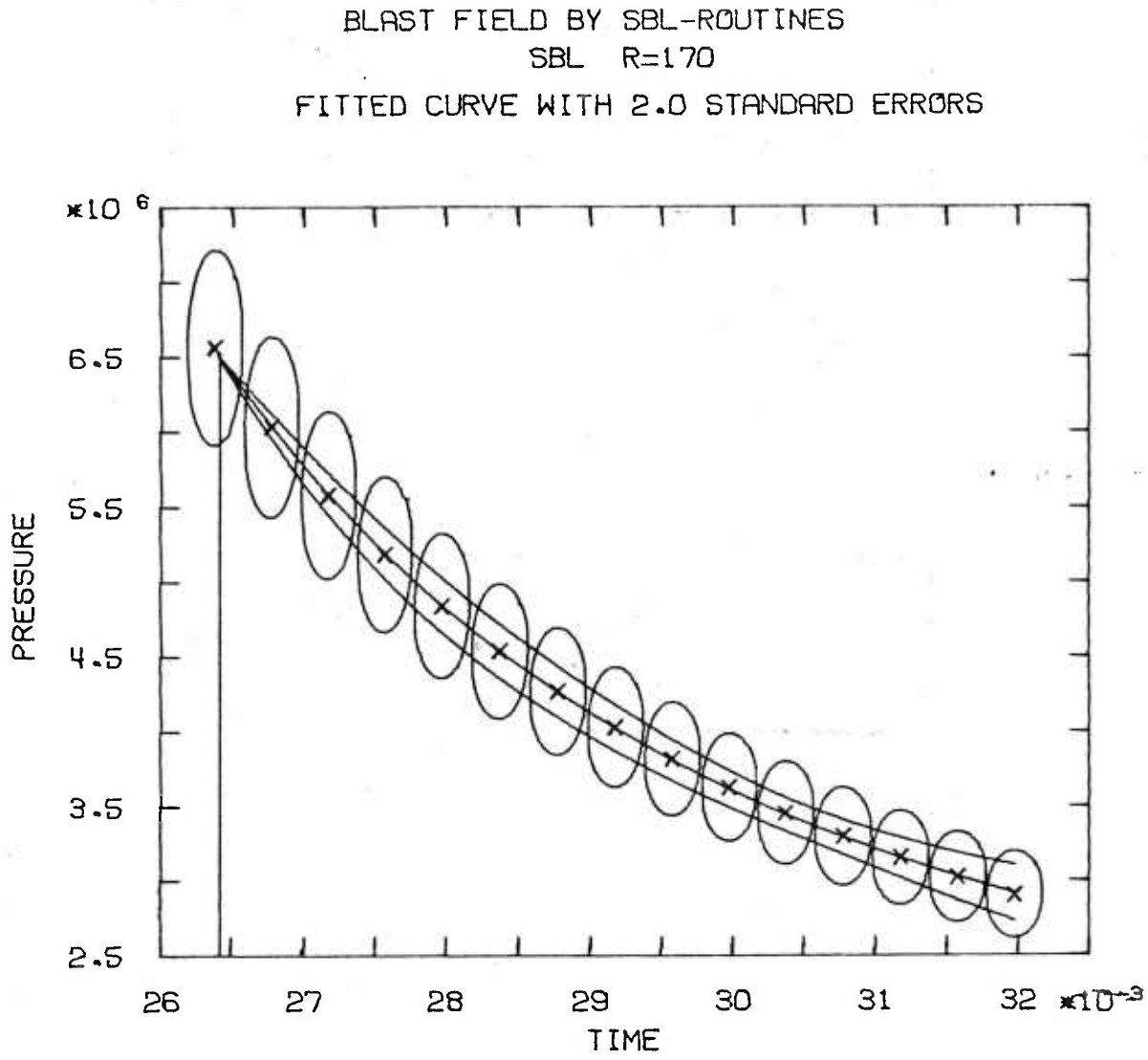

Figure 8. Fitting of Pressure at 170 m in Theoretical Test Example

(The data accuracy is indicated by a two standard error ellipse around each observed point.)

Time is expressed in seconds and pressure is expressed in pascals.

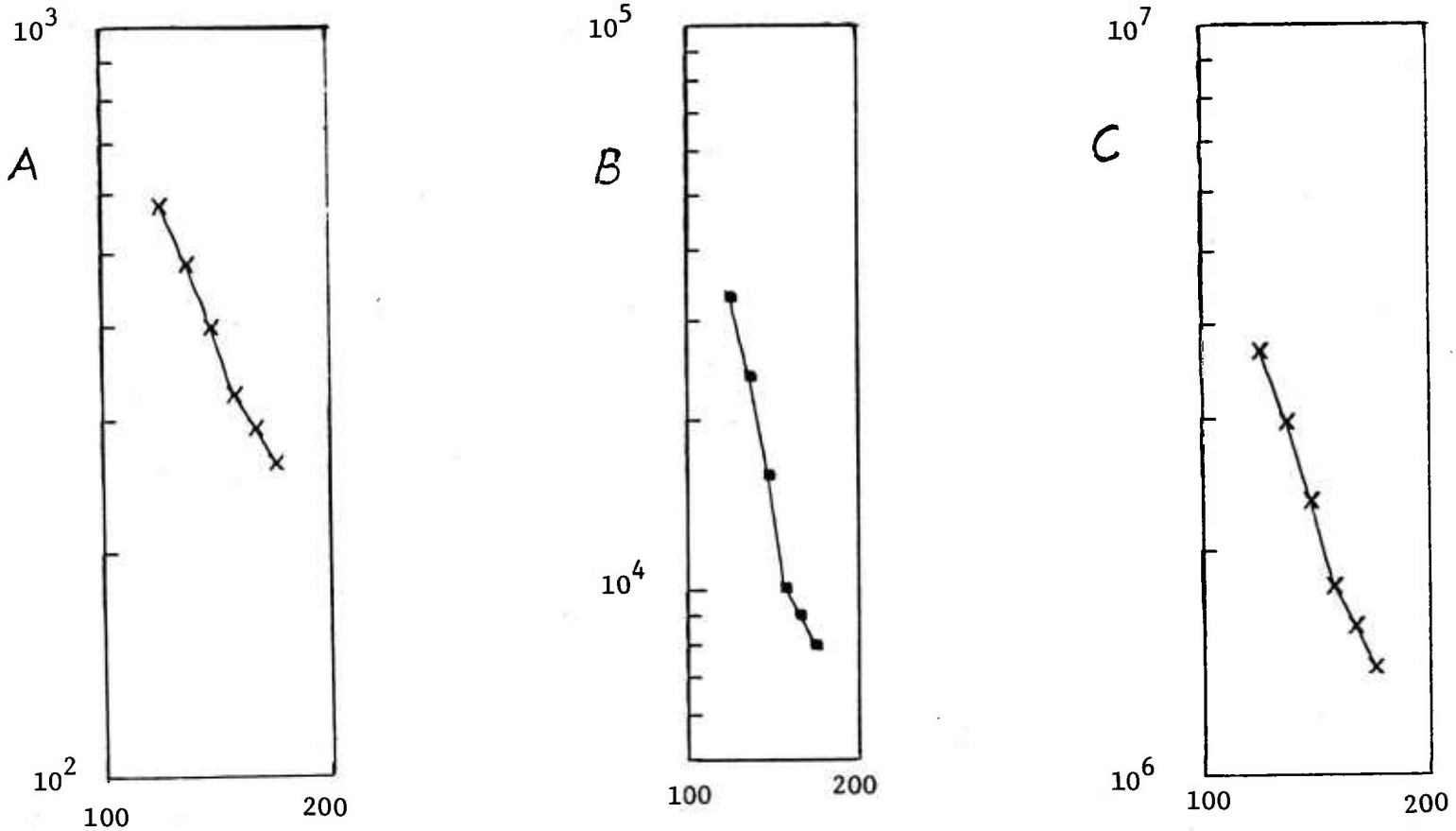

Figure 9. Log-log Plots of History Parameters vs. Distance in Theoretical Test Example

A test fitting, for which $A_2=B_2=0$ was assumed, produced indeed an almost as good approximation to the overpressure field as the function defined by Eqs. (7.1) and (7.2). For subsequent calculations, however, the full parameter set of Table 4 was used, because all five parameters are likely to be needed for real life observations.

Finally, the results of the field fitting and shock fitting were used to compute flow field histories at 150 m and 160 m from the explosion.

TABLE 4. OVERPRESSURE FIELD PARAMETERS OF THE THEORETICAL TEST EXAMPLE

The model is given by Eq. (7.1)
The total number of observed (p,t,r)-sets is 92

Parameters and Standard Errors

$$A_1 = (-3.706 \pm 0.918)\cdot 10^7 \ m^{2.3}/s$$

$$A_2 = (2.210 \pm 6.111)\cdot 10^4 \ m^{1.3}/s$$

$$B_1 = (1.027 \pm 1.231)\cdot 10^{14} \ m^{4.5}/s$$

$$B_2 = (-2.384 \pm 8.292)\cdot 10^{11} \ m^{3.5}/s$$

$$C_1 = (3.840 \pm 0.301)\cdot 10^{12} \ m^{2.9}\cdot Pa$$

Standard error of weight one, $m_o = 0.1650$, is not included in the standard errors of the parameters. (See NOTE in Table 3)

Correlation Matrix of the Parameters

$$\begin{pmatrix} 1.0 & -0.98719841 & -0.93452111 & 0.92814584 & -0.09747745 \\ -0.98719841 & 1.0 & 0.94741921 & -0.94678284 & -0.05480633 \\ -0.93452111 & 0.94741921 & 1.0 & -0.99916227 & -0.07989523 \\ 0.92814584 & -0.94678284 & -0.99916227 & 1.0 & 0.11085262 \\ -0.09747745 & -0.05480633 & -0.07989523 & 0.11085262 & 1.0 \end{pmatrix}$$

The flow histories of 150 m are shown in Figures 10 through 14. The length of the computable history is limited to the end time of about 22 ms, at which time the leftmost particle path reaches the distance 150 m (see Figure 3). If the field history at 150 m is needed beyond 22 ms, then additional observations are necessary at distances closer than 110 m to the explosion. The pressure history, Figure 10, shows close agreement between fitted values and theoretical values. The magnitude of the estimated variances of the pressure is of the same order (5 percent) as the assumed accuracy of pressure observations, indicating that excessive error amplification does not take place.

The particle velocity history is shown in Figure 11. The figure also contains, as a dashed line, the results of the control calculation by the quadrature (2.15). The difference between both velocity curves is of the same order as the estimated standard error of the velocity. Therefore, one can conclude from the test that the pressure field model is consistent with the assumed accuracy of the data. Also shown in the figure is the theoretical particle velocity as predicted by the strong blast theory. The deviation between the calculated velocity and the theoretical velocity is always in the same direction, indicating a systematic cause for the difference. A systematic reason is indeed present, because for the strong blast theory one sets in all formulas the ratio p_o/p_s equal to zero, whereas, the present calculation takes the ratio properly into account. The difference in the result can be easily checked at the initial point of the velocity history. One obtains the value of the velocity as predicted by strong blast theory by using Eqs. (4.3) and (4.4) with $p_o/p_s = 0$, whereas the full formulas produce the value shown as "calculated result." It is apparent from this comparison that a shock pressure ratio of about 0.01 cannot be neglected for the calculation of details of the blast field.

Figure 12 shows the density history at 150 m. The calculation of the density makes use of both the pressure and velocity calculation results. Nevertheless, the estimated variance of the result is moderate, indicating that the computing method is numerically stable. A systematic deviation between the calculated density and the strong blast density is again present and caused by the neglect of the ratio p_o/p_s in the strong blast theory. The effect of the ratio on Eq. (4.15) is stronger for lower shock pressures and, therefore, the difference is larger at the beginning of the density history, where the particles have been subjected to a less strong shock.

The dynamic pressure history at 150 m is shown in Figure 13. The dynamic pressure is computed from the velocity and density and, therefore, one obtains the same systematic deviation as discussed above between the calculated result and the strong blast theory. More interesting is the estimated variance of the calculated dynamic pressure. It is of the order of five percent, i.e., of the same order as the assumed accuracy of the pressure data. This result is very encouraging for the application of the method to field experiments, because it shows that the computation method is sufficiently stable to produce accurate dynamic pressure histories from overpressure observations with typical uncertainties.

Figures 14 through 17 show the calculated field histories at 160 m distance from the explosion. The results are similar to the corresponding results for 150 m distance, and the same comments apply as before to the systematic differences and estimated variances of the calculated histories.

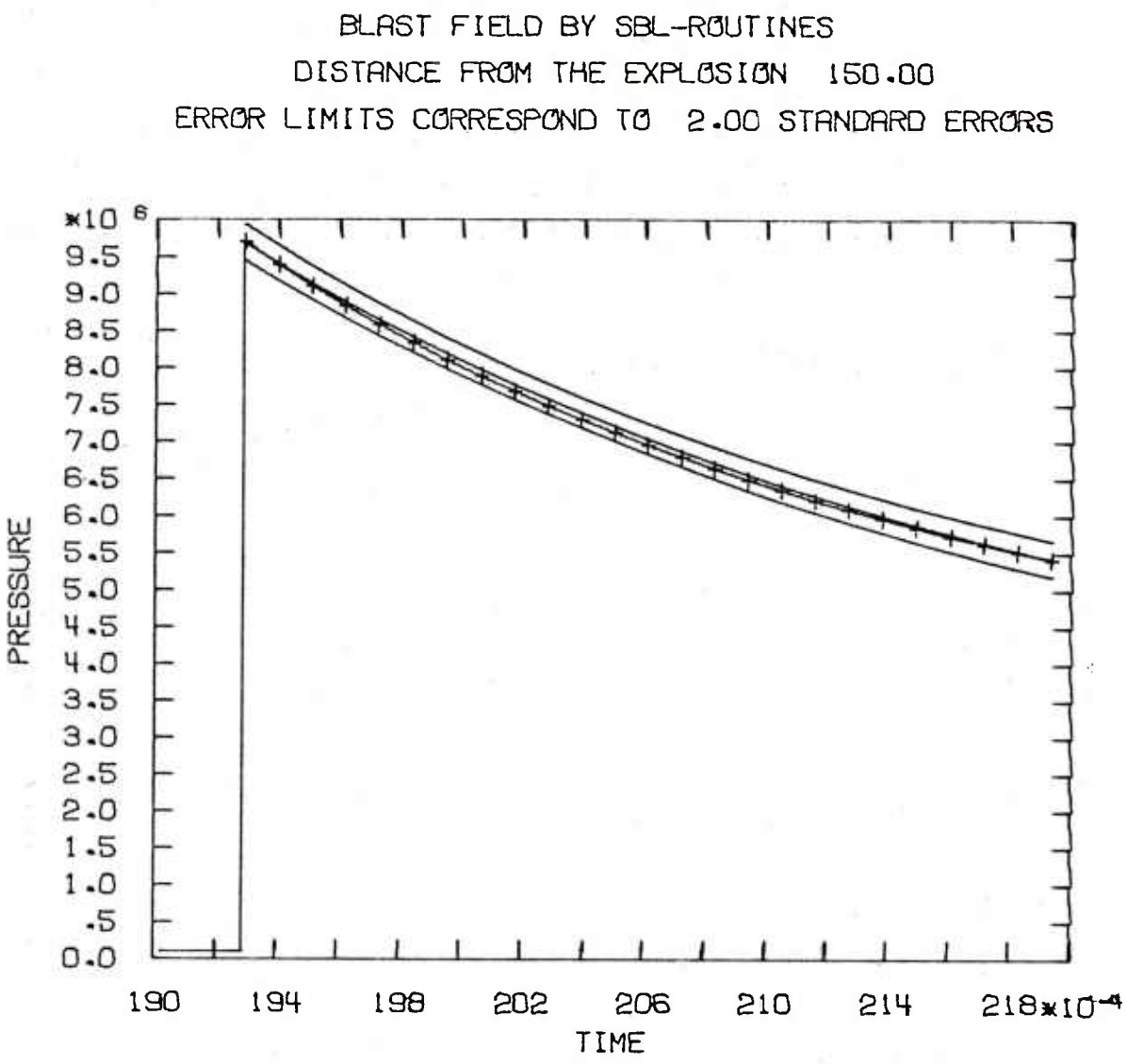

Figure 10. Pressure History at 150 m in Theoretical Test Example

Field fitting results with confidence limits

Strong blast theory

Time is expresses in seconds and pressure is expressed in pascals.

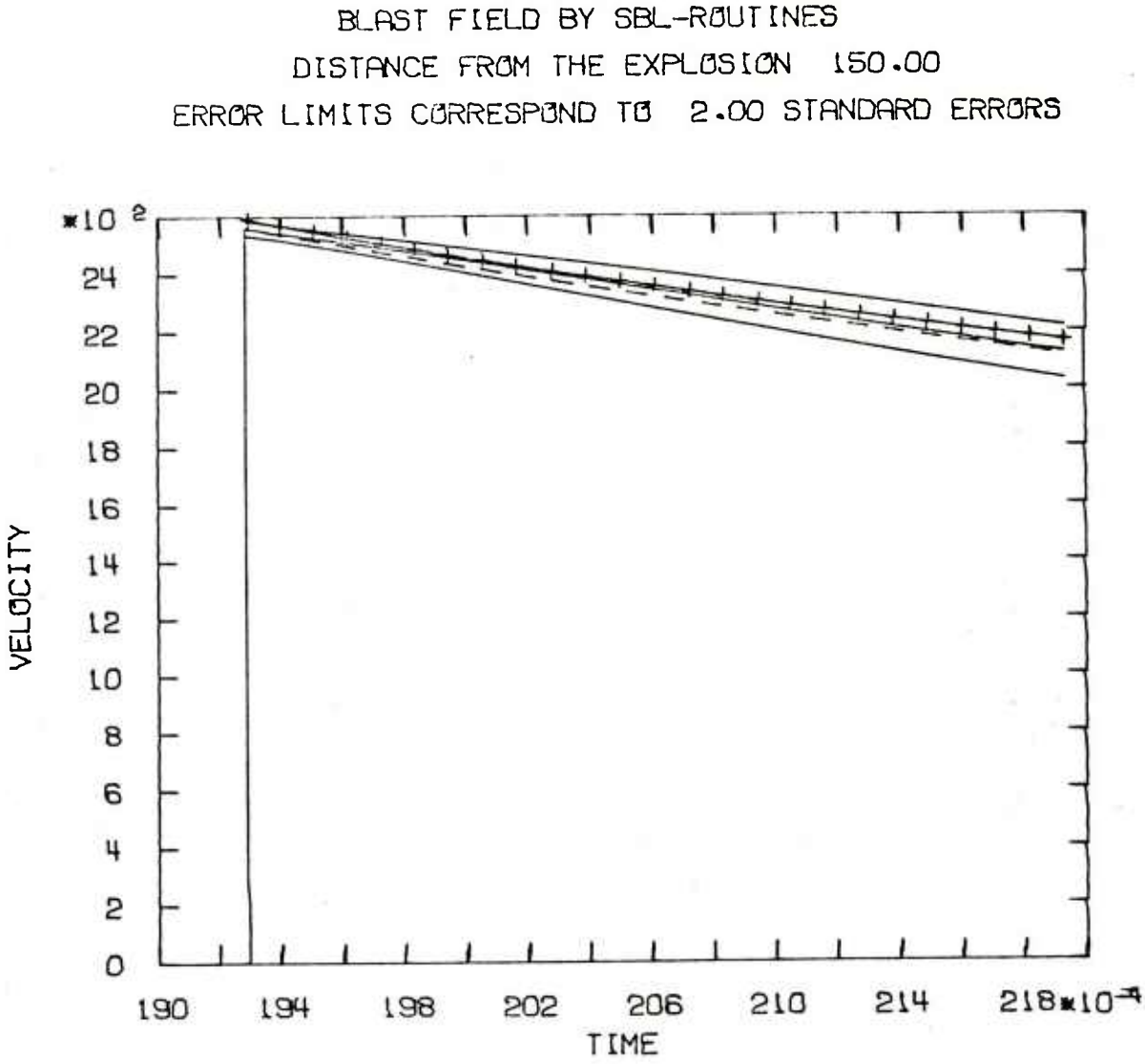

Figure 11. Particle Velocity History at 150 m in Theoretical Test Example

Calculated result with confidence limits

Control calculation

Strong blast theory

Time is expressed in seconds and velocity is expressed in m/s.

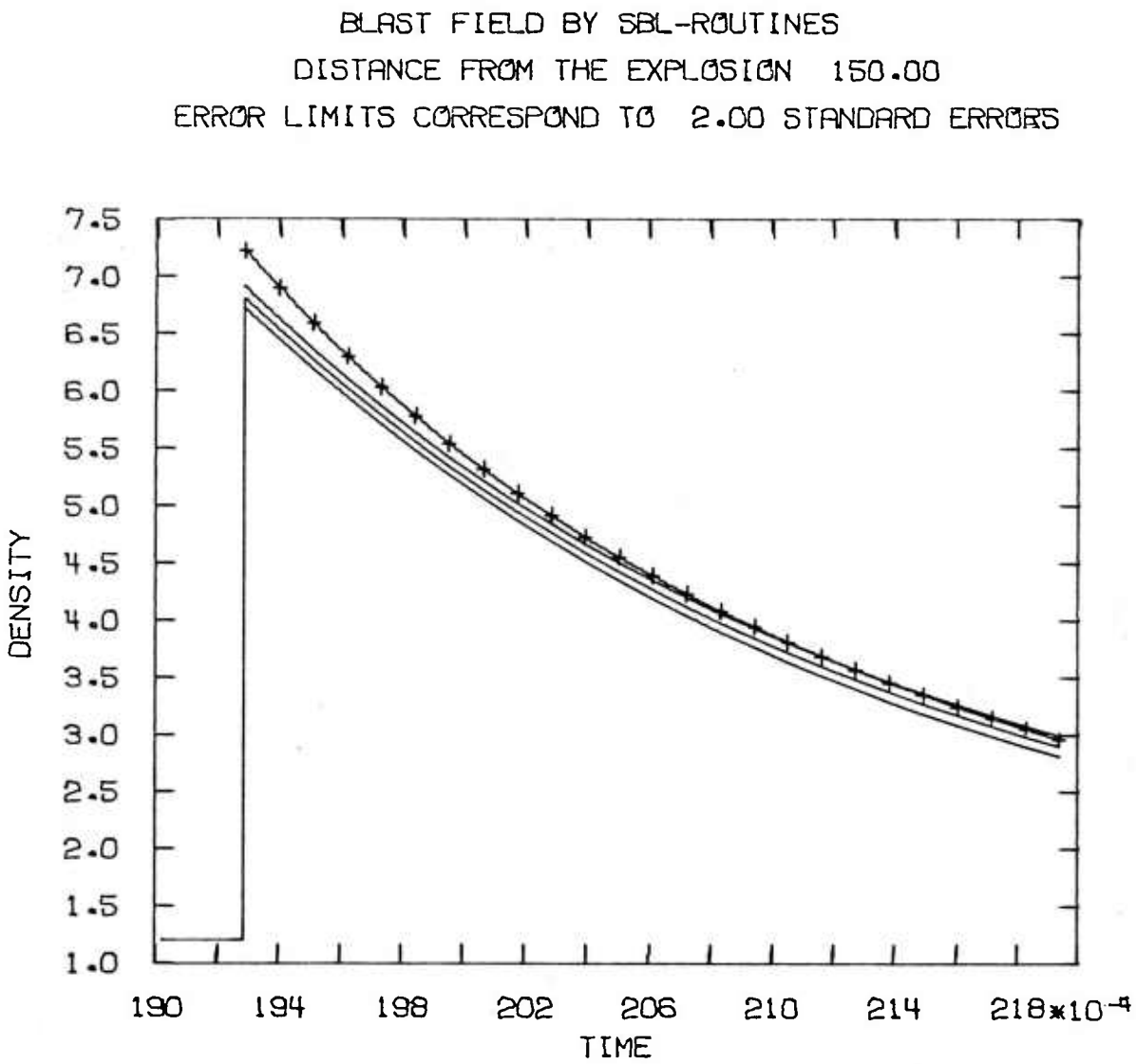

Figure 12. Density History at 150 m in Theoretical Test Example

Calculated result with confidence limits

Strong blast theory

Time is expressed in seconds and density is expressed in kg/m^3.

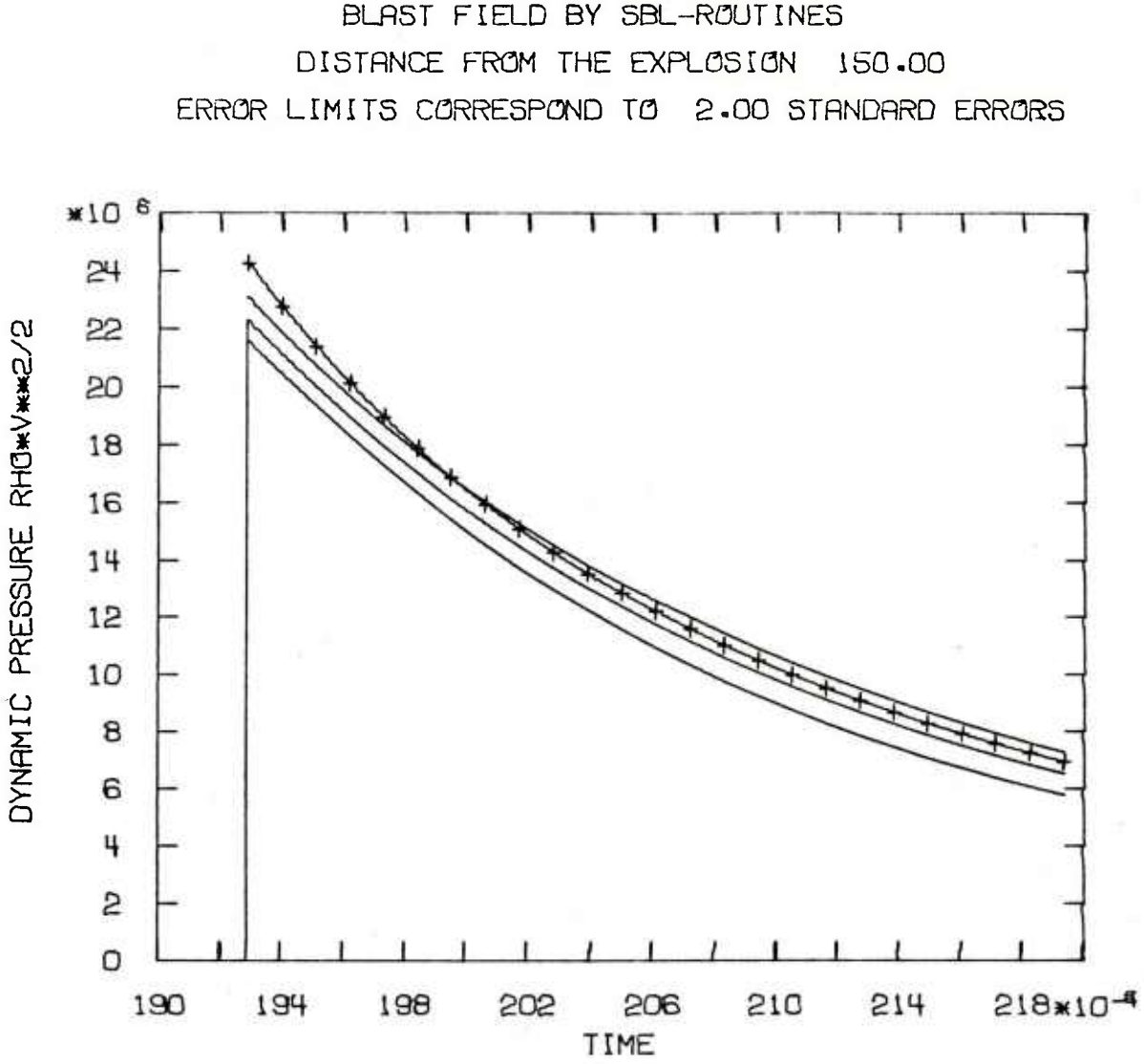

Figure 13. Dynamic Pressure History at 150 m in Theoretical Test Example

Calculated result with confidence limits

Strong blast theory

Time is expressed in seconds and dynamic pressure is expressed in pascals.

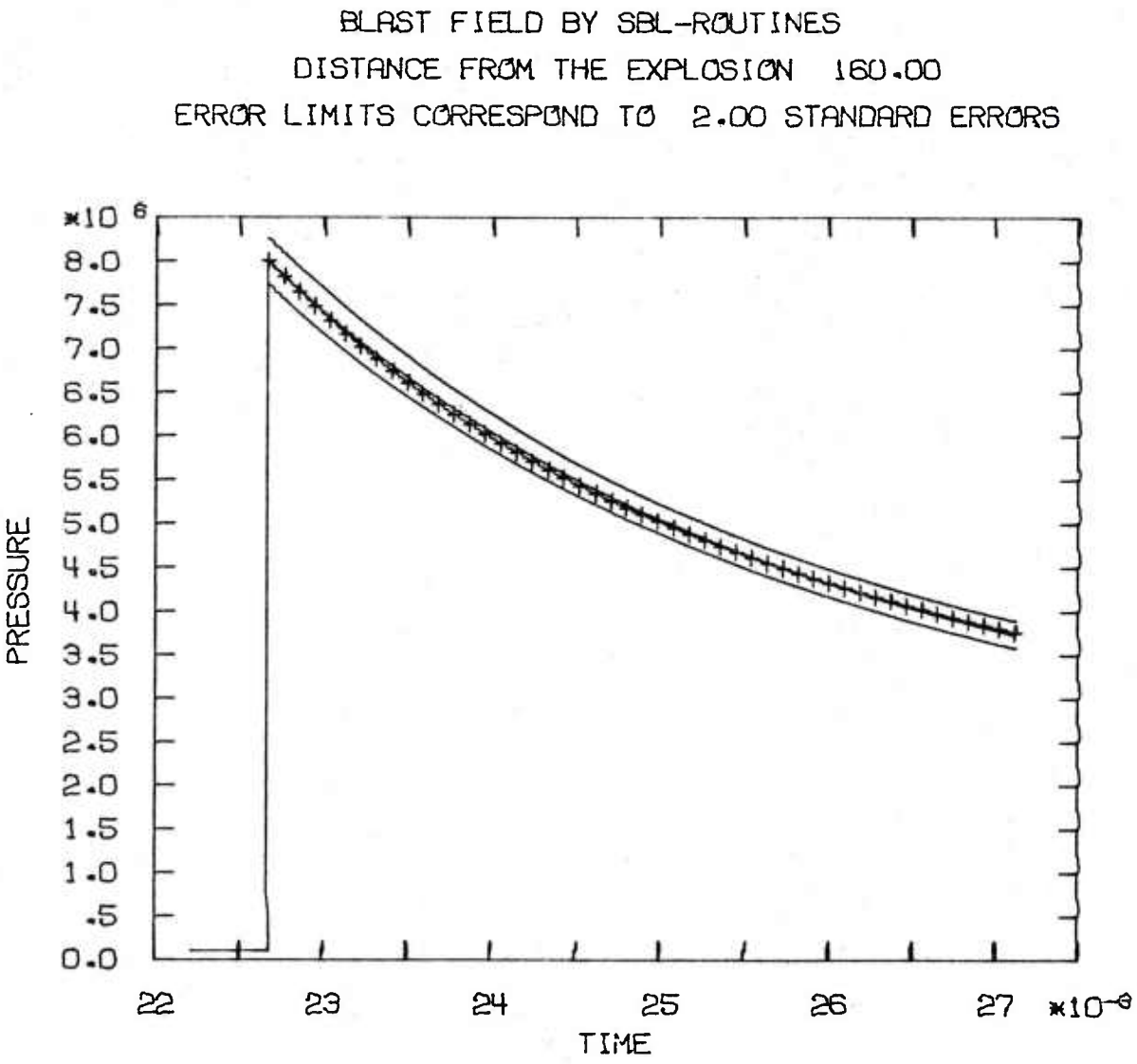

Figure 14. Overpressure History at 160 m in Theoretical Test Example

Field fitting with confidence limits

Strong blast theory

Time is expressed in seconds and pressure is expressed in pascals.

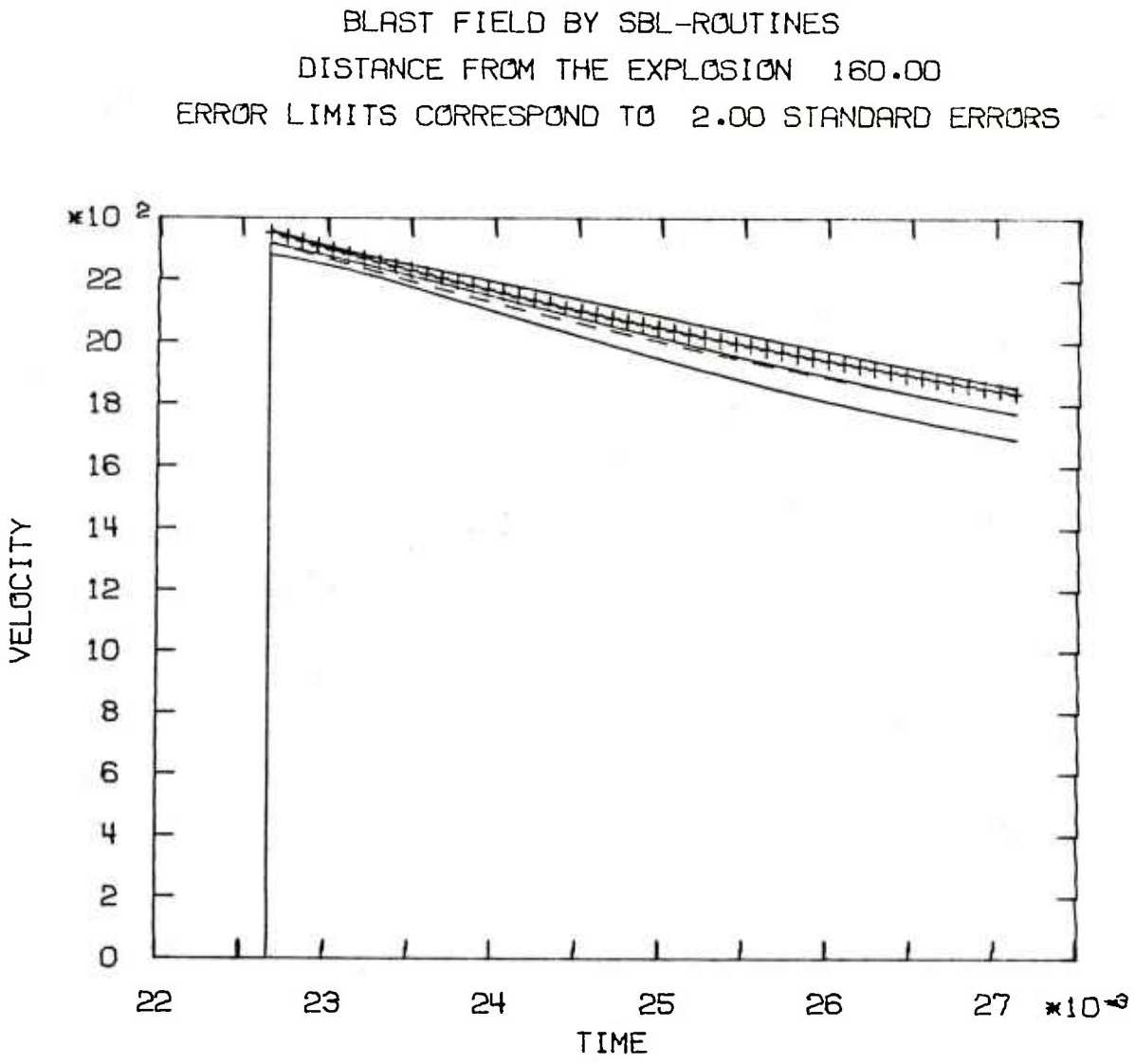

Figure 15. Particle Velocity History at 160 m in Theoretical Test Example

Calculated result with confidence limits

Control calculation

Strong blast theory

Time is expressed in seconds and velocity is expressed in m/s.

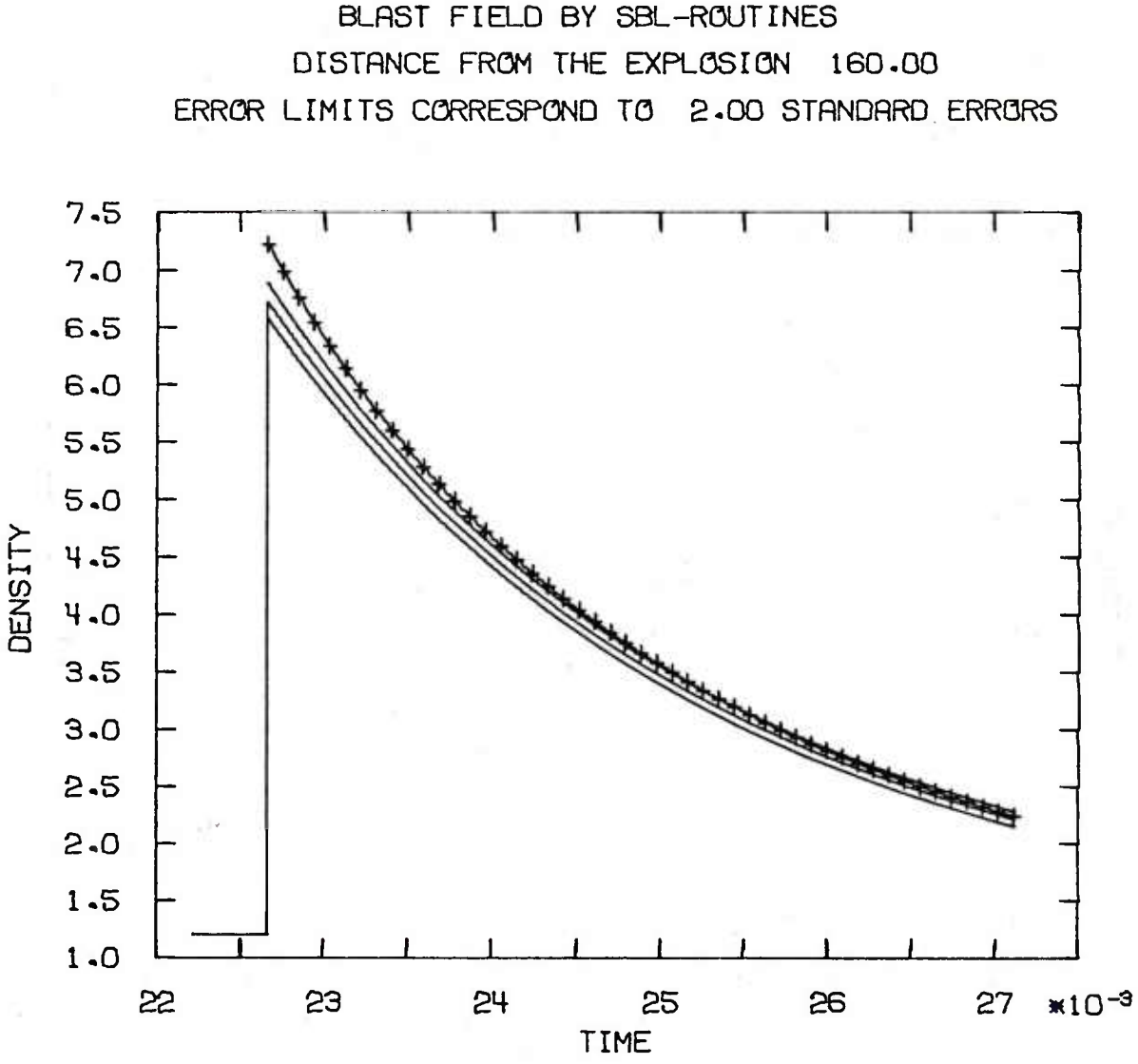

Figure 16. Density History at 160 m in Theoretical Test Example

Calculated result with confidence limit

Strong blast theory

Time is expressed in seconds and density is expressed in kg/m^3.

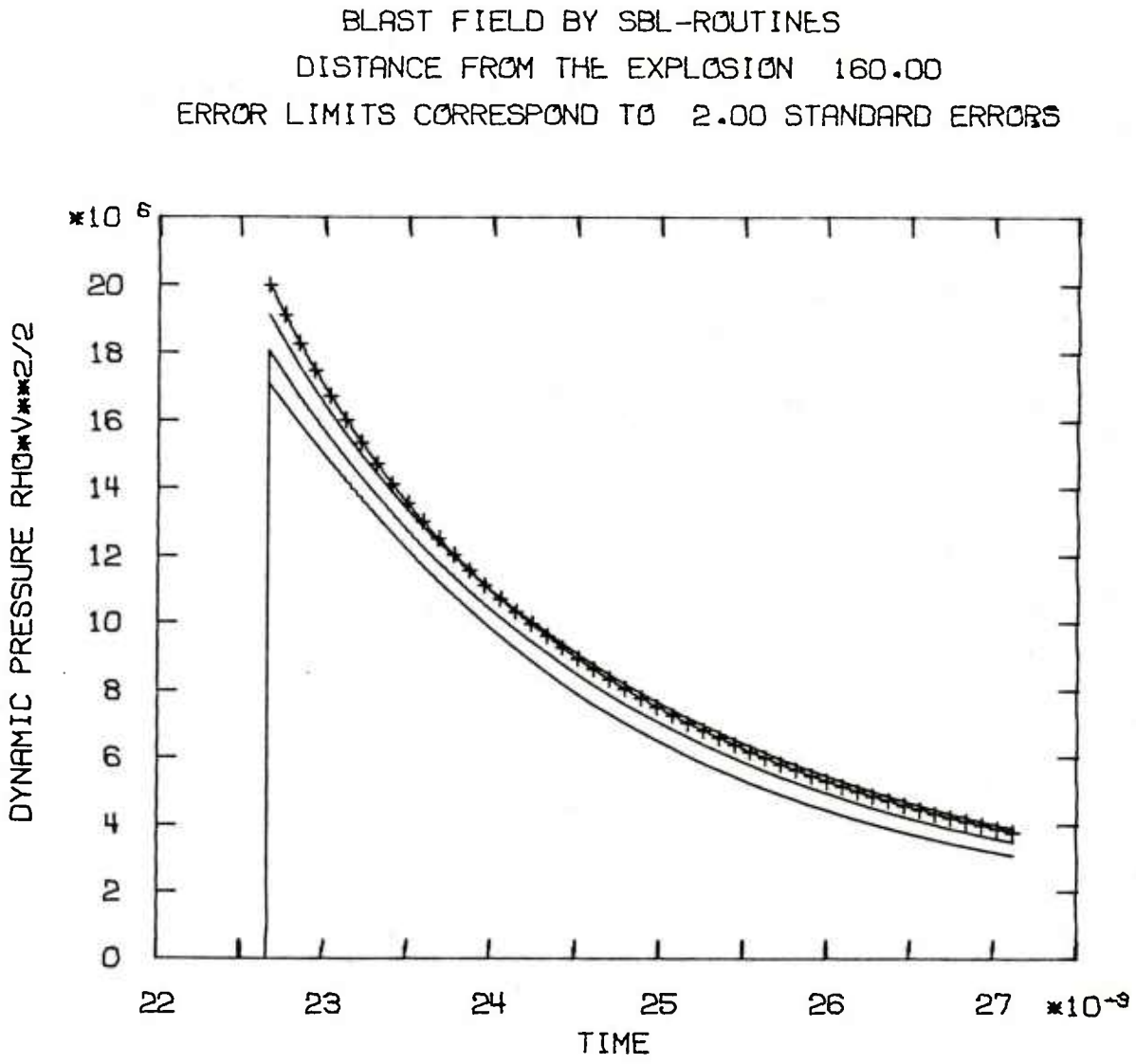

Figure 17. Dynamic Pressure History at 160 m in Theoretical Test Example

Calculated result with confidence limit

Strong blast theory

Time is expressed in seconds and dynamic pressure is expressed in pascals.

8. APPLICATION TO DATA FROM MISERS BLUFF II

In order to test the applicability of the flow field calculation method and corresponding computer programs to real problems, we used the computer programs on data from the event MISERS BLUFF II[9].

For the shock fitting, we used data consisting of 18 shock arrival times and overpressure measurements at ranges between 89.7 m and 715 m. The shock data and data describing the ambient conditions are listed in Table 5. Table 6 gives the numerical results of the shock fitting. Comparing the results with corresponding results in Table 3 for the theoretical test example, one notices that now there are no indications of a redundancy of parameters. Their estimated standard errors are relatively small and correlations between them are less strong than in the theoretical example. The standard error of weight one has a value close to one, indicating that the estimated standard errors of the observations are consistent with the shock model and with the scatter of the data.

Figures 18, 19, and 20 show the shock fitting results graphically. The increase of the estimated confidence interval outside the fitting region is much more gradual than in the theoretical test example (Figures 4, 5, and 6). This behavior of the confidence limits can be attributed to the fact that the model contains no redundant parameters for the treatment of the given data set.

In order to test and illustrate the flow field calculation capability of the computer program we assumed that the stations of interest were located at 120 m and 150 m from the explosion; i.e., we assumed that the goal is to compute flow histories at these distances. Then the first step is to establish pressure field functions in the vicinity of the stations of interest. Available were overpressure history data at eight stations between 89.7 m and 211 m, as shown in Figure 21.

The overpressure history data and fitting curves for the individual histories are shown in Figures 22 through 29. For this data fitting, as well as for the subsequent pressure field fitting, we assumed the following standard errors of the data:

Pressure: 5% of the initial overpressure

Time: 1 ms

Range and Elevation: 1 m

---

[9] *G. Teel, "Free Field Airblast Definition," Proceedings of the MISERS BLUFF Phase II Results Symposium, 27-29 March 1979, Defence Nuclear Agency Report POR 7013-1, 1979.*

TABLE 5. AMBIENT AND SHOCK DATA OF MISERS BLUFF II

Ambient Conditions

Molar mass	M = 28.94 g/mole
Specific heat ratio	γ = 1.4
Temperature	T = 312.05 K
Pressure	p_o = 92.92 kPa

Charge

Released Energy	418.4 GJ
Elevation	0.0 m

Shock Observations

Range (m)	Elevation (m)	Overpressure (kPa)	Time (ms)
89.7	0.0	478	56.6±1
96.0	0.0	340	64.8±1
103.0	0.0	294	75.0±1
114	0.0	198	92.4±2
114	0.0	204	95.7±2
120.3	0.0	149	104±2
150.3	0.0	83.1	164±2
174	0.0	57.3	217±2
190	0.0	49.2	254±2
206	1.22	42.1	292±2
206	2.44	41.1	293±2
211	0.0	38.9	304±3
264	0.0	25.8	436±3
309	1.22	19.8	551±3
344	0.0	19.4	643±3
388	0.0	14.6	760±4
532	0.0	9.78	1150±5
715	0.0	6.59	1660±10

The range and elevation accuracies were assumed to be 1.0 m.
The overpressure accuracy was assumed to be 5 percent.

TABLE 6. SHOCK PARAMETERS OF MISERS BLUFF II

The model is given by Eqs. (4.7) and (4.8).
The data are listed in Table 5.

Parameters and Standard Errors

$$a = (6.093 \pm 0.435) \cdot 10^{6} \text{ Pa} \cdot \text{m}$$

$$b = (-1.134 \pm 0.217) \cdot 10^{9} \text{ Pa} \cdot \text{m}^2$$

$$c = (3.343 \pm 0.235) \cdot 10^{11} \text{ Pa} \cdot \text{m}^3$$

$$d = 57.934 \pm 0.766 \text{ ms} = \text{arrival time at } 89.7 \text{ m}$$

The standard error of weight one, $m_o = 1.156$,
is included in the quoted standard errors.

Correlation Matrix of the Parameters

$$\begin{pmatrix} 1.0 & -0.93948052 & 0.83556376 & 0.01536038 \\ -0.93948052 & 1.0 & -0.96070389 & -0.03520487 \\ 0.83556376 & -0.96070389 & 1.0 & 0.09994155 \\ 0.01536038 & -0.03520487 & 0.09994155 & 1.0 \end{pmatrix}$$

NOTE: In this example, the standard error of weight one, m_o, is close to one, indicating that the data scatter is consistent with the data standard error as specified by input. However, because m_o is larger than one, the inaccuracies might have been slightly underestimated. We have multiplied the calculated standard errors of the parameters by m_o in order to account for the possible underestimate.

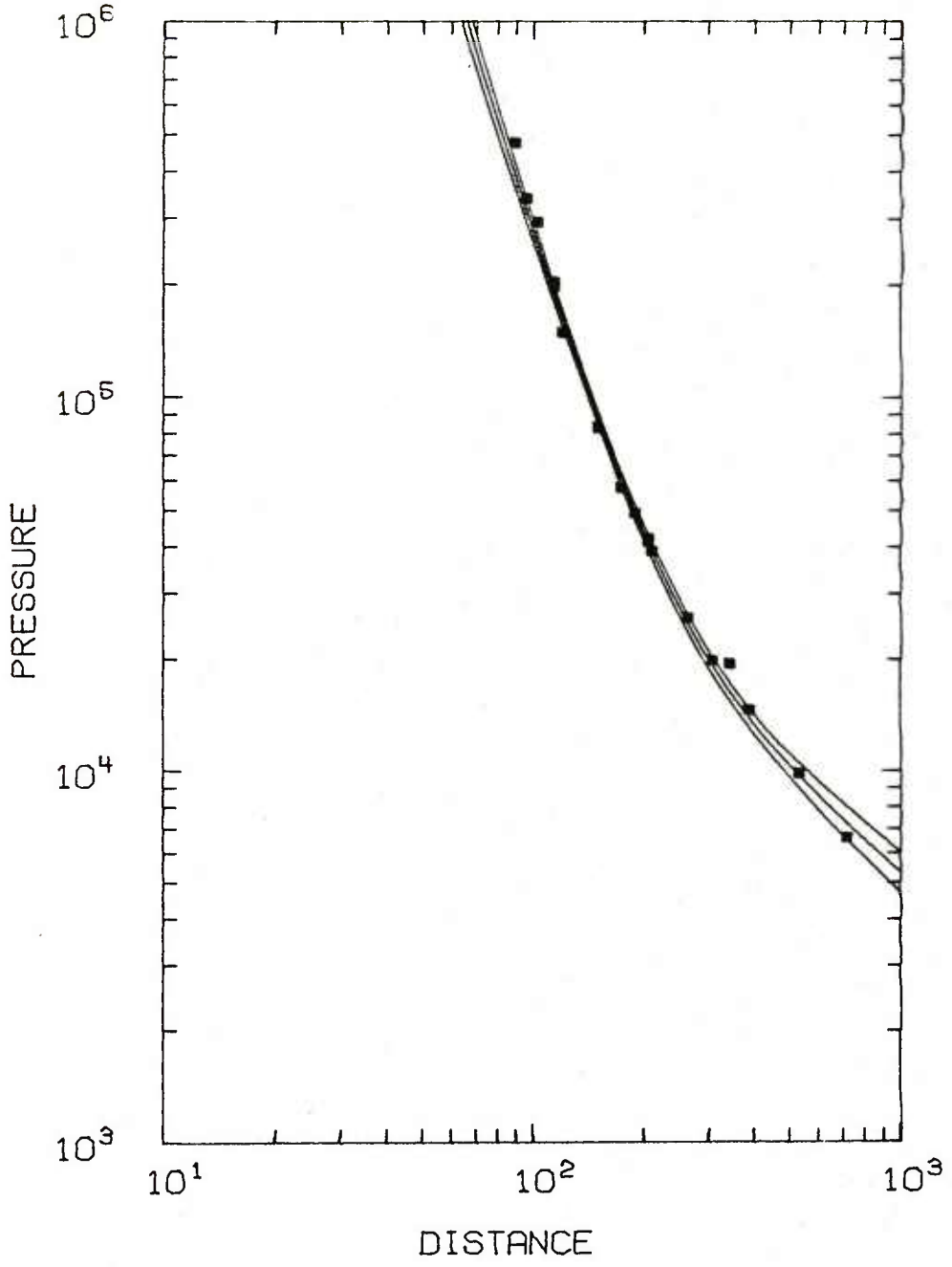

Figure 18. Shock Overpressure Versus Distance in MISERS BLUFF II

Distance is expressed in meters and pressure is expressed in pascals.

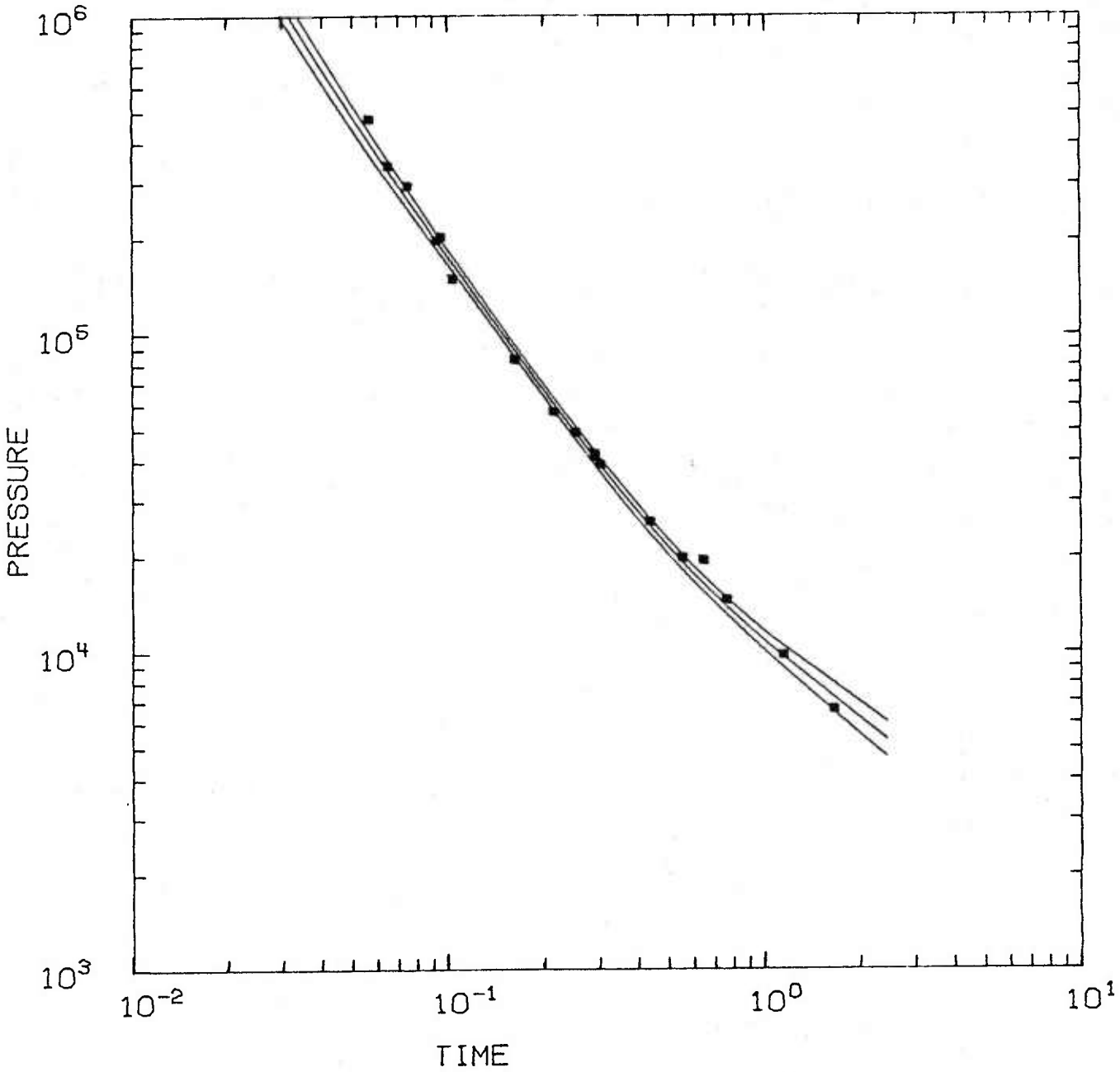

Figure 19. Shock Overpressure Versus Time in MISERS BLUFF II

Time is expressed in seconds and pressure is expressed in pascals.

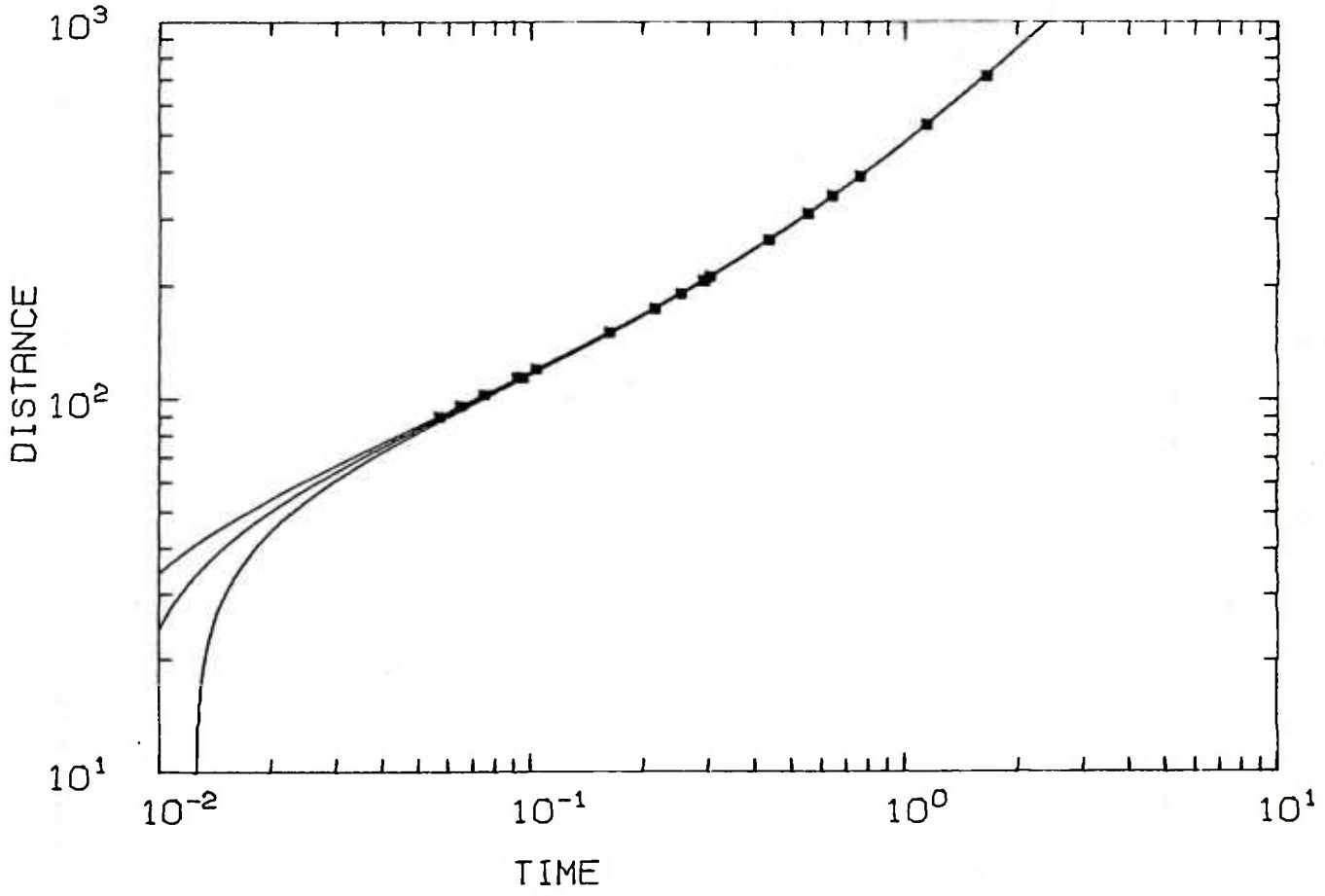

Figure 20. Shock Distance Versus Time in MISERS BLUFF II

Time is expressed in seconds and distance is expressed in meters.

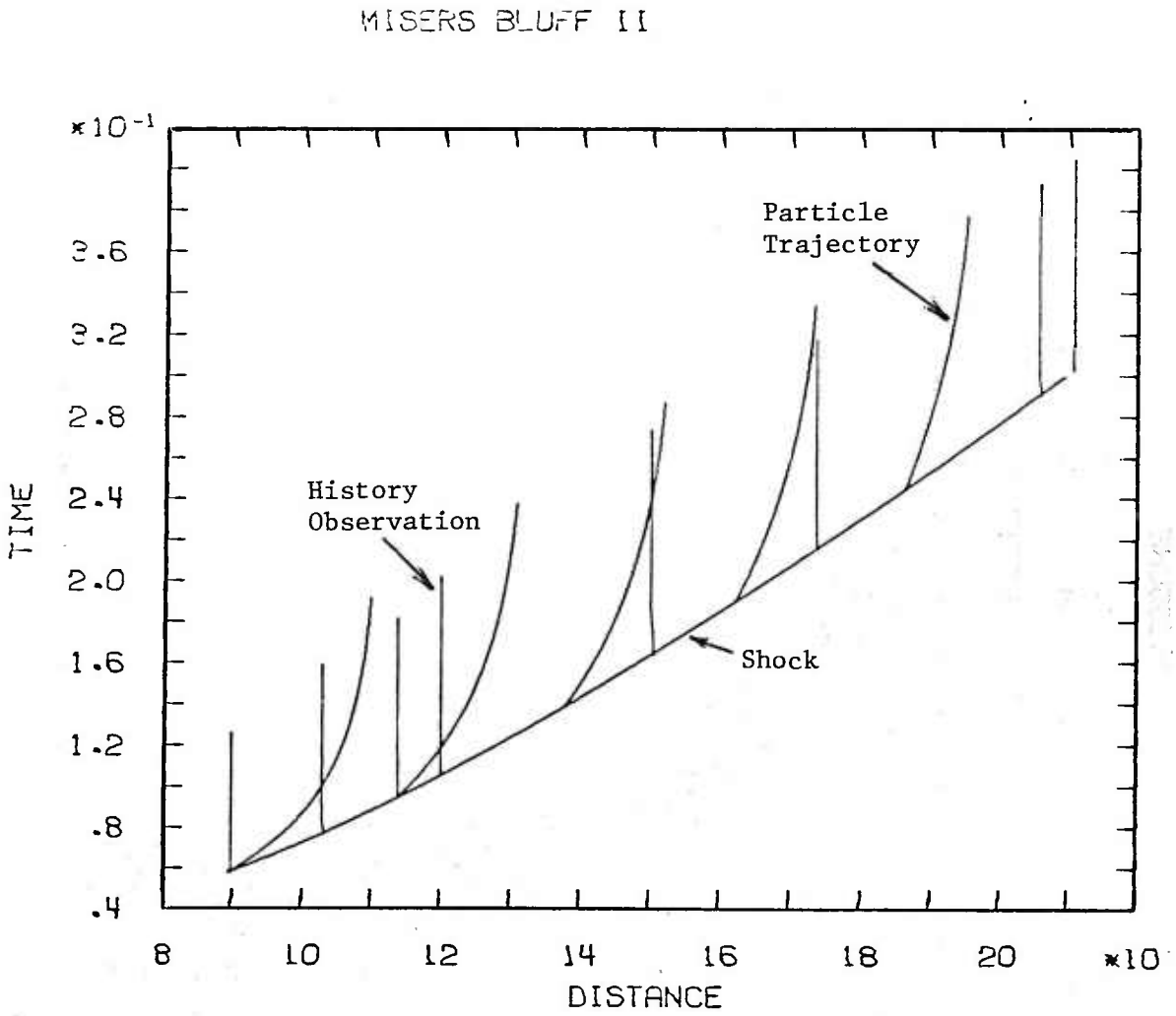

Figure 21. Locations of History Observations in MISERS BLUFF II

Distances are expressed in meters and times are expressed in seconds.

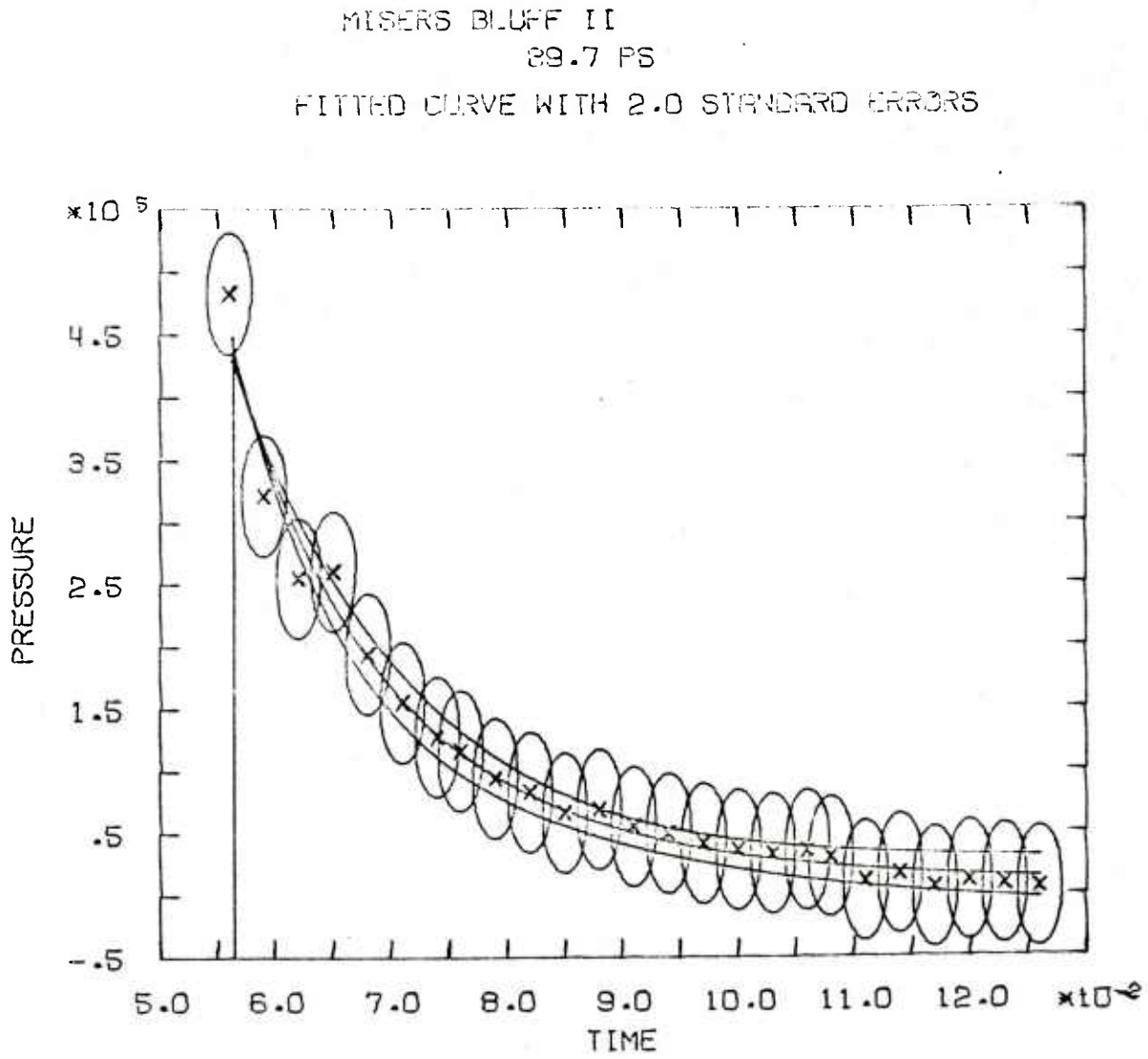

Figure 22. Fitting of Pressure at 89.7 m in MISERS BLUFF II

The data accuracy is indicated by a two-standard error ellipse around each observed point.

Time is expressed in seconds and pressure is expressed in pascals.

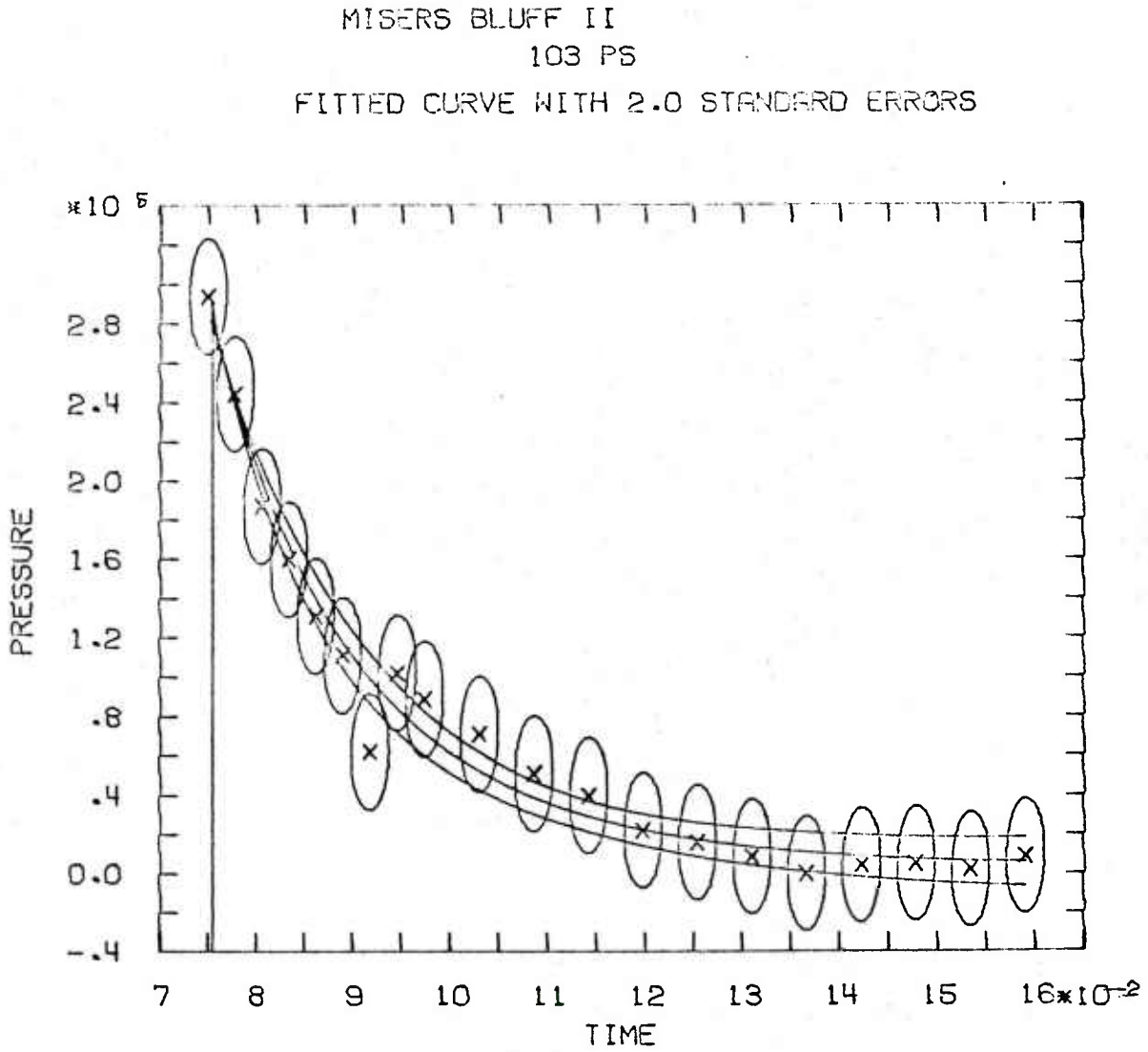

Figure 23. Fitting of Pressure at 103 m in MISERS BLUFF II

The data accuracy is indicated by a two-standard error ellipse around each observed point.

Time is expressed in seconds and pressure is expressed in pascals.

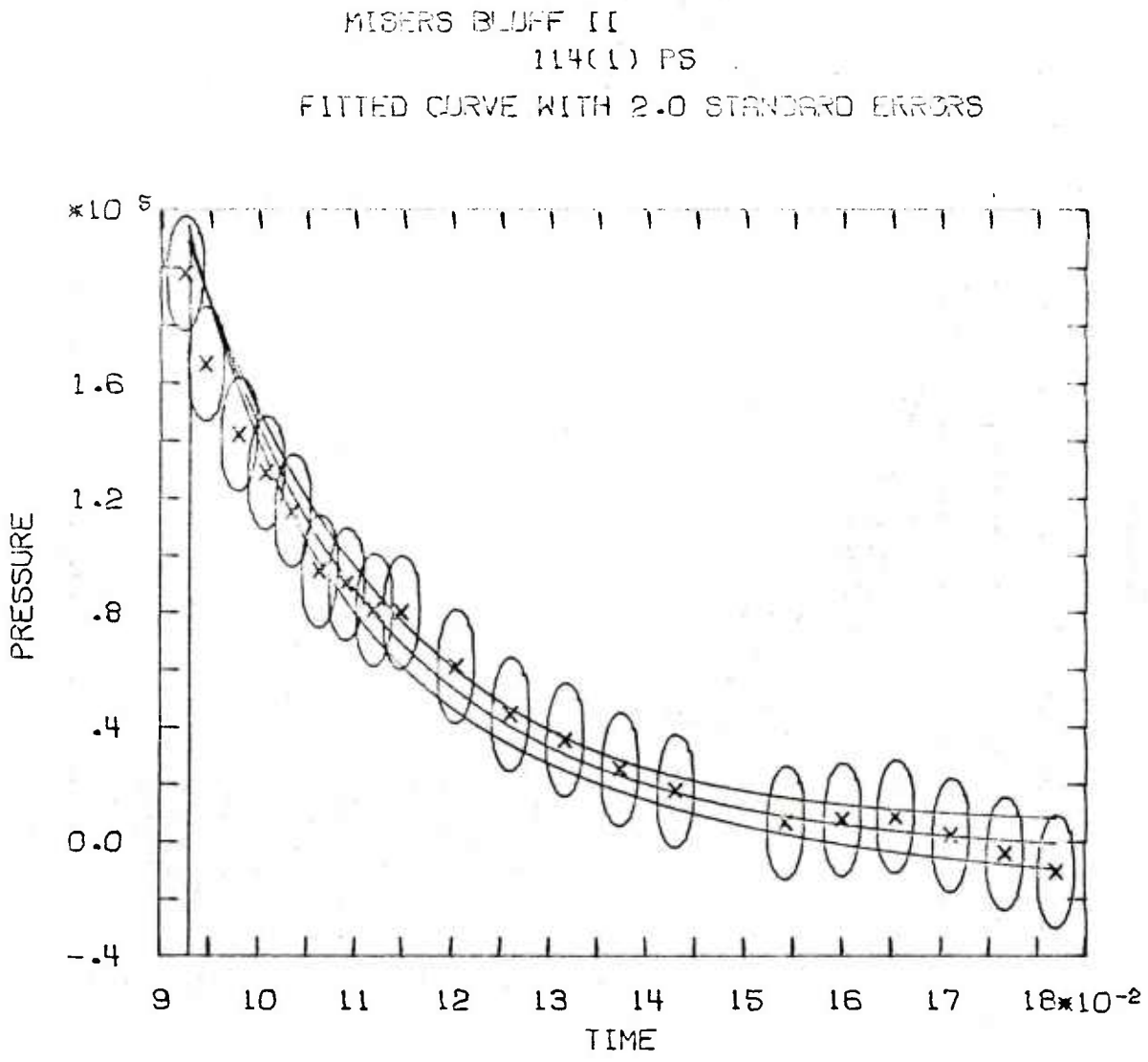

Figure 24. Fitting of Pressure at 114 m in MISERS BLUFF II

The data accuracy is indicated by a two-standard error ellipse around each observed point.

Time is expressed in seconds and pressure is expressed in pascals.

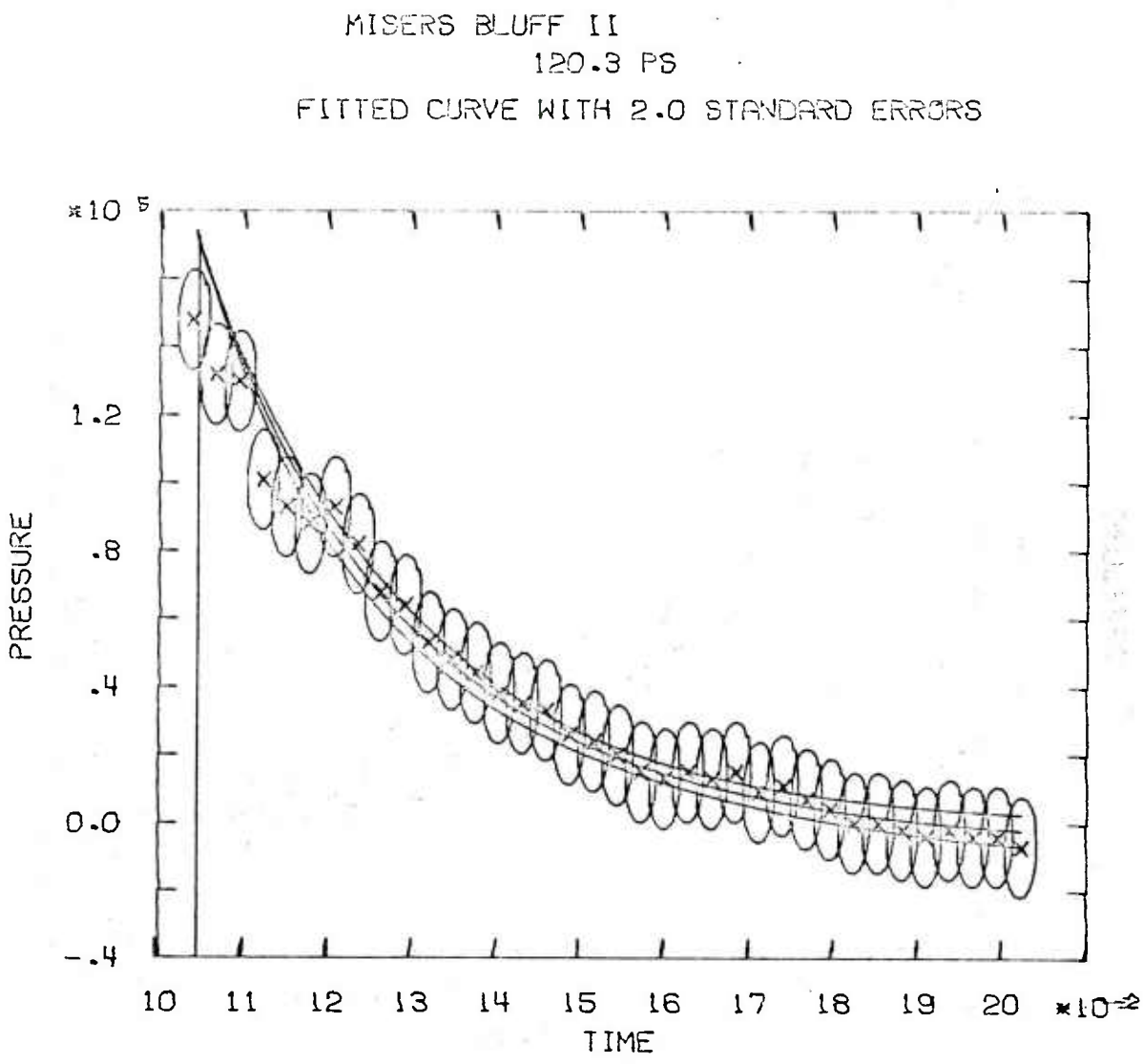

Figure 25. Fitting of Pressure at 120.3 m in MISERS BLUFF II

The data accuracy is indicated by a two-standard error ellipse around each observed point.

Time is expressed in seconds and pressure is expressed in pascals.

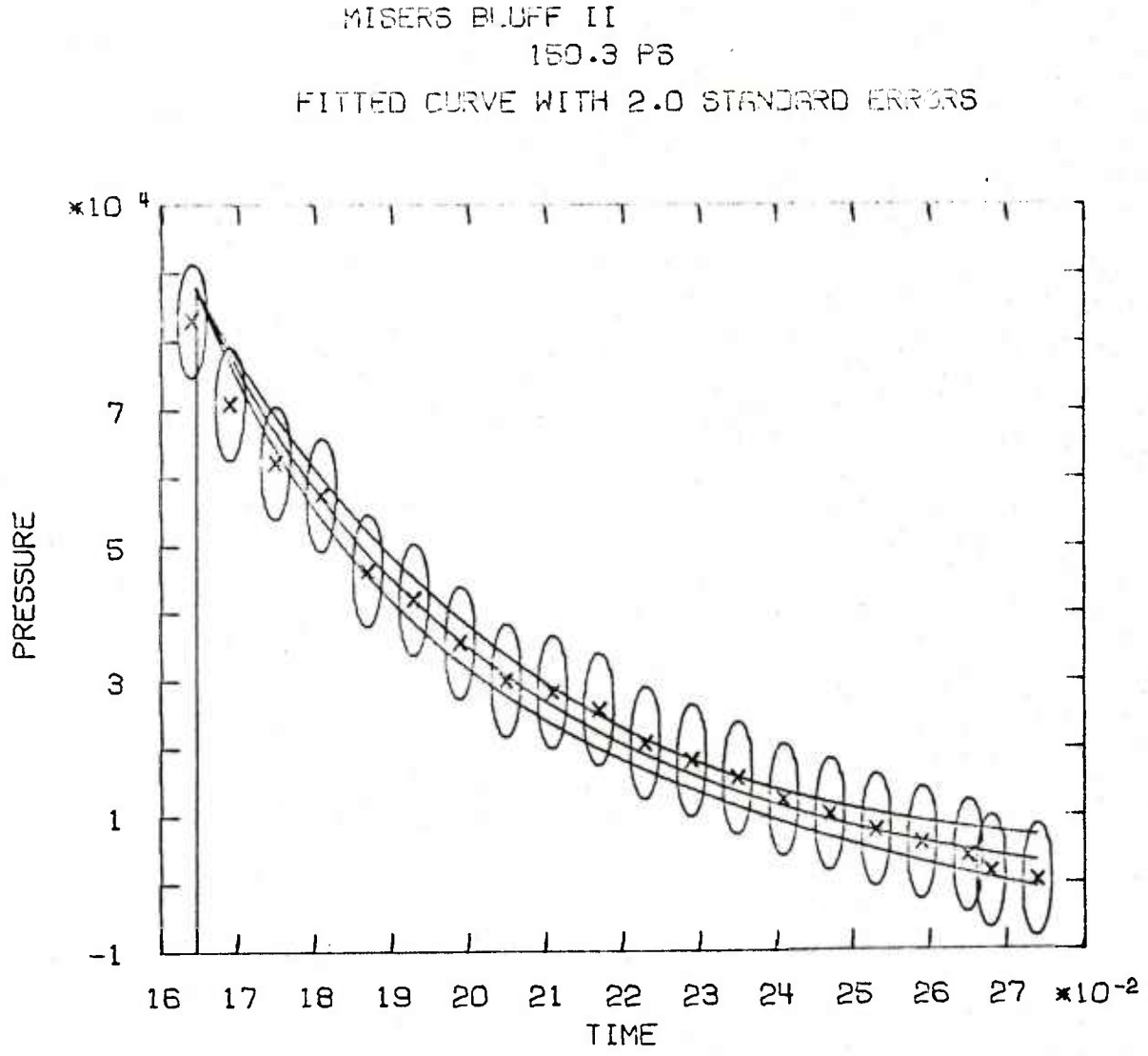

Figure 26. Fitting of Pressure at 150.3 m in MISERS BLUFF II

The data accuracy is indicated by a two-standard error ellipse around each observed point.

Time is expressed in seconds and pressure is expressed in pascals.

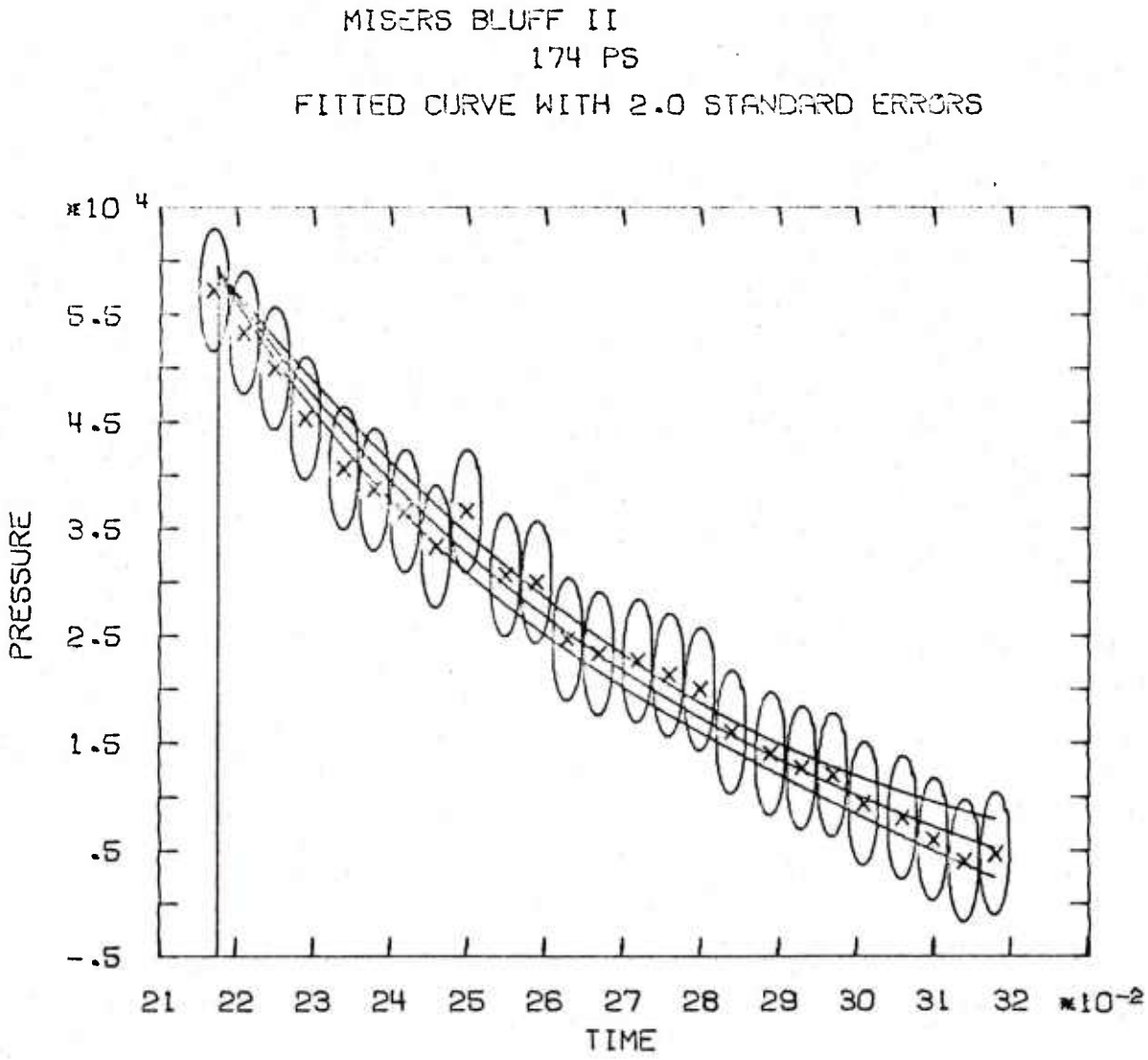

Figure 27. Fitting of Pressure at 174 m in MISERS BLUFF II

The data accuracy is indicated by a two-standard error ellipse around each observed point.

Time is expressed in seconds and pressure is expressed in pascals.

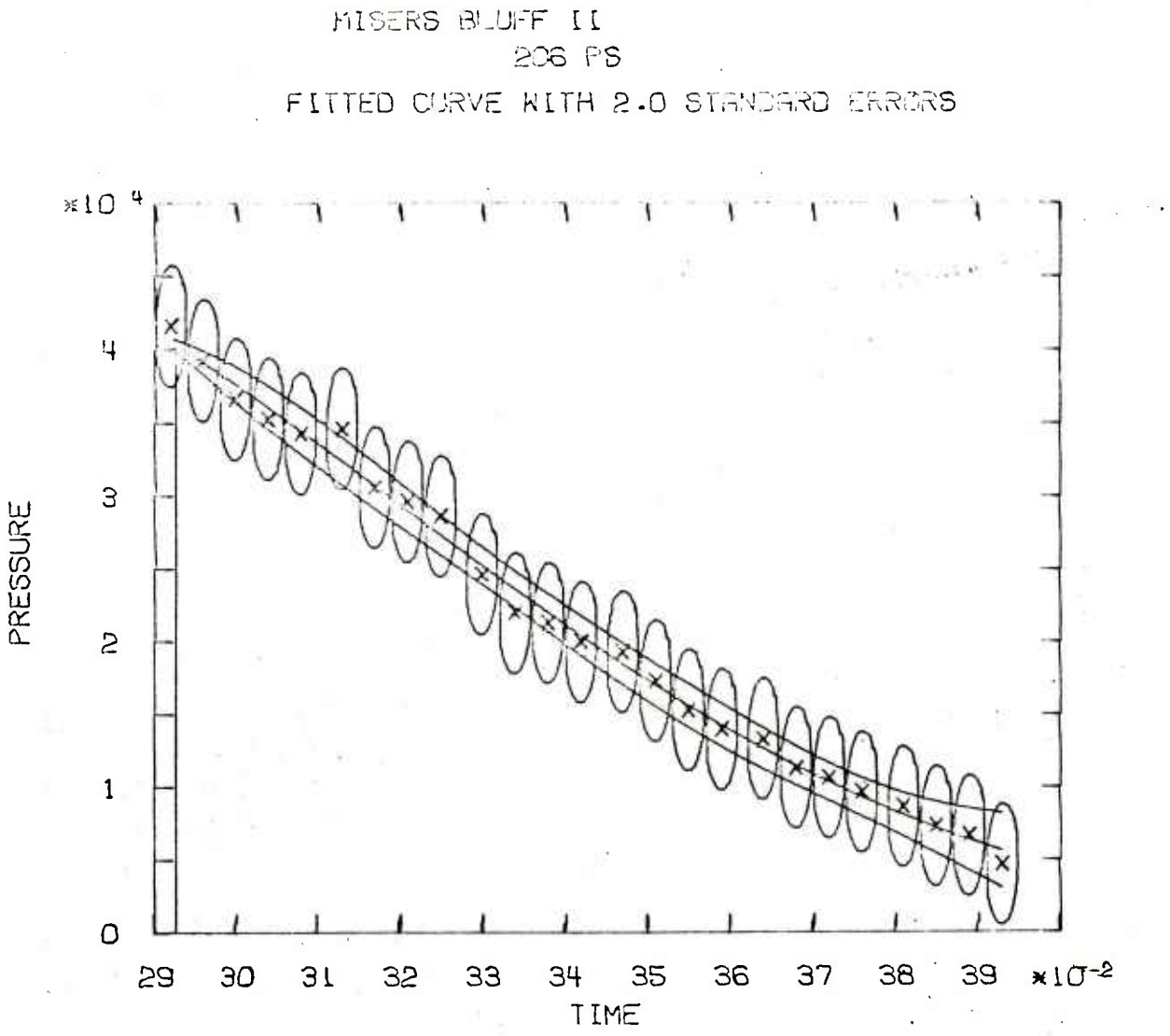

Figure 28. Fitting of Pressure at 206 m in MISERS BLUFF II

The data accuracy is indicated by a two-standard error ellipse around each observed point.

Time is expressed in seconds and pressure is expressed in pascals.

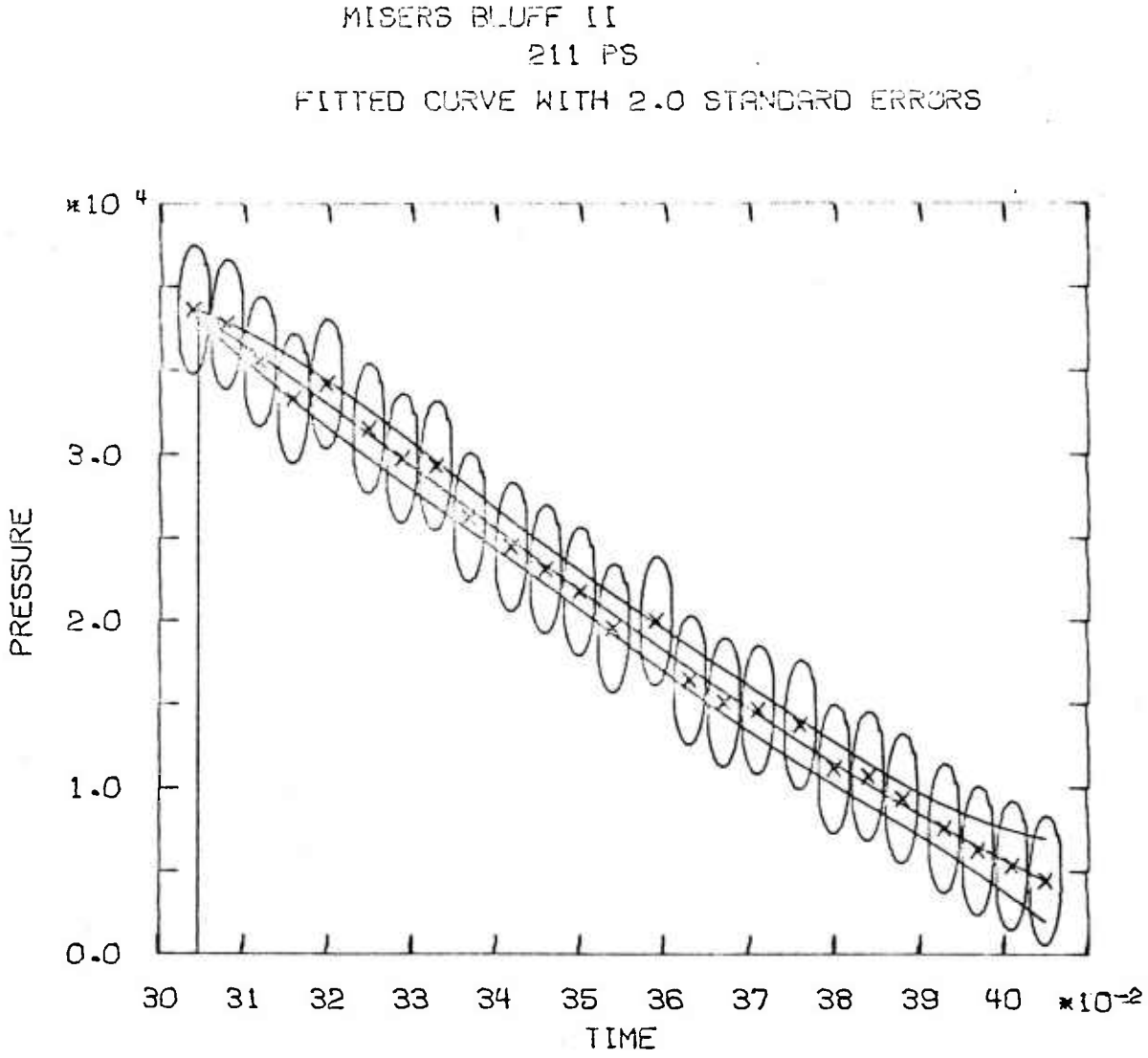

Figure 29. Fitting of Pressure at 211 m in MISERS BLUFF II

The data accuracy is indicated by a two-standard error ellipse around each observed point.

Time is expressed in seconds and pressure is expressed in pascals.

Comparing the overpressure histories, one notices that the last two histories, Figures 28 and 29, have shapes that are different from the other curves. This observation is confirmed by the plots of the individual history fitting parameters versus distance, Figure 30. The parameters corresponding to the last two histories do not follow the trends of the other parameters. Based on this observation, one should check the experimental setup and see if any causes for the different behavior of the last two histories can be detected that may render the observations less reliable. For the present example, we assumed that all data are valid and equally accurate.

The next step in computing the flow history at, say, 120 m is to choose a range of observations for the overpressure field fitting. The range should be sufficiently large to enable one to calculate the flow and the test velocity for the time interval of interest. On the other hand, the range should not be too large, because systematic differences between the model and the solution of the governing equations may become excessive in a large fitting region. We illustrate the choice of a fitting region by using two regions for the 120 m history. One region includes all histories between 89.7 m and 174 m, and the other region includes histories between 103 m and 174 m. (Figure 21 shows that the 174 m history data must be included, at least partially, in order to compute the test velocity for the total duration of the 120 m observation.)

Results based on field fitting in the first region (89.7 m - 174 m) are shown in Figures 31 through 34. The dynamic pressure, which is an important quantity for applications, has in Figure 34 very reasonable estimated confidence limits. However, the test velocity in Figure 32 deviates from the particle path velocity by two standard errors throughout the history. Because the test velocity is computed using data at distances beyond 120 m, the difference indicates a discrepancy between data below 120 m and beyond 120 m, respectively.

This discrepancy indication disappears if one uses field data only between 103 m and 174 m; i.e., if the history at 89.7 m is not used. The results of such a computation are shown in Figures 35 through 38. The velocity plot in Figure 36 now shows good agreement between the original and the test velocities. Comparing Figure 36 with Figure 32, one sees that the test velocity in both figures is practically equal, whereas the original velocity, which depends more directly on data below 120 m, has changed by the exclusion of the 89.7 m history. Short of other information about the experiment, one should in such a case use only field data between 103 m and 174 m to calculate histories at 120 m, because then the results are self consistent. We notice, in passing, that the absolute differences between the dynamic pressures in both calculated cases are small, although they are of the order of two standard errors.

For the computation of the flow histories at 150 m range, again two different pressure field functions were used. One function was obtained by fitting overpressure data from ranges between 120.3 m and 206 m. This corresponds to the minimum coverage of the pressure field that is necessary for the computation of the histories at 105 m for the complete duration of the pressure observations. The computed histories are shown in Figures 39 through 42.

Another pressure function was obtained by adding two more observed overpressure histories to the data base, one at each end of the range covered. Now, the overpressure field function was fitted to data between 114 m and 211 m. The corresponding histories at 150 m were found to be identical within the

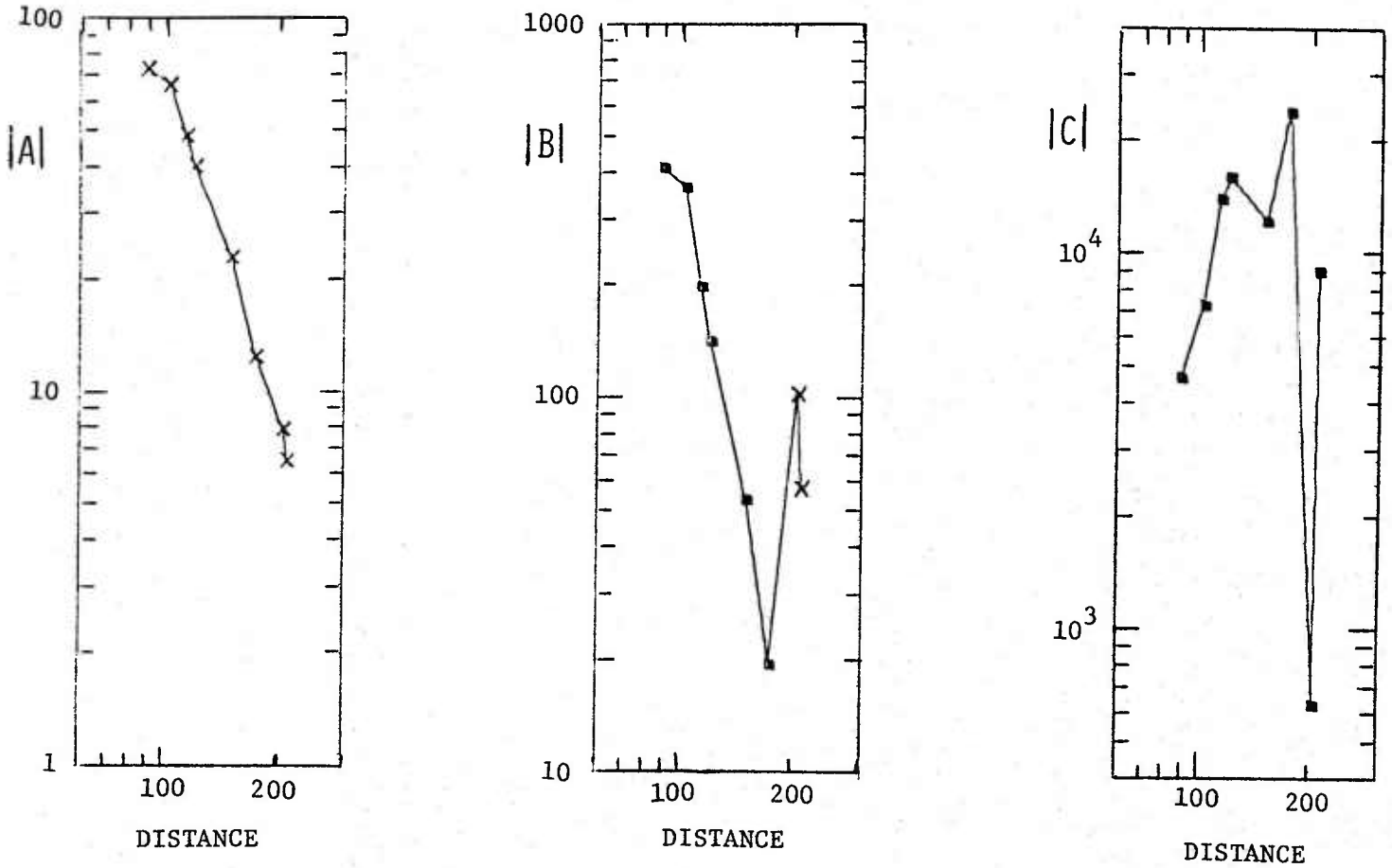

Figure 30 . Log-log Plots of History Parameters versus Distance in MISERS BLUFF II

X - Negative parameter

■ - Positive parameter

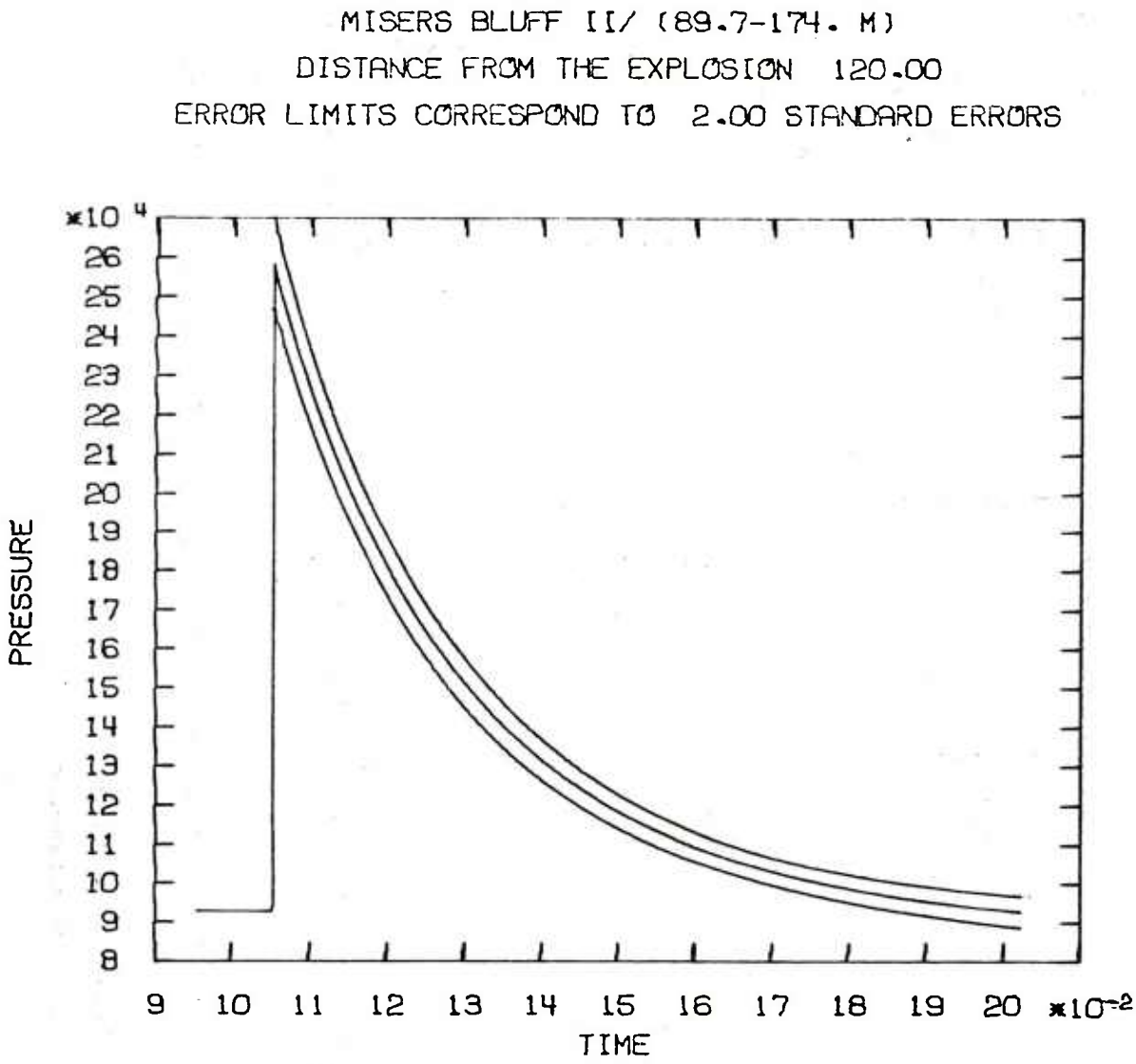

Figure 31 . Pressure History at 120 m in MISERS BLUFF II/(89.7-174 m)

Time is expressed in seconds and pressure is expressed in pascals.

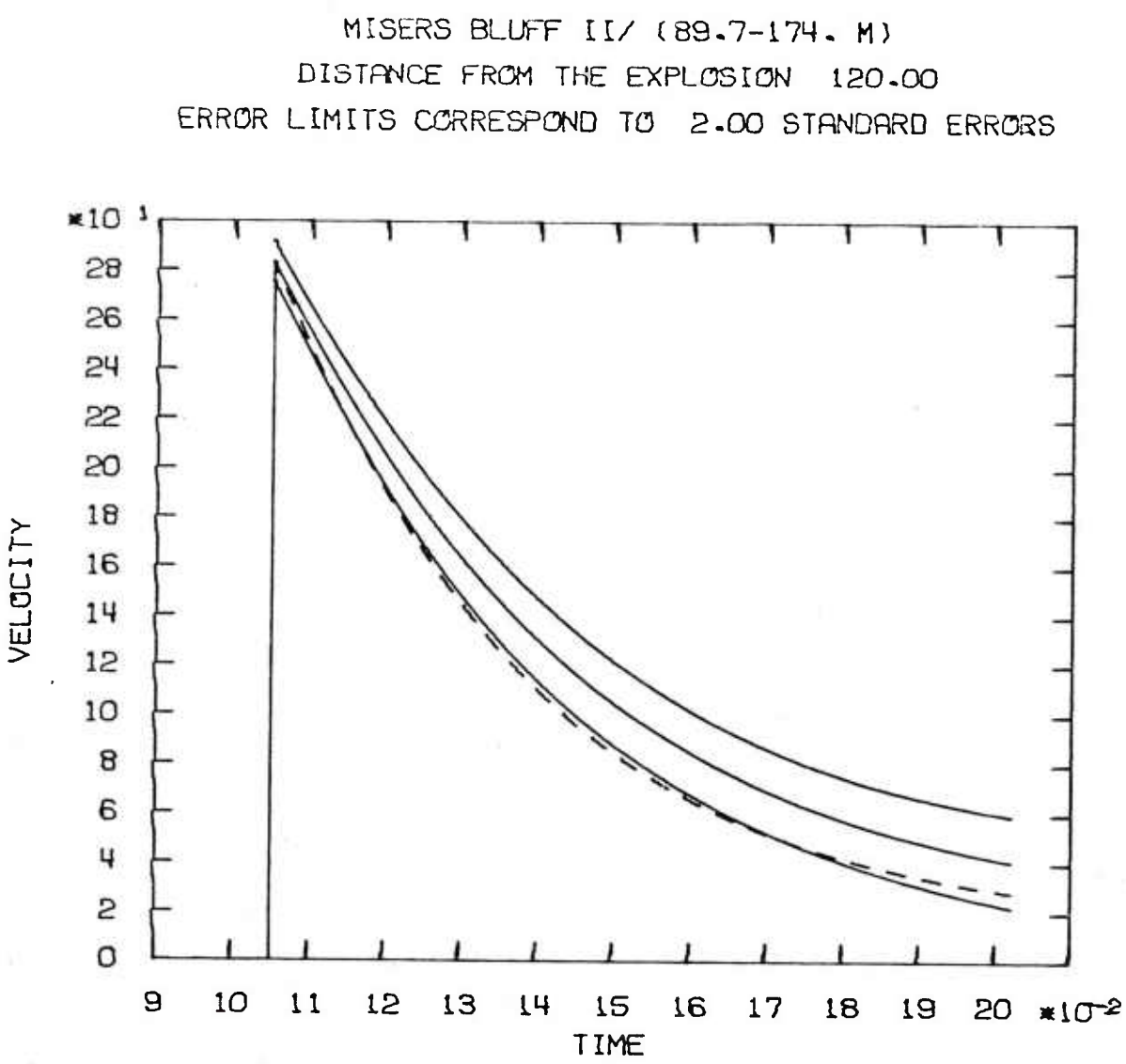

Figure 32 . Velocity History at 120 m in MISERS BLUFF II/(89.7-174 m)

Velocity and confidence limits computed along particle paths

Control calculation

Time is expressed in seconds and velocity is expressed in m/s.

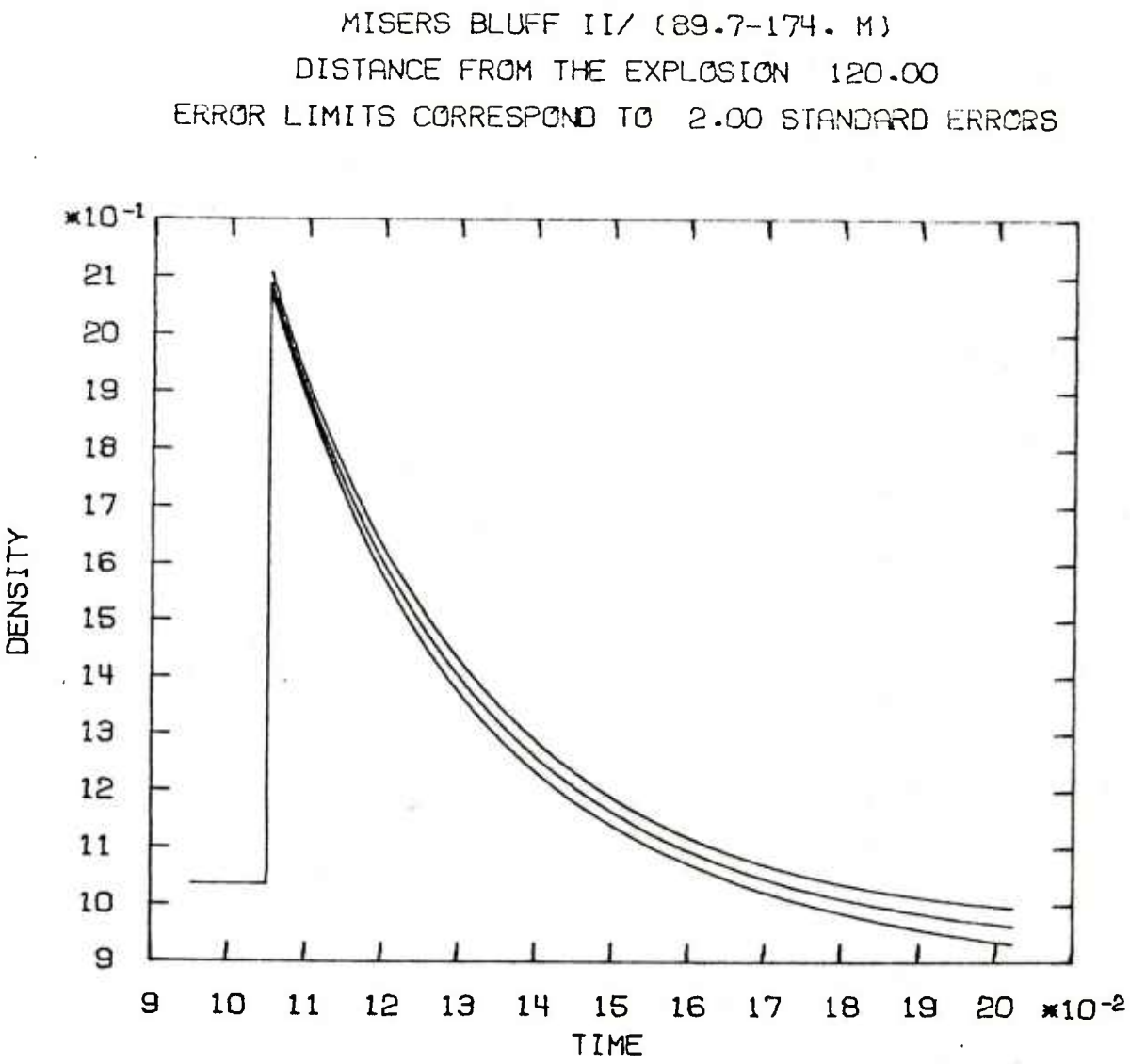

Figure 33. Density History at 120 m in MISERS BLUFF II/(89.7-174 m)

Time is expressed in seconds and density is expressed in kg/m^3.

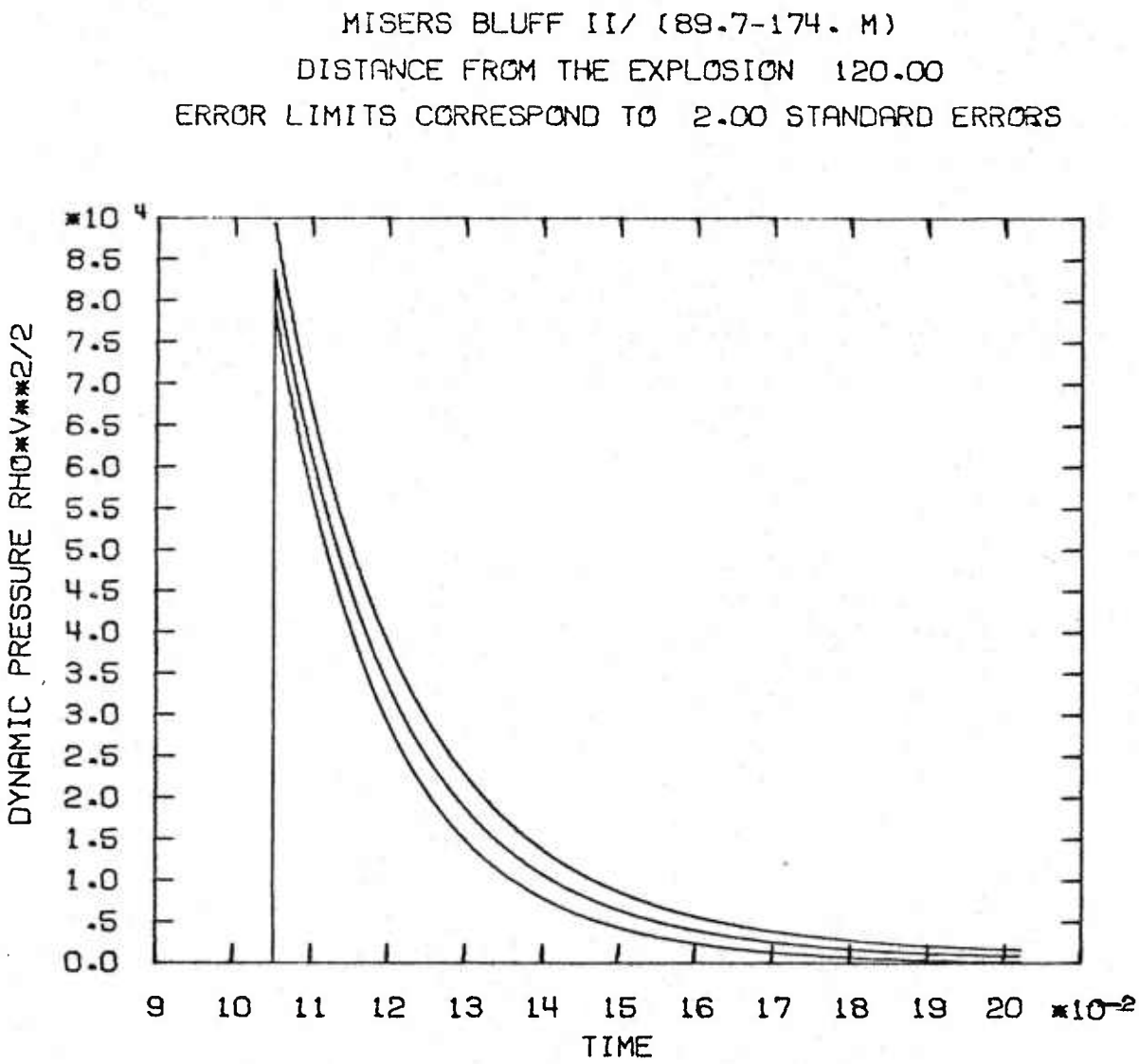

Figure 34. Dynamic Pressure History at 120 m in MISERS BLUFF II/(89.7-174 m)

Time is expressed in seconds and dynamic pressure is expressed in pascals.

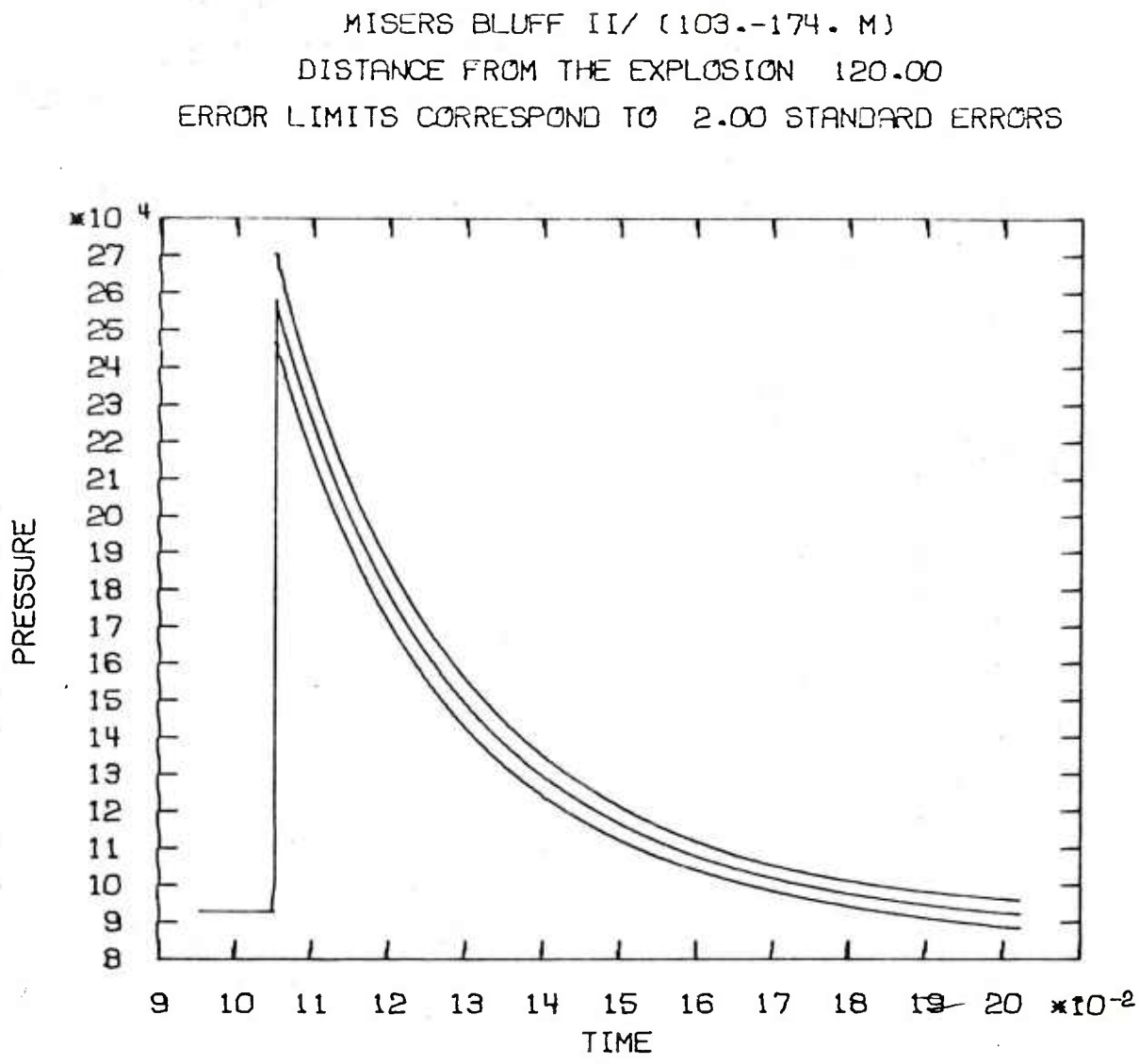

Figure 35. Pressure History at 120 m in MISERS BLUFF II/(103-174 m)

Time is expressed in seconds and pressure is expressed in pascals.

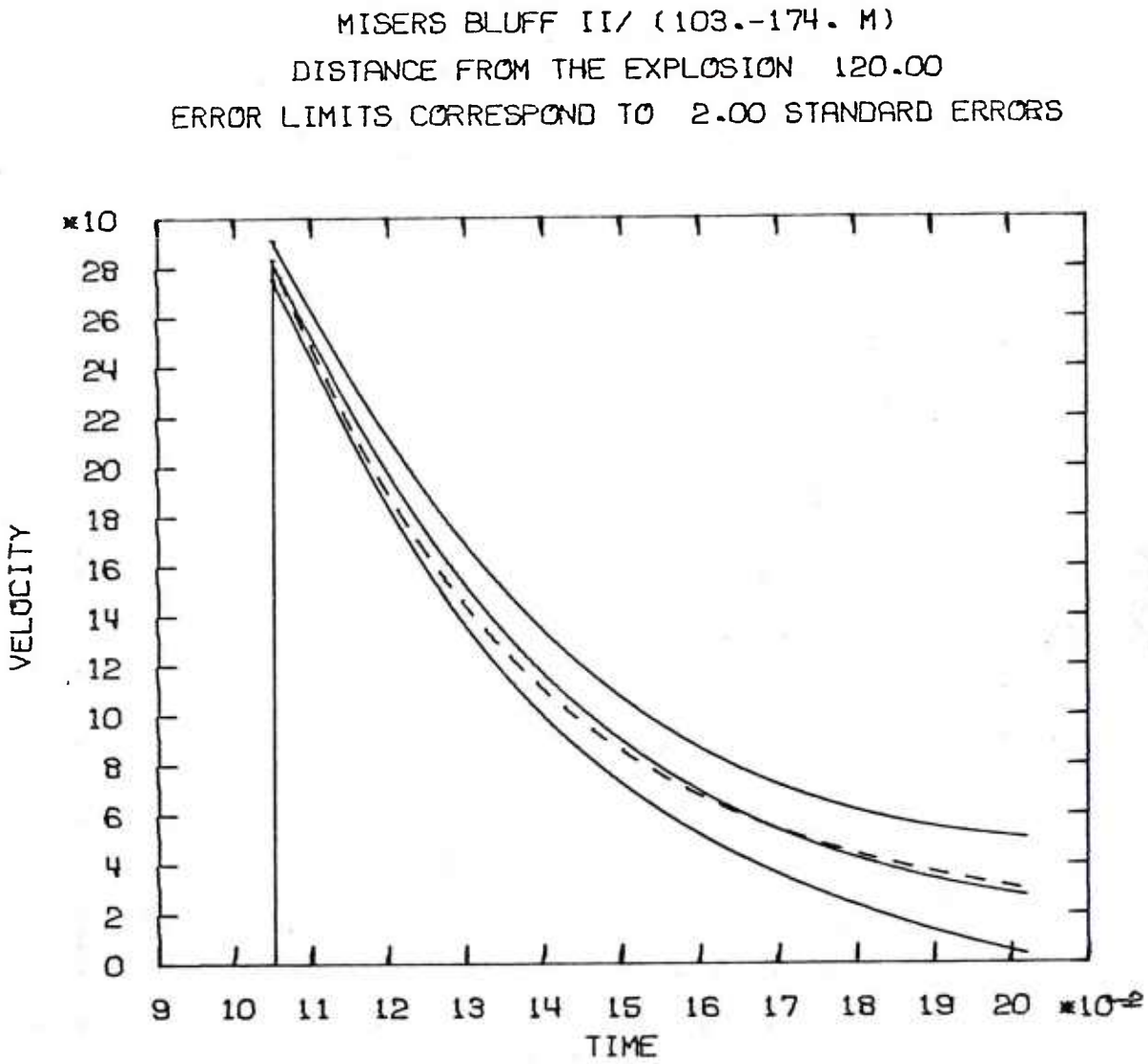

Figure 36. Velocity History at 120 m in MISERS BLUFF II/(103-174 m)

Velocity and confidence limits computed along particle path

Control calculation

Time is expressed in seconds and velocity is expressed in m/s.

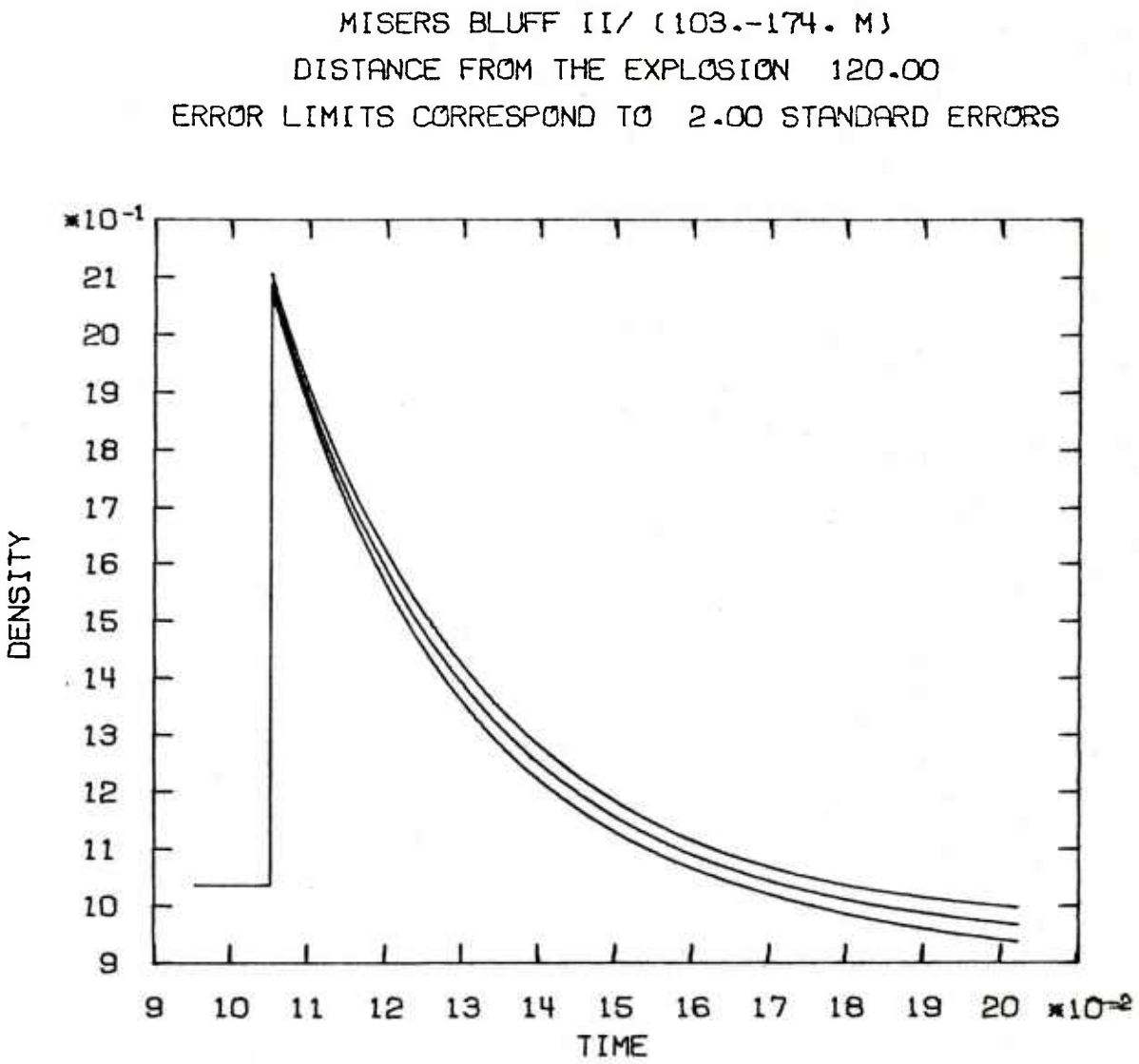

Figure 37. Density History at 120 m in MISERS BLUFF II/(103-174 m)

Time is expressed in seconds and density is expressed in kg/m^3.

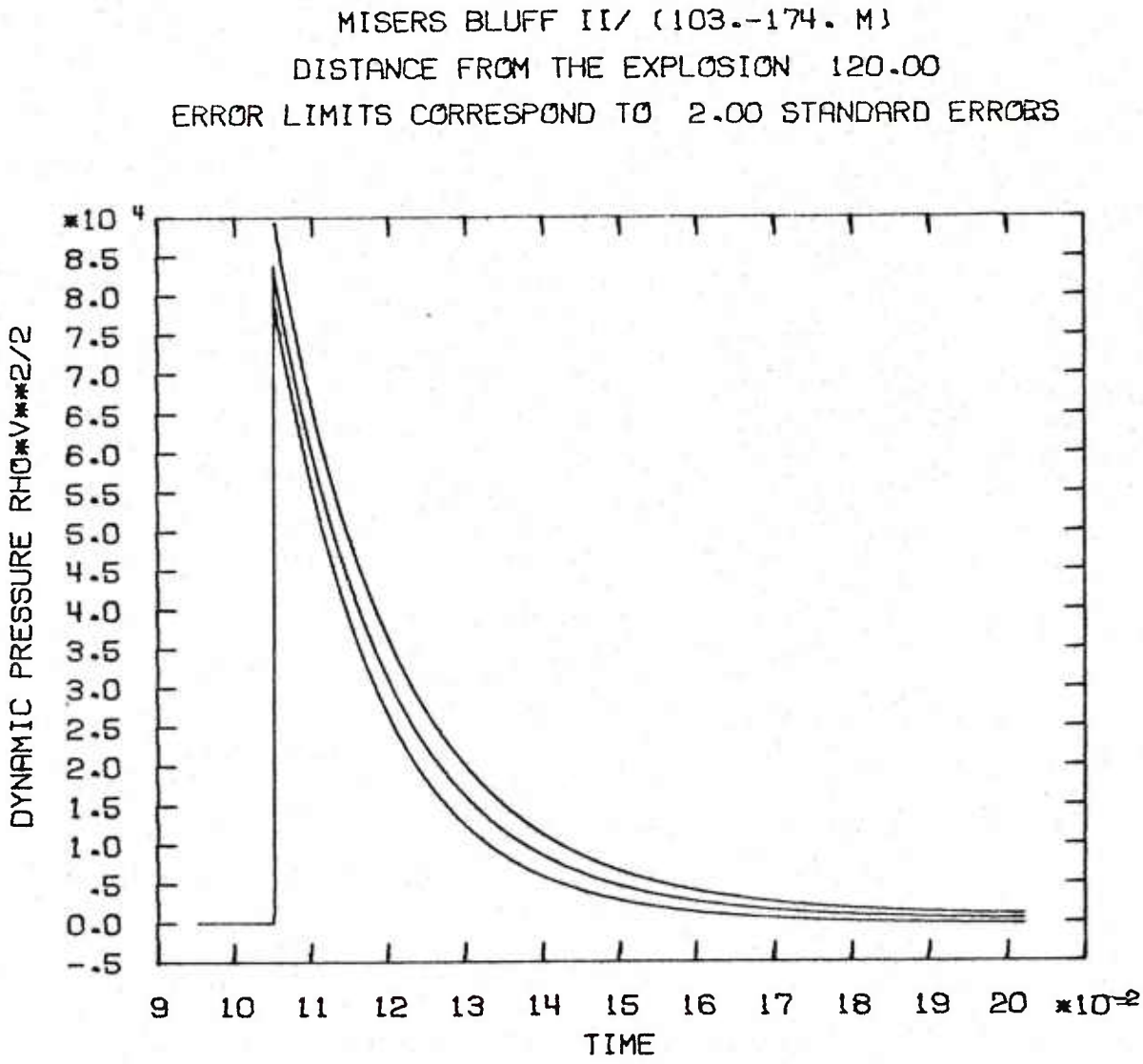

Figure 38. Dynamic Pressure History at 120 m in MISERS BLUFF II/(103-174 m)

Time is expressed in seconds and dynamic pressure is expressed in pascals.

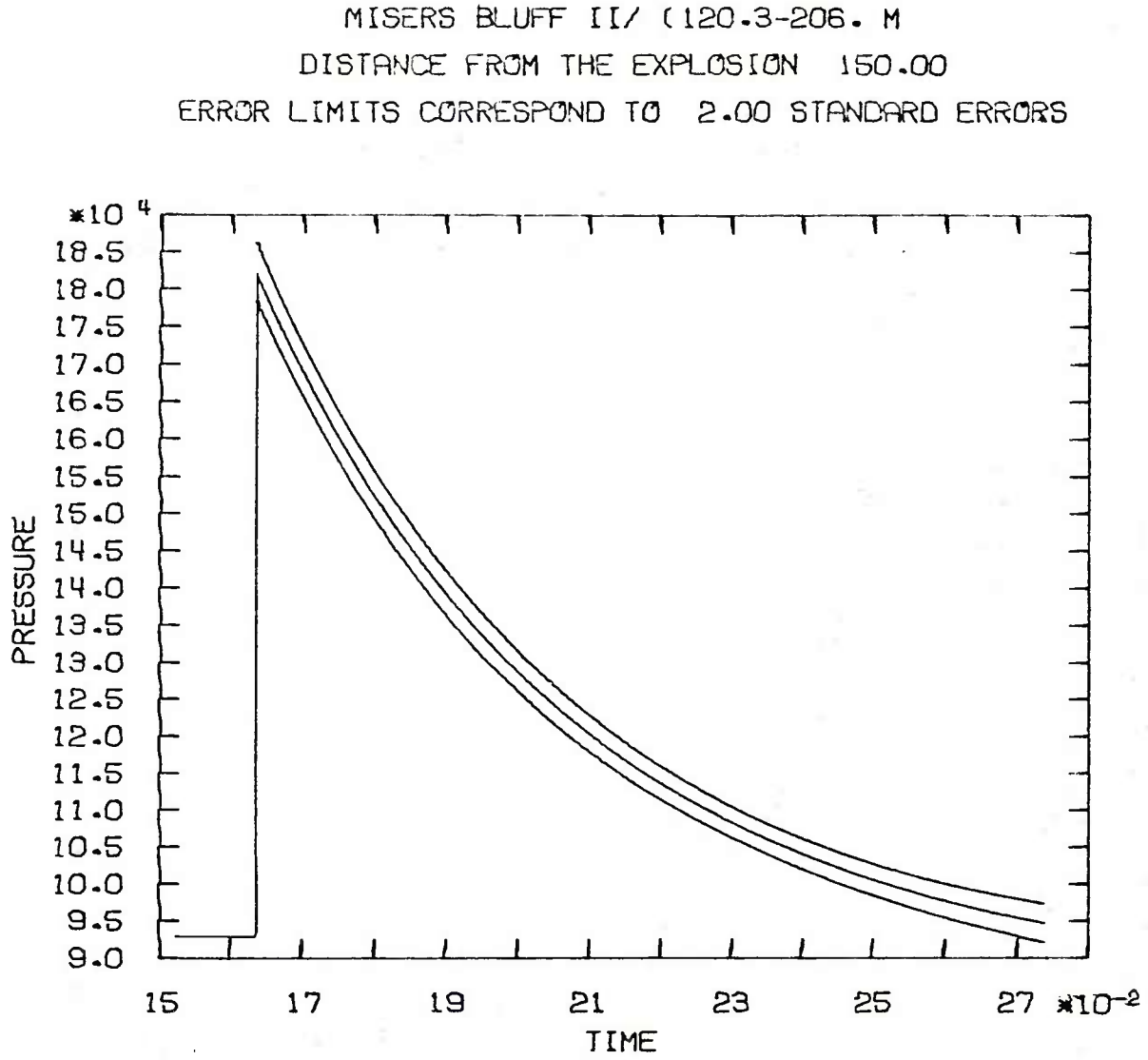

Figure 39. Pressure History at 150 m in MISERS BLUFF II/(120.3-206 m)

Time is expressed in seconds and pressure is expressed in pascals.

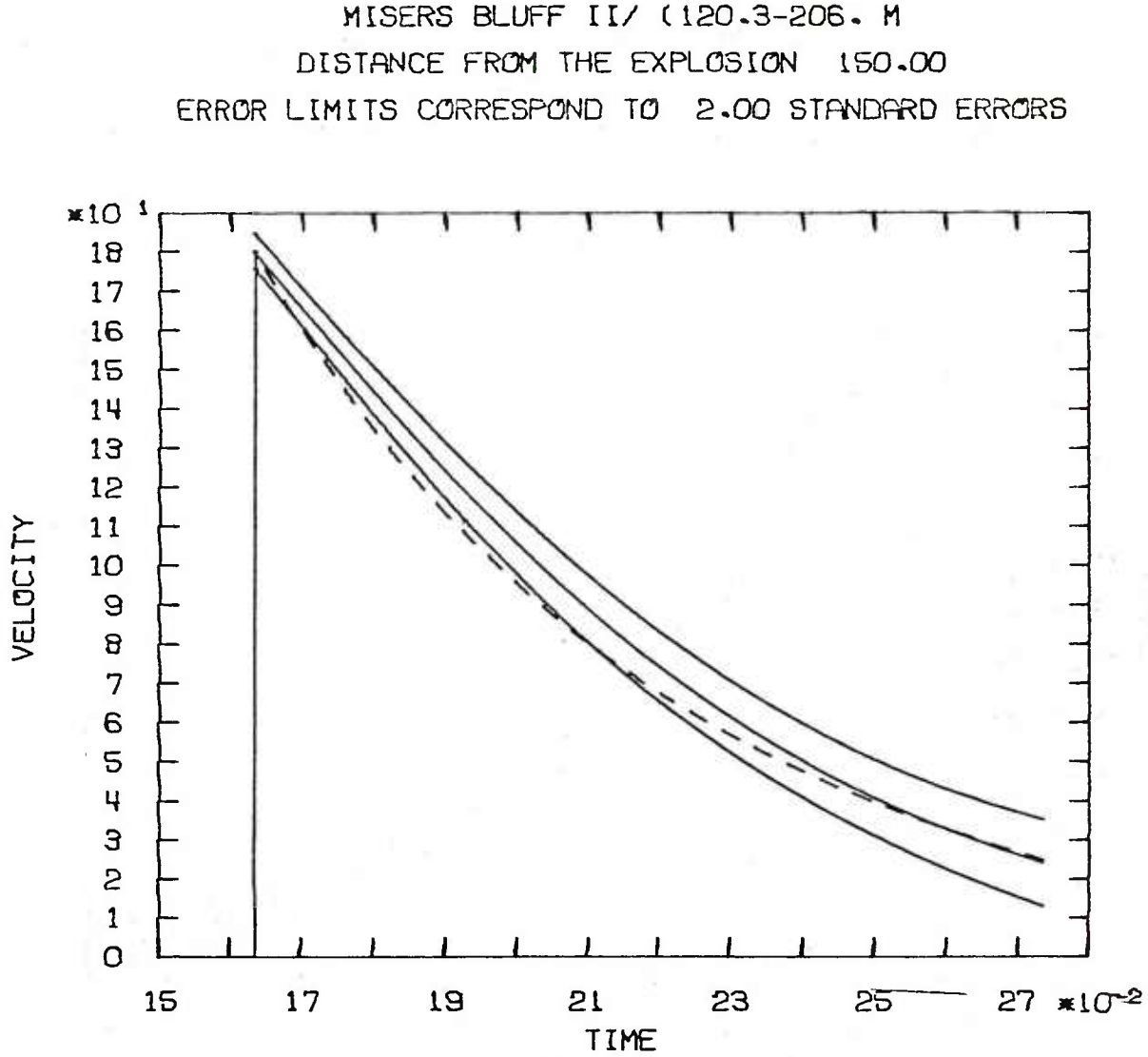

Figure 40. Velocity History at 150 m in MISERS BLUFF II/(120.3-206 m)

Velocity and confidence limits computed along particle paths

Control calculation

Time is expressed in seconds and velocity is expressed in m/s.

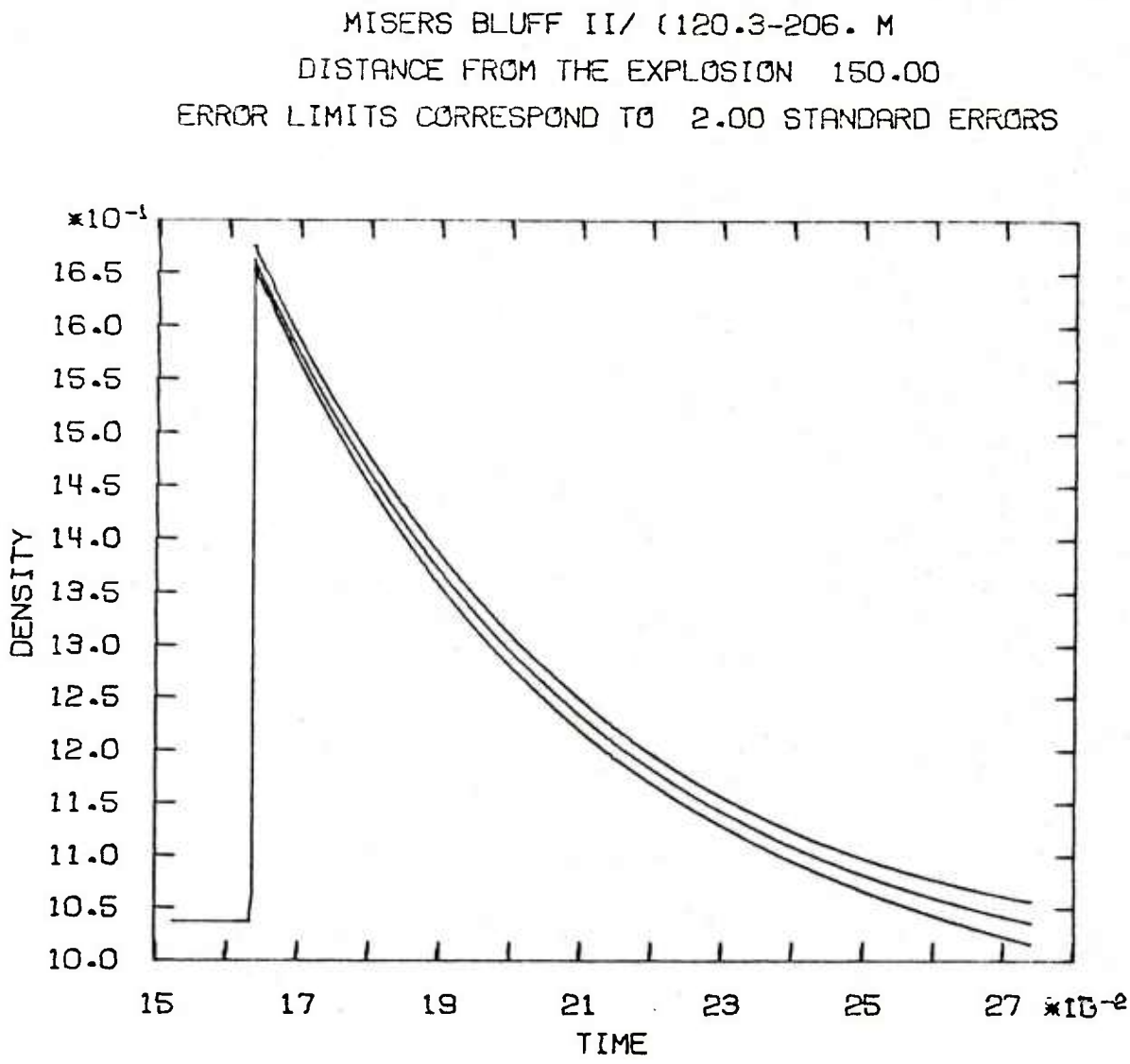

Figure 41. Density History at 150 m in MISERS BLUFF II/(120.3-206 m)

Time is expressed in seconds and density is expressed in kg/m^3.

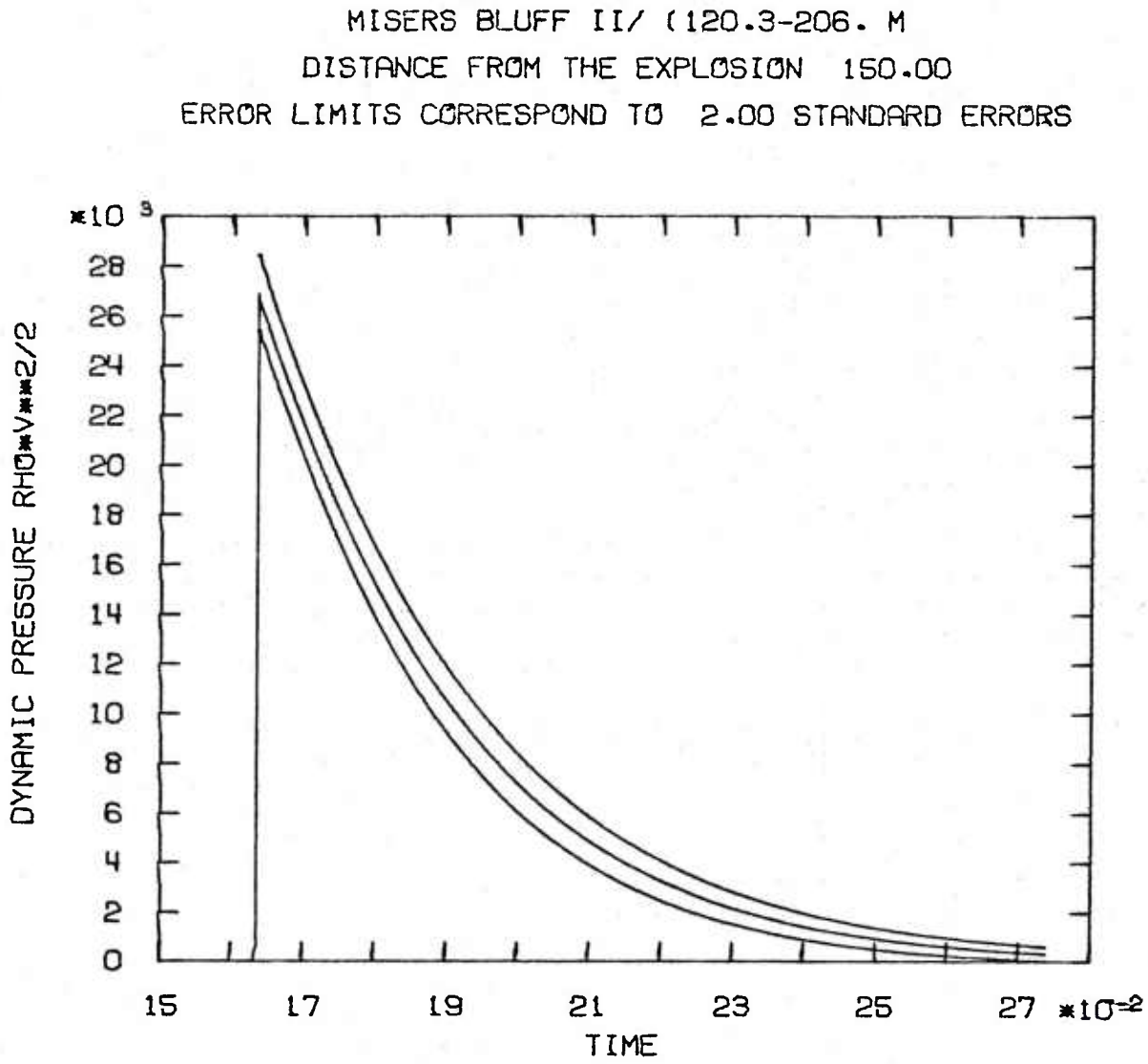

Figure 42. Dynamic Pressure History at 150 m in MISERS BLUFF II/(120.3-206 m)

Time is expressed in seconds and dynamic pressure is expressed in pascals.

plotting accuracy to those of the previous calculation. A closer inspection of the numerical output indicates that the variance estimates are slightly reduced by the addition of the two observed histories. However, the difference between streamline velocity and test velocity is increased. The latter observation confirms the experience with history calculations at 120 m, where it was also found that best results are obtained when the range for the fitting of the pressure field function is as small as practically possible.

Of some concern in the present example is the large difference between the original and test velocity, which is of the order of two standard errors. This difference may be attributed to disturbances in the flow field at ranges beyond 150 m, that can violate some of the basic assumptions for the flow model, e.g., the spherical symmetry. In a practical application, one would reexamine the data and then decide, depending on the purpose of the history calculations, whether the proposed analysis is adequate.

The example makes it clear that one needs a good definition of the pressure field around the reference ground range where the flow history is of interest. The range interval in which additional pressure histories should be recorded depends on the size of the explosion, on the reference range, and on the anticipated duration of the history observation. For a planned experiment, one may assume that typically the duration of interest will approximate the duration of positive overpressure. Estimates of positive overpressure duration are available from past experiments. Figure 43 shows such an estimate[10] for an 0.1 kton TNT experiment, like MISERS BLUFF.

Estimates of corresponding range intervals can be calculated, e.g., assuming that the shock trajectory and the particle paths are straight lines within the area of interest. Range intervals computed with this assumption are overestimates, as can be seen from Figure 21. The results are as follows.

The downstream range interval that is needed to carry out the control calculation for a history of duration Δt can be estimated by

$$\Delta r_{control} = \Delta t \cdot U \qquad (8.1)$$

where U is the shock velocity. The corresponding upstream interval that is needed to compute the flow field history at the reference range for the duration Δt can be estimated by

$$\Delta r_{computing} = \Delta t(1/u_s - 1/U)^{-1} = \Delta t \cdot U \cdot (U/u_s - 1)^{-1} \quad , \qquad (8.2)$$

where u_s is the particle velocity behind the shock. Using the shock formula (4.4) one can also express Eq. (8.2) in the form

$$\Delta r_{computing} = \Delta t \cdot U \frac{1}{\gamma} \frac{p_s}{p_o} \left(1 + \frac{\gamma-1}{2\gamma} \frac{p_s}{p_o}\right)^{-1} \qquad (8.3)$$

---

[10] *Klaus Opalka, Terminal Ballistics Division, USA ARRADCOM/Ballistic Research Laboratory, private communication, March 1981.*

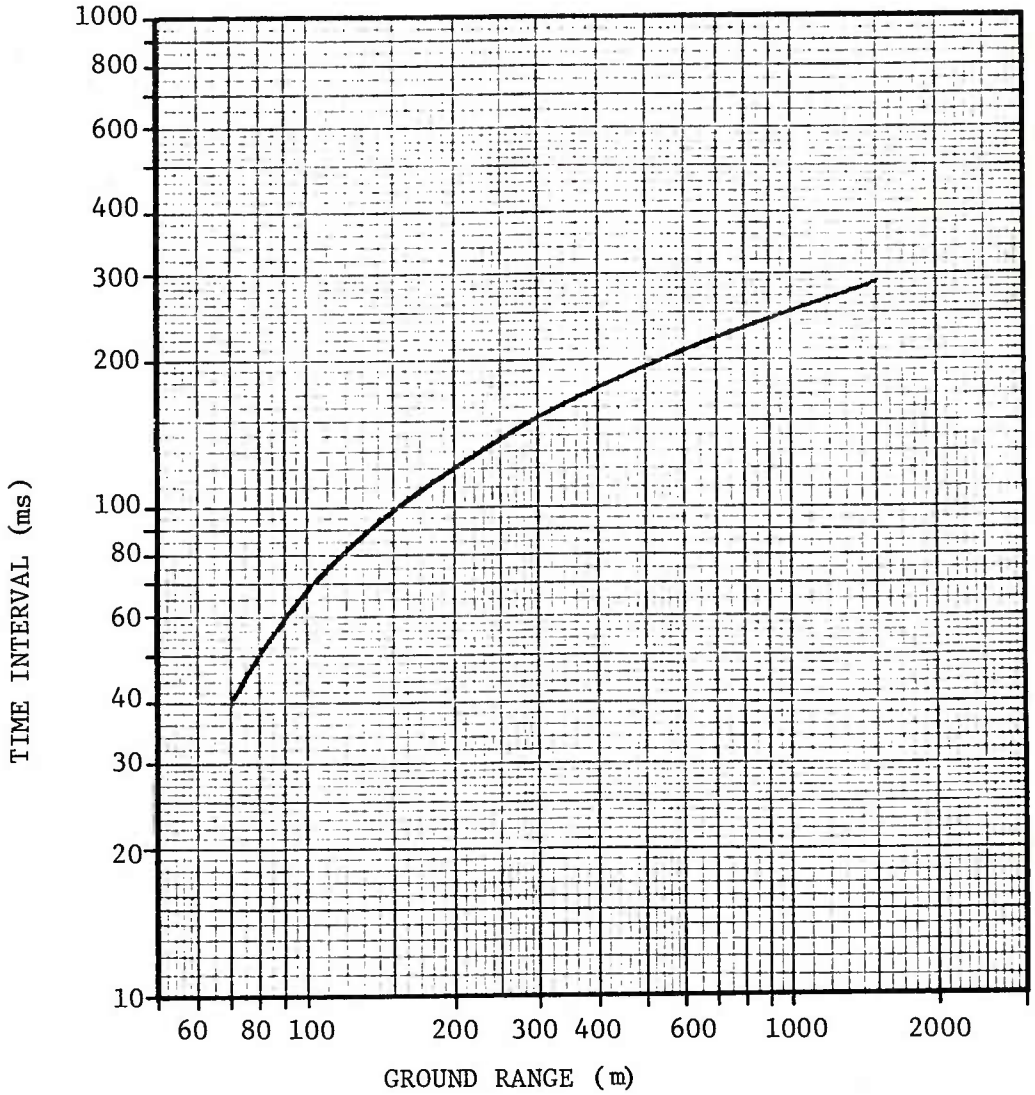

Figure 43. Estimated Positive Overpressure Duration in a 0.1 kton TNT Experiment

where p_s is the shock overpressure and p_o is the ambient pressure. The estimates (8.1) and (8.3) of the downstream and upstream range intervals are plotted in Figure 44 as functions of the reference range, using the Δt from Figure 43.

In order to check the quality of the approximate range interval formulas, we also have determined the range intervals by an analysis of Figure 21. The resulting upstream intervals are plotted in Figure 44. The plot shows that for close ranges the approximate formulas overestimate the range interval by more than a factor of two. For ranges larger than 200 m the factor is smaller because the path line curvatures decrease with increasing range.

The downstream range intervals computed by an analysis of Figure 21 differ only insignificantly from the curve in Figure 44 and, therefore, are not plotted.

9. CONCLUSIONS

A distinct feature of the described method for blast field reconstruction from overpressure measurements is the calculation of variance estimates of all field variables concurrently with the calculation of the variables themselves. The estimates can be used in the planning of blast experiments; e.g., to determine pressure gage arrangements that enhance the predicted accuracy of the calculated flow field. In examples where the method was applied to actual measurements, it was found that the sensitivity of the computed results to observational inaccuracies was up to ten times smaller than that of some previous methods.

Another unique feature of the method is the control calculation of a flow velocity based on the continuity equation. The control calculation provides an indicator for the consistency of the data with the basic assumption for the mathematical model. Numerical experimentation with this indicator shows that more consistent results can be expected when the pressure field function is fitted to data covering smaller ranges of distances. This means for the planning of experiments that one should provide a sufficient number of pressure history observations in the vicinity of the range of interest. Favorable arrangements of stations and durations of pressure recordings can be obtained from test runs of the field calculation programs on approximate expected data sets.

The nine parameter pressure field function of this report was found to be sufficiently flexible for the description of the pressure within a wide range of theoretical and real problems.

One part of the analysis, having independent applications, is the determination of shock functions from shock data. The method described in this report has the advantage of using all available data, including incomplete sets and adjusting simultaneously measurements of pressure, time, and distance. The method can be expected to produce more reliable results than previous numerical shock fittings.

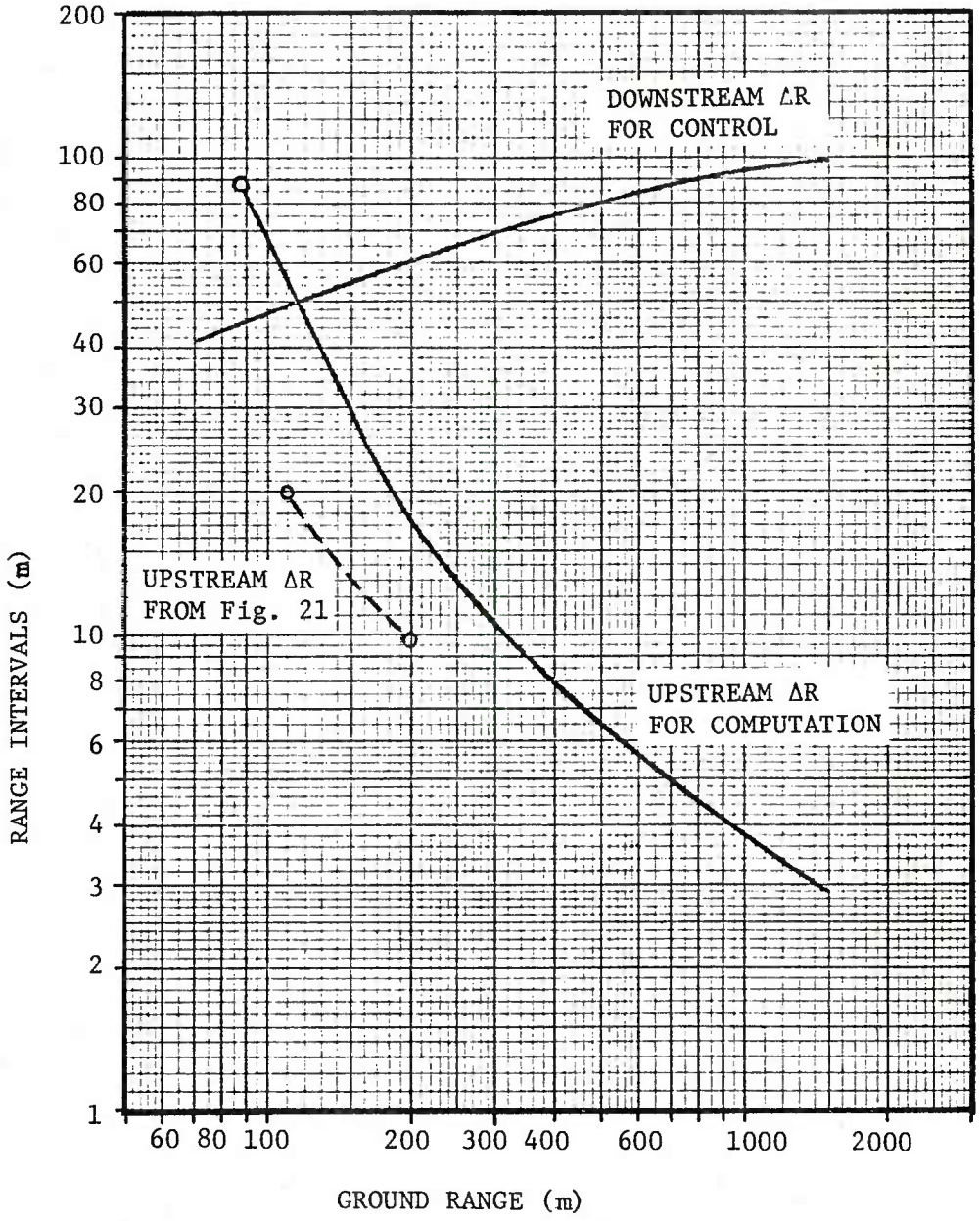

Figure 44. Range Intervals for a 0.1 kton TNT Experiment

ACKNOWLEDGMENT

Mr. Noel Ethridge, Terminal Ballistics Division, Ballistic Research Laboratory, suggested using Makino's theoretical work as a basis for the development of the presented method. The author also wishes to thank Mr. Ethridge for his continued interest and support.

REFERENCES

1. George D. Teel, "Free-Field Airblast Definition - Event DICE THROW," Proceedings of the DICE THROW Symposium, 21-23 June 1977, Volume I, Defence Nuclear Agency Report DNA 4377P-1, pp. 7-76, July 1977.

2. James J. Gottlieb and David V. Ritzel, "Flow Properties of a Spherical Blast Wave," presentation at the Sixieme Symposium International sur les Applications Militaires de la Simulation de Souffle, Cahors, France, 25-29 June 1979.

3. Ray C. Makino, "An Approximation Method in Blast Calculations," USA Ballistic Research Laboratory Memorandum Report 1034, February 1956. (AD #114875)

4. Richard von Mises, "Mathematical Theory of Compressible Fluid Flow," Academic Press, NY, 1958.

5. Aivars Celmiņš, "A Manual for General Least Squares Model Fitting," USA ARRADCOM/Ballistic Research Laboratory Report ARBRL-TR-02167, June 1979. (AD #B040229L)

6. Aivars Celmiņš, "Strong Blast Wave Computer Programs," USA ARRADCOM/Ballistic Research Laboratory Report ARBRL-TR-02264, September 1980. (AD #A092346)

7. L.I. Sedov, "Similarity and Dimensional Methods in Mechanics," Academic Press, NY, 1959.

8. O. Laporte and T.S. Chang, "Curved Characteristics Behind Strong Blast Waves," Physics of Fluids, Volume 15, pp. 502-504, 1972.

9. G. Teel, "Free Field Airblast Definition," Proceedings of the MISERS BLUFF Phase II Results Symposium, 27-29 March 1979, Defence Nuclear Agency Report POR 7013-1, September 1979.

10. Klaus Opalka, Terminal Ballistics Division, USA ARRADCOM/Ballistic Research Laboratory, Private communication, March 1981.

LIST OF SYMBOLS

(a,b,c,d) - shock parameters

(A,B,C) - overpressure field parameter functions

(A_1,A_2,B_1,B_2,C_1) - overpressure field parameters

c - sound speed (m/s)

e - specific internal energy (J/kg)

E - function defined by Eq. (5.3)

f - model function for data fitting

H - flow field vector defined by Eq. (3.17)

M - molar mass (kg/mole)

p,P - pressure (Pa)

p_f - overpressure field function (Pa)

p_h - overpressure history function (Pa)

Q - function defined by Eq. (4.16)

r,R - distance from the center of explosion

t,T - time after explosion (s)

T_o - ambient temperature (K)

u - particle velocity (m/s)

U - shock velocity (m/s)

V - variance-covariance matrix

γ - ratio of specific heats

$\Gamma = (\gamma+1)/(2\gamma p_o)$ - constant in Section 4 (Pa^{-1})

θ - parameter vector for model fitting

ρ - density (kg/m^3)

SUBSCRIPTS

s - pertaining to shock

o - pertaining to ambient conditions

DISTRIBUTION LIST

No. of Copies	Organization
12	Commander Defense Technical Info Center ATTN: DDC-DDA Cameron Station Alexandria, VA 22314
2	Director Defense Civil Preparedness Agency ATTN: G. Sission/RF-SR Technical Library Washington, DC 20301
1	Director Defense Advanced Research Projects Agency ATTN: Technical Library 1400 Wilson Boulevard Arlington, VA 22209
5	Director Defense Nuclear Agency ATTN: DDST/Dr. Conrad DDST/Dr. Oswald DDST/Dr. Knowles SPSS/Dr. Goering SPSS/Dr. Ullrich Washington, DC 20305
5	Director Defense Nuclear Agency ATTN: STSI/Archives STSP STTL/Tech Lib (2 cys) STVL Washington, DC 20305
7	Commander US Army Engineer Waterways Experiment Station ATTN: Technical Library W. Flathau L. Ingram G. Jackson J.N. Strange S.A. Kiger R.D. Crowson P.O. Box 631 Vicksburg, MS 39180
1	Commander US Army Materiel Development and Readiness Command ATTN: DRCDMD-ST 5001 Eisenhower Avenue Alexandria, VA 22333
1	Commander US Army Materiel Development and Readiness Command ATTN: Technical Library 5001 Eisenhower Avenue Alexandria, VA 22333
2	Commander US Army Armament Research and Development Command ATTN: DRDAR-TSS Dover, NJ 07801
2	Commander US Army Armament Research and Development Command ATTN: DRDAR-LCN, P. Angelotti Dover, NJ 07801
1	Commander US Army Armament Materiel Readiness Command ATTN: DRSAR-LEP-L, Tech Lib Rock Island, IL 61299
1	Director US Army ARRADCOM Benet Weapons Laboratory ATTN: DRDAR-LCB-TL Watervliet, NY 12189
1	Commander US Army Aviation Research and Development Command ATTN: DRDAV-E 4300 Goodfellow Boulevard St. Louis, MO 63120

DISTRIBUTION LIST

No. of Copies	Organization
1	Director US Army Air Mobility Research and Development Laboratory Ames Research Center Moffett Field, CA 94035
1	Commander US Army Communications Research and Development Command ATTN: DRDCO-PPA-SA Fort Monmouth, NJ 07703
2	Commander US Army Electronics Research and Development Command Technical Support Activity ATTN: DELSD-L R. Freiberg Fort Monmouth, NJ 07703
5	Commander US Army Harry Diamond Labs ATTN: DRXDO-TI DRXDO-TI/012 DRXDO-NP DRXDO-RBH, Mr. Caldwell DELHD-RBA, J. Rosado 2800 Powder Mill Road Adelphi, MD 20783
5	Commander US Army Harry Diamond Labs ATTN: L. Belliveau J. Gaul J. Gwaltney B. Vault J. Meszaros 2800 Powder Mill Raod Adelphi, MD 20783
1	Commander US Army Missile Command ATTN: DRSMI-R Redstone Arsenal, AL 35809
1	Commander US Army Missile Command ATTN: DRSMI-YDL Redstone Arsenal, AL 35809
1	Commander US Army Tank Automotive Research and Development Command ATTN: DRDTA-UL Warren, MI 48090
4	Commander US Army Nuclear Agency ATTN: ACTA-NAW Technical Library Dr. Davidson MAJ J. Sims 7500 Backlick Road, Bldg. 2073 Springfield, VA 22150
1	Director US Army TRADOC Systems Analysis Activity ATTN: ATAA-SL, Tech Lib White Sands Missile Range, NM 88002
1	Director Strategic Systems Project Office ATTN: NSP-43, Tech Lib Department of the Navy Washington, DC 20360
1	Commander Naval Surface Weapons Center ATTN: DX-21, Library Branch Dahlgren, VA 22448
2	Commander Naval Surface Weapons Center ATTN: Code WX21, Tech Lib Code 240, C.J. Aronson Silver Spring, MD 20910
1	AFWL/DE-I Kirtland AFB, NM 87117
1	AFWL/DEX Kirtland AFB, NM 87117

DISTRIBUTION LIST

No. of Copies	Organization
1	AFWL, R. Henny Kirtland AFB, NM 87117
1	AFWL/SUL, M.A. Plamondon Kirtland AFB, NM 87117
2	Director Lawrence Livermore Laboratory ATTN: Tech InfoDept L-3 H.D. Glenn P.O. Box 808 Livermore, CA 94550
4	Director Los Alamos Scientific Laboratory ATTN: Doc Contr for Rpts Lib A. Davis R.A. Gentry G.R. Spillman P.O. Box 1663 Los Alamos, NM 87544
4	Sandia National Laboratories ATTN: Doc Control for 3141 Sandia Rpt Collection M.L. Merritt L.J. Vortman J.M. McGlaun P.O. Box 5800 Albuquerque, NM 87115
1	The Aerospace Corporation ATTN: H. Mirel El Segundo, CA 90245
3	Agbabian Associates ATTN: M. Agbabian F.B. Safford S.F. Masri 250 North Nash Street El Segundo, CA 90245
1	Analytical Services, Inc. ATTN: G. Hessellracher 712 F North Valley Street Anaheim, CA 92801
1	The BMD Corporation ATTN: R. Hensely P.O. Box 9274 Albuquerque International Albuquerque, NM 87119
1	Boeing Aerospace Corporation Shock Physics & Applied Math Department MIS 42-37 ATTN: R.M. Schmidt P.O. Box 3999 Seattle, WA 98124
1	General Electric Company-TEMPO ATTN: DASIAC P.O. Drawer QQ Santa Barbara, CA 93102
1	General Electric Company-TEMPO ATTN: E. Bryant 220 S. Main Street, Rm 206 Bel Air, MD 21014
2	Kaman Avidyne ATTN: N.P. Hobbs S. Criscione 83 Second Avenue Northwest Industrial Park Burlington, MA 01830
2	Kaman Sciences Corporation ATTN: Library F.H. Shelton Suite 855 101 Continental Boulevard El Segundo, CA 90245
1	Pacific Sierra Research Corp. ATTN: H. Brode 1456 Cloverfield Boulevard Santa Monica, CA 90404
1	Physics International Corp. ATTN: F.M. Sauer J.M. Thomsen Technical Library 2700 Merced Street San Leandro, CA 94577

DISTRIBUTION LIST

No. of Copies	Organization
1	R&D Associates ATTN: H. Cooper Suite 500 1401 Wilson Boulevard Arlington, VA 22209
6	R&D Associates ATTN: J. Carpenter A.L. Kuhl A.L. Latter J.G. Lewis W.B. Wright Technical Library P.O. Box 9695
2	The Rand Corporation ATTN: C.C. Mow Library-D 1700 Main Street Santa Monica, CA 90406
2	Science Applications, Inc. ATTN: J. Cockayne W. Layson 1710 Goodridge Drive P.O. Box 1303 McLean, VA 22101
1	Science Applications, Inc. 2450 Washington Avenue San Leandro, CA 94577
2	Science Applications, Inc. ATTN: Technical Library M. McKay P.O. Box 2351 La Jolla, CA 92037
2	Science Applications, Inc. ATTN: J.F. Dishon, III R.I. Miller Albuquerque, NM 87115
2	Systems, Science and Software ATTN: C.E. Needham J.E. Crepeau P.O. Box 8243 Albuquerque, NM 87198
3	Terra Tek, Inc. ATTN: S. Green A.H. Jones Technical Library 420 Wakara Way Salt Lake City, UT 84108
2	TRW Systems Group ATTN: B. Sussholts Tech Info Ctr/S-1930 One Space Park Redonodo Beach, CA 92078
1	Weidlinger Associate Consulting Engineers ATTN: M.L. Baron 110 East 59th Street New York, NY 10022
2	Drexel Institute of Technology ATTN: P.C. Chou Mechanics and Structures Group 32 and Chestnuts Streets Philadelphia, PA 19137
1	Massachusetts Institute of Technology Aeroelastic and Structures Research Laboratory ATTN: E.A. Witmer Cambridge, MA 02139
2	Southwest Research Institute ATTN: W.E. Baker A.B. Wenzel 8500 Culebra Road San Antonio, TX 78206
2	SRI International ATTN: G.R. Abrahamson C. Peterson 333 Ravenswood Avenue Menlow Park, CA 94025

DISTRIBUTION LIST

No. of Copies	Organization
2	University of Denver Denver Research Institute ATTN: J. Wisotski Technical Library P.O. Box 10127 Denver, CO 80210
1	J. D. Haltiwanger Consulting Services B106a Civil Engineering Bldg. 208 N. Romine Street Urbana, IL 61801
1	University of Washington ATTN: K.A. Holsapple Seattle, WA 98195

Aberdeen Proving Ground

Dir, USAMSAA
ATTN: DRXSY-D
DRSXY-MP, H. Cohen
Cdr, USATECOM
ATTN: DRSTE-TO-F
Dir, USACSL, Bldg. E3516, EA
ATTN: DRDAR-CLB-PA

USER EVALUATION OF REPORT

Please take a few minutes to answer the questions below; tear out this sheet, fold as indicated, staple or tape closed, and place in the mail. Your comments will provide us with information for improving future reports.

1. BRL Report Number _____

2. Does this report satisfy a need? (Comment on purpose, related project, or other area of interest for which report will be used.)

_____

_____

_____

3. How, specifically, is the report being used? (Information source, design data or procedure, management procedure, source of ideas, etc.) _____

_____

_____

4. Has the information in this report led to any quantitative savings as far as man-hours/contract dollars saved, operating costs avoided, efficiencies achieved, etc.? If so, please elaborate.

_____

_____

5. General Comments (Indicate what you think should be changed to make this report and future reports of this type more responsive to your needs, more usable, improve readability, etc.) _____

_____

_____

_____

6. If you would like to be contacted by the personnel who prepared this report to raise specific questions or discuss the topic, please fill in the following information.

Name: _____

Telephone Number: _____

Organization Address: _____

_____

_____